The Study of Some Physical Properties

of High Temperature Superconductors

Dissertation

zur Erlangung des Doktorgrades
des Fachbereichs Physik
der Universität Hamburg

vorgelegt von
Atif Mahmoud Ismail
aus Gharbia, Ägypten

Hamburg
2008

Gutachter der Dissertation:	Prof. Dr. K. Scharnberg Prof. Dr. A. Lichtenstein
Gutachter der Disputation:	Prof. Dr. K. Scharnberg Prof. Dr. M. Potthoff
Datum der Disputation:	24.06.2008
Vorsitzender des Prüfungsausschusses:	PD Dr. A. Chudnovskiy
Vorsitzender des Promotionsauaschusses:	Prof. Dr. J. Bartels
Dekan des Fachbereiches für Mathematik, Informatik und Naturwissenschaften:	Prof. Dr. Arno Frühwald

To the ***Honesty, Justice, Truth, and Honor*** *that we are missing nowadays in our world.*

Kurzfassung

Das Phänomen der Supraleitung, die Entdeckung der Hochtemperatursupraleitung in den Kupraten und die Eigenschaften dieser Materialien werden in dem einführenden Kapitel beschrieben. Dieses beinhaltet auch eine Diskussion der Pseudolücke, welche bis heute Rätsel aufgibt, ebenso wie die hohen Übergangstemperaturen. Es wird ein Überblick über mögliche Anwendungen der Hochtemperatursupraleitung gegeben, bevor die Theorien von Bardeen, Cooper, Schrieffer (BCS) und von Ginzburg und Landau in aller Kürze vorgestellt werden. Der letzte Abschnitt enthält Auszüge aus der inzwischen fast unübersehbaren Literatur zu diesem Thema, wobei die Bedeutung von Störstellen für die Eigenschaften von Hochtemperatursupraleitern im Mittelpunkt steht.

Im zweiten Kapitel werden die mathematischen Hilfsmittel und der theoretische Hintergrund für die Beschreibung von Vielteilchensystemen entwickelt. Verschiedene Green's Funktionen werden eingeführt, welche dann zur Beschreibung der Streuung von Quasiteilchen an Defekten beliebiger Stärke benutzt werden. Sie werden auch zur Berechnung der Wechselstromleitfähigkeit, für welche mit Hilfe der linearen Antworttheorie ein mikroskopischer Ausdruck hergeleitet wird, benötigt. Die Konvergenzprobleme, denen man bei der Berechnung der Leitfähigkeit begegnet, werden kurz erörtert. Detaillierte Berechnungen der Leitfähigkeit im Normalzustand werden im dritten Kapitel und im Anhang dargestellt.

Das dritte Kapitel beginnt mit einer ausführlichen Darstellung des tight binding Modells für die Energiedispersion, da dieses Modell die elektronischen Eigenschaften der Hochtemperatursupraleiter anscheinend sehr viel zutreffender beschreibt als das Modell nahezu freier Electronen. Die Gestalt der zweidimensionalen Fermifläche wird als Funktion der Bandfüllung und des Hüpfmatrixelements B zwischen übernächsten Nachbarn berechnet und dargestellt. B spielt eine wichtige Rolle bei der Ausbildung sogenannter hot-spots. Die Quasiteilchenzustandsdichte und deren Hilbertransformierte $F(\omega)$ werden durch vollständige elliptische Integrale Formalismus gelöst . Diese Ergebnisse werden benutzt, um die an Störstellen gebundenen Zustände zu erhalten.

Auf der Basis von hot spots und Pseudolücke wird ein einfaches Modell für die Supraleitung in den Kupraten entwickelt, welches insbesondere für die elektrondotierten Materialien relevant sein sollte, weil, abhängig von der Dotierung, dort Elektronen und Löcher koexistieren könnten.

Abstract

The phenomenon of superconductivity, the discovery of high temperature superconductivity in the Cuprates and the properties of these materials is described in the introductory chapter. It also includes a discussion of the pseudogap, which has remained a mystery as has the high transition temperature. Possible applications of high temperature superconductivity are reviewed before the theories by Bardeen, Cooper, and Schrieffer (BCS) and Ginzburg and Landau are briefly sketched. The last section gives excerpts of the by now vast literature on this subject, focussing on the role impurities play in this context.

The second chapter develops the mathematical tools and the theoretical background for the description of many-body systems. Various Green's functions are introduced which are then used to describe scattering of quasiparticles off defects of arbitrary strength. They are also required to calculate the a.c. conductivity, for which an expression is derived using linear response theory. The convergence problems one encounters when actually calculating the conductivity are briefly discussed. Detailed calculations for the normal state are presented in the third chapter and in the appendix.

The third Chapter begins with a detailed presentation of the tight binding model for the energy dispersion because this model appears to give a more accurate description of the electronic properties of high temperature superconductors than the nearly free electron model. The shape of the two-dimensional Fermi surface is calculated and displayed as function of band filling and the next-nearest neighbor hopping integral B, assuming a rigid band. B plays an important role in the formation of so-called hot spots. The quasiparticle density of states and its Hilbert transform $F(\omega)$ are solved by means of complete elliptic integrals formalism. These results are used to obtain impurity bound states.

A simple model for the superconductivity in the cuprate materials is developed on the basis of hot spots and the pseudogap, particularly relevant for the electron doped materials, where electrons and holes might coexist, depending on the degree of doping.

Acknowledgements

Before all and after all I thank $\mathcal{ALLAH}$ that $\mathcal{ALLAH}$ always was beside me and supported me in overcoming all the problems that I did encounter during all my existence interval at the university of Hamburg.

I would like to thank my supervisor *Prof. Dr. K. Scharnberg* for his kindness and hospitality. I have to mention his support, during my existence at the institute, in overcoming most of the problems that i did encounter at the institute, I have to mention also without his actions I think the thesis could not be.

I would like to thank *Dr. C. T. Rieck* for his help in fortran programs and for his kindness.

I would like to thank the *University of Hamburg* for financial support from Oktober 1, 2007 to March 31, 2008.

I would like to thank *Prof. Dr. G. El Gemeie* and his former assistant *Dr. D. Salama* for their kindness and support during my mission.

At the end I would like to thank my *Egyptian Government* for financial support from Oktober 7, 2002 to July 6, 2007.

Date, *Atif Ismail*
Jun. 24, 2008

Contents

List of Figures

List of Tables

Chapter 1

Introduction

Superconductivity, see Fig.(1.1), is a fascinating and challenging field of physics. Scientists and engineers throughout the world have been striving to develop an understanding of this remarkable phenomenon for many years. For nearly 75 years superconductivity has been a relatively obscure subject, see Fig.(1.4).

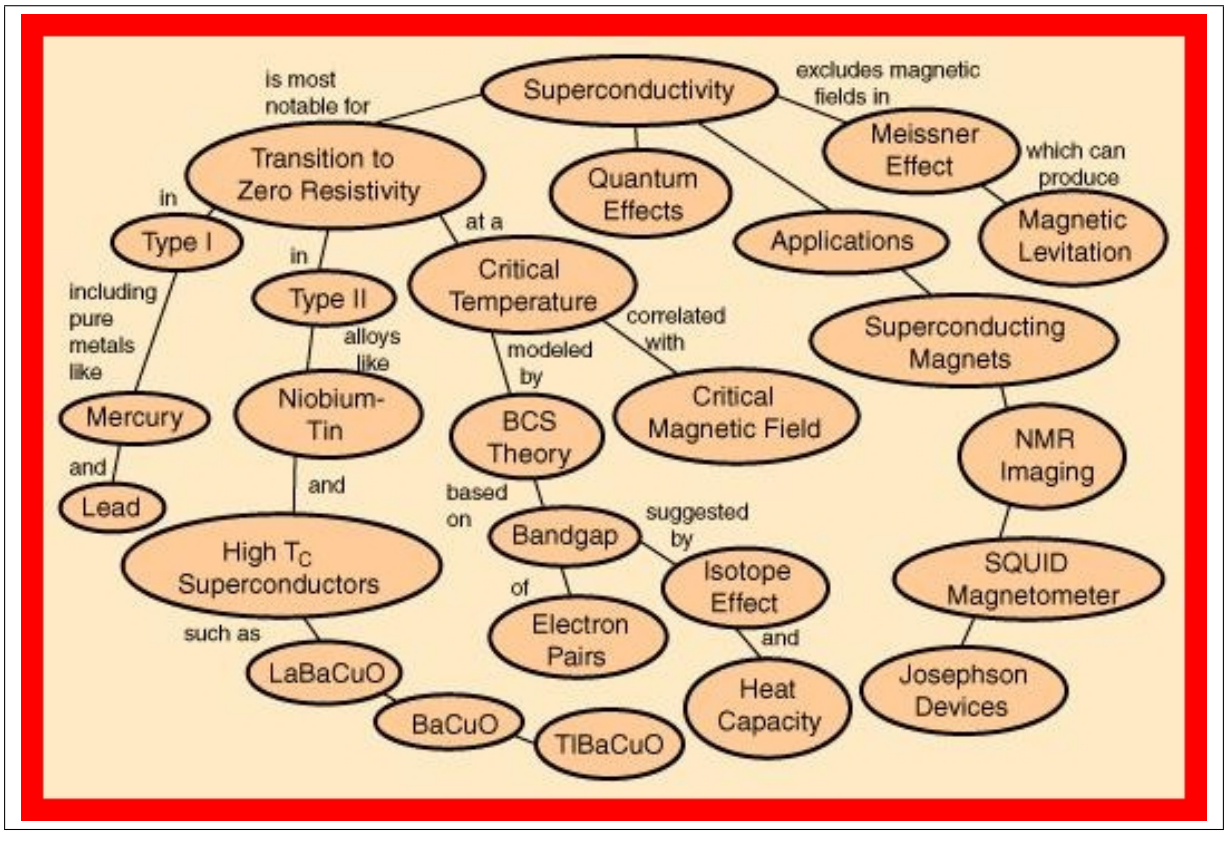

Figure 1.1: Characteristic lengths in superconductors,taken from ref.[1]

Nowadays however, superconductivity is being applied to many diverse areas such as: medicine, theoretical and experimental science, the military, transportation, power production, electronics, as well as many other areas [2; 3].

1.1 Historical Background

Major advances in low-temperature refrigeration were made during the late 19th century. Superconductivity was first discovered in 1911 by the Dutch physicist, Heike Kammerlingh Onnes *. He dedicated his scientific career to exploring extremely cold refrigeration. On 1908, he successfully liquified helium by cooling it to ($4K$).

Onnes produced only a few milliliters of liquid helium that time, but this was to be the new beginnings of his explorations in temperature regions previously unreachable. Liquid helium enabled him to cool other materials closer to absolute zero (0 K).

In 1911, Onnes began to investigate the electrical properties of metals in extremely cold temperatures. It had been known for many years that the resistance of metals fell when cooled below room temperature, but it was not known what limiting value the resistance would approach, if the temperature were reduced to very close to $0K$. Some scientists, such as William Kelvin, believed that electrons flowing through a conductor would come to a complete halt as the temperature approached absolute zero. Other scientists, including Onnes, thought that a cold wire's resistance would dissipate. This suggested that there would be a steady decrease in electrical resistance, allowing for better conduction of electricity. At some very low temperature point, scientists expected that there would be a leveling off as the resistance reached some ill-defined minimum value allowing the current to flow with little or no resistance. Onnes passed a current through a very pure mercury wire and measured its resistance as he steadily lowered the temperature. Much to his surprise there was no leveling off of resistance, let alone the stopping of electrons as suggested by Kelvin. At 4.2 K the resistance suddenly vanished. Current was flowing through the mercury wire and nothing was stopping it, the resistance was zero. Fig. (1.2) shows resistance versus temperature in mercury wire as measured by Onnes . According to Onnes, "Mercury has passed into a new state, which on account of its extraordinary electrical properties may be called the "superconductive state". The experiment left no doubt about the disappearance of the resistance of a mercury wire. Onnes called this newly discovered state, Superconductivity. Onnes recognized the importance of his discovery to the scientific community as well as its commercial potential. An electrical conductor with no resistance could carry current any distance with no losses. In one of Onnes experiments he started a current flowing through a loop of lead wire cooled to 4 K. A year later the current was still flowing without significant current loss. Onnes found that the superconductor exhibited what he called persistent currents, electric currents that continued to flow without an electric potential driving them. Onnes was anounced the Nobel Prize in 1913, for his discovery of superconductivity.

By 1933 Walther Meissner and R. Ochsenfeld discovered that superconductors are more than a perfect conductor of electricity, they also have an interesting magnetic property of excluding a magnetic field. A superconductor will not allow a magnetic field to penetrate its interior. It causes currents to flow that generate a magnetic field inside the superconductor that just balances the field that would have otherwise penetrated the material.

This effect, called the Meissner Effect, causes a phenomenon that is a very popular demonstration of superconductivity. Fig.(1.3) is a sketch of magnetic field lines from a magnet

*Original paper: The Discovery of Superconductivity, Comm. Phys. Lab. Univ. Leiden, volume 12, Number 120,1911

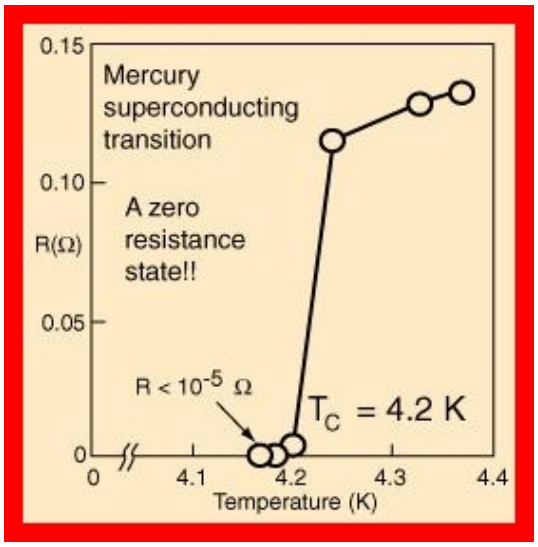

Figure 1.2: Data from Onnes' pioneering works. The plot shows the electric resistance of the mercury vs. temperature, taken from ref.[4]

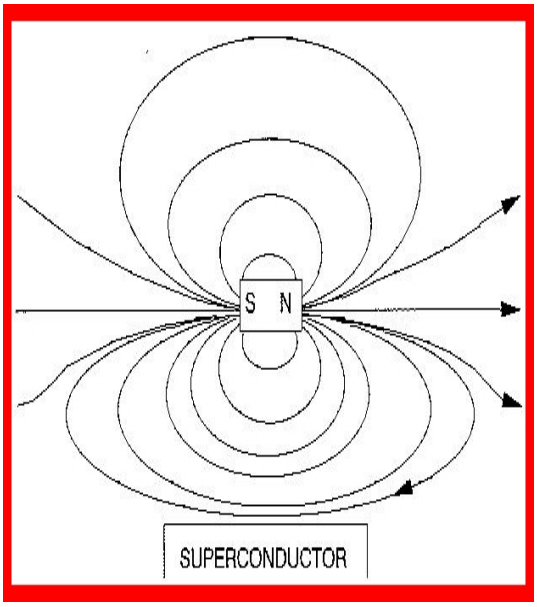

Figure 1.3: The phenomena of diamagnetism in SC, taken from ref.[3; 5]

levitating above a superconductor. The Meissner Effect will occur only if the magnetic field is relatively small. If the magnetic field becomes too great, it penetrates the interior of the metal and the metal loses its superconductivity.

In 1957 scientists began to unlock the mysteries of superconductors. Three American physicists at the University of Illinois, John Bardeen, Leon Cooper, and Robert Schrieffer, developed a model that has since stood as a good mental picture of why superconductors behave as they do. The model is expressed in terms of advanced ideas of the science of quantum mechanics, but the main idea of the model suggests that electrons in a superconductor condense into a quantum ground state and travel together collectively and coherently. In 1972, Bardeen, Cooper, and Schrieffer received the Nobel Prize in Physics for their theory of superconductivity, which is now known as the BCS theory, after the initials of their last names [2].

1.2 What is a superconductor?

Superconducting materials have two fundamental properties:

- **No dc-resistivity ($\rho = 0$ for all $T < T_c$)**: Zero resistivity, i.e., infinite conductivity, is observed in a superconductor at all temperatures below the critical temperature T_c , as depicted in Fig.(1.5). However, if the passing current is higher than the critical current j_c , superconductivity disappears.*Why is the resistivity of a superconductor zero?* If a superconducting metal like Al or Hg is cooled below the critical temperature T_c , the gas of repulsive individual electrons that characterizes the normal state transform itself into a different type of fluid, a quantum fluid of highly correlated pairs of electrons. A conduction electron of a given momentum and spin gets weakly coupled with another electron of the opposite momentum and spin. These pairs are called Cooper pairs. The

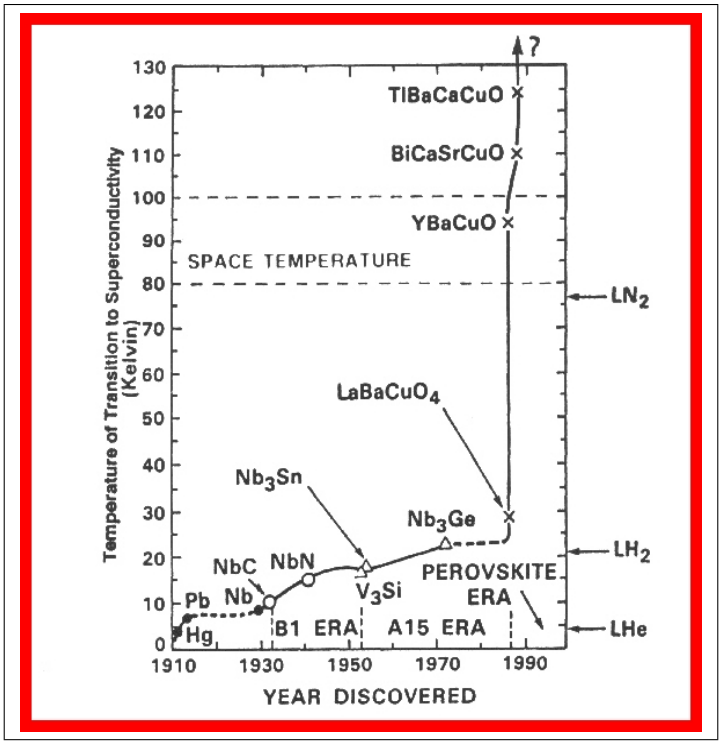

Figure 1.4: The following figure summarizes the history of superconductivity in terms of the discovery or synthesis of materials of increasingly higher transition temperatures, taken from ref. [6]

coupling energy is provided by lattice elastic waves, called *phonons*. The behavior of such a fluid of correlated Cooper pairs is different from the normal electron gas. They all move in a single coherent motion. A local perturbation, like an impurity, which in the normal state would scatter conduction electrons (and cause resistivity), cannot do so in the superconducting state without immediately affecting the Cooper pairs that participate in the collective superconducting state. Once this collective, highly coordinated, state of coherent super-electrons (Cooper pairs) is set into motion (like the supercurrent induced around the loop), its flow is without any dissipation. There is no scattering of individual pairs of the coherent fluid, and therefore no resistivity.

- **No magnetic induction ($B = 0$ inside the superconductor)**: In magnetic fields lower the critical field B_c the magnetic inductance becomes zero inside the superconductor when it is cooled below T_c. The magnetic flux is expelled from the interior of the superconductor (see Fig.(1.6)). This effect is called the Meissner-Ochsenfeld effect after its discoverers. To test whatever a material is superconducting both properties $\rho = 0$ and $B = 0$ must be present simultaneously [7].

1.2.1 Normal metal vs. superconductor

In this section a discussion is presented about the origin of electrical resistivity in the normal metal and contrast it with the absence of resistivity in the superconductor.

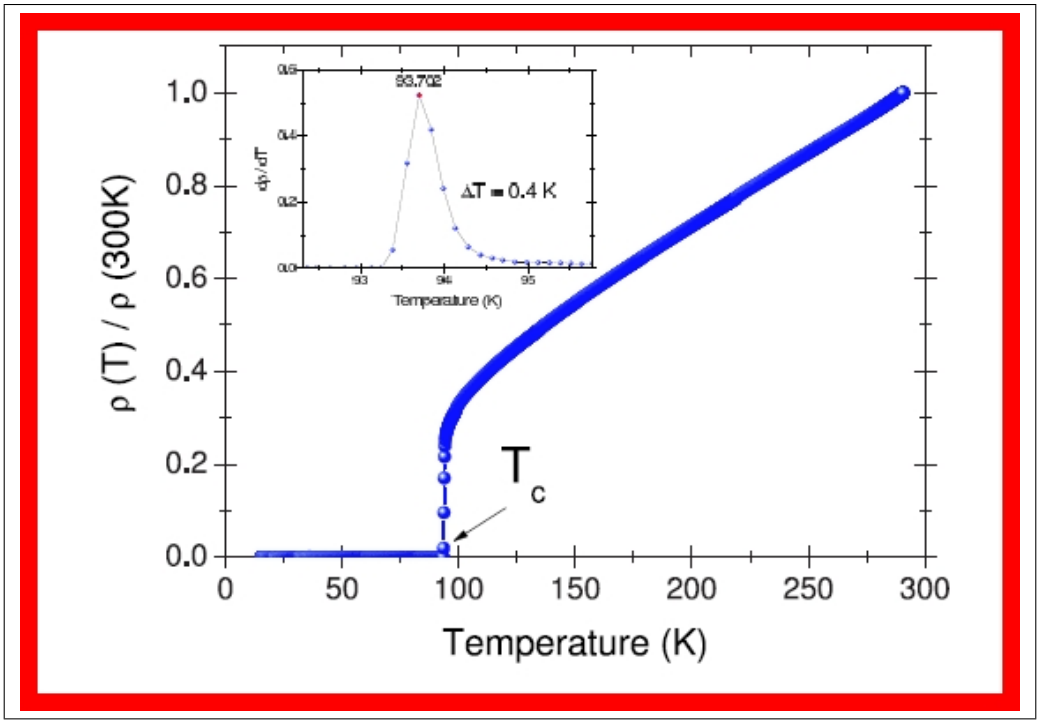

Figure 1.5: Temperature dependence of the resistivity of a thin film of the high-T_c superconductor $YBa_2Cu_3O_{7-\delta}$.

1.2.1.1 Description of the normal state

A normal metal consists of a regular crystalline lattice of positively charged ions and a gas of free, non-interacting conduction electrons that fill the space between the ions. If there is typically one electron per ion, this means 10^{23} electrons/cm^3. As the electrons are of opposite charge as the ions, the total charge is balanced and at equilibrium, the model metal is electrically neutral. If we apply an electric field as an external perturbation to the gas of free electrons within the metal, the external force will accelerate the electrons and create a current flow of free electrons. As the ions are arranged in perfectly regular array, they do not scatter conduction electrons at $T = 0$ [†]. The scattering of electrons at $T = 0$ is actually caused by deviations from the ideal periodic potential of the lattice, i.e., by impurities, imperfections in periodicity like dislocations. Since every real metal contains some imperfections and impurities, one observes some finite resistivity at very low temperatures. This resistivity, extrapolated to $T = 0$, is called residual resistivity, ρ_i. As we increase the temperature, the electrons also get scattered by thermal vibrations of the lattice (called phonons) so the resistivity rises with temperature. This contribution is called phonon resistivity, ρ_{ph}. Therefore the temperature dependance of resistivity of a good metal can be described as : $\rho(T) = \rho_i + \rho_{ph}$. This is empirical Matthiessens rule and provides a basis for understanding the resistivity of metal at low temperature. In order to derive a simple expression for the residual resistivity of the metal, first some characteristic quantities of the normal state should be considered. At $T = 0$ the maximum kinetic energy of an electron inside the metal is called Fermi energy (E_F). It is related to the number of carriers per unit volume,

[†]If the crystal was perfect, at $T = 0$, the electron waves would propagate without scattering and there would be no resistivity, i.e., conductivity of an ideal crystal at $T = 0$ should be infinite.

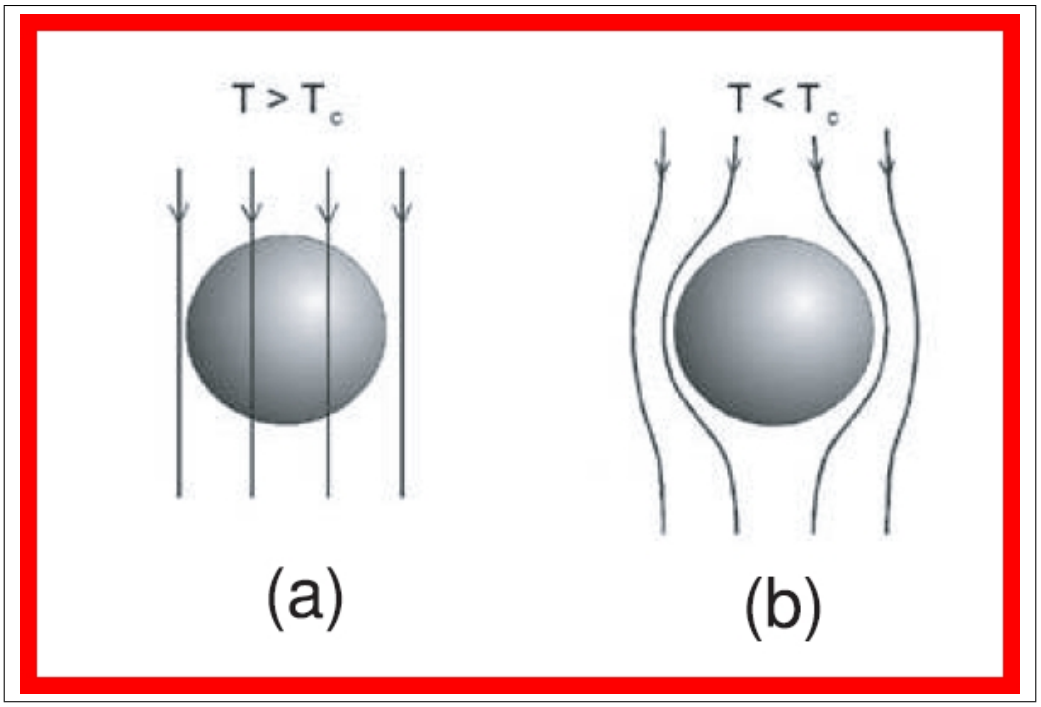

Figure 1.6: Expulsion of a weak external magnetic field from the interior of the superconducting material.

n, by the simple relation: $E_F = \frac{\hbar}{2m}(2\pi^2 n)$, where $\hbar$ is the Planck constant and m is the mass of the electron. The Fermi energy of a typical metal is of the order of electron volts (see Table (1.1)). Conduction electrons of maximum energy, E_F, propagate with the Fermi velocity v_F

Material	n $[10^{23} cm^{-3}]$	v_F $[10^6 ms^{-1}]$	l [nm]	$\rho(100K)$ $[\mu\Omega cm]$
Al	180	2	130	0.3
Nb	56	1.4	29	3
$La_{1.85}Sr_{0.15}CuO_4$	5	0.1	~ 5	~ 100
$YBa_2Cu_3O_{7-\delta}$	7	0.1	~ 10	~ 60

Table 1.1: Some characteristic quantities of the normal state of classical and high-T_c superconductor materials.

related to the Fermi momentum P_F by $P_F = mv_F$. We have $E_F = \frac{1}{2}P_F v_F$. We also define the Fermi wave vector, k_F; as in quantum mechanics a wave is always associated with a particle by de-Broglie relation $P_F = \hbar k_F$. The conduction electrons that propagate through the crystal with a characteristic Fermi velocity v_F are scattered by impurities or lattice imperfections. This gives rise to resistivity. Between two scattering events an electron covers on average a characteristic distance l_e, called the electron mean free path. The resistivity ρ_i of a metal, according to the Drude model, is given by

$$\rho_i = \frac{mv_F}{ne^2 l_e} \tag{1.2.1}$$

where e and m represent the charge and mass of the electron. In isotropic metals, the conductivity is equal to the inverse of the resistivity; both quantities are tensors in the

anisotropic case. Eq.(1.2.1) shows that in the normal state of a given metal the resistivity is inversely proportional to the electron mean free path. The shorter the average distance between the scattering events the higher is the resistivity. The introduction of impurities into a metal obviously reduces l_e and increases ρ_i. This can be clearly seen in Table (1.1), in which typical values for ρ and l_e for several superconducting materials are presented.

1.2.1.2 The superconducting state

The electrical dc-resistivity in superconductors is zero for temperatures below the critical temperature T_c . So, one can apply a dc electrical current (supercurrent) without energy dissipation. Let us see what happens in a supercondcting state and what are its characteristic properties compared with the normal state taken Al as an example for classical superconductor material. In the normal state above the critical temperature $(T_c = 1.1K)$ Al is a good conductor and behaves just like an ideal metal or like copper which exhibits no superconducting behavior down to the lowest temperature. Its conduction electrons behave like a gas of nearly free electrons that are scattered by lattice vibrations, lattice imperfections, etc. which contributes to the resistivity. However, when Al is cooled below T_c , its dc-resistance abruptly vanishes, the resistivity is zero. One natural question is, what happens to the scattering of conduction electrons which contributed to the resistivity in the normal state? Why does it disappear? A satisfactory explanation to these questions can be given only within the rather involved quantum mechanical description of the microscopic BCS-theory, which shall be briefly discussed in the present chapter. When Al is cooled below the critical temperature T_c , the gas of the repulsive individual electrons that characterizes the normal state transforms itself into a different type of fluid. A quantum fluid of highly correlated pairs of electrons (in the reciprocal, momentum space, not in a real space). Below T_c a conduction electron of a given momentum and spin gets weakly coupled with another electron of exactly the opposite momentum and spin. These pairs are called Cooper pairs. The glue is provided by the elastic waves of the lattice, called phonons. One can visualize this attraction by a real-space picture. As the lattice consists of positive ions, the moving electron creates a lattice distortion. Due to the heavy mass of lattice ions, this positively charged distortion relaxes slowly and is therefore able to attract another electron. The distance between the two electrons of the Cooper pair, called the coherence length, ξ, is large in classical superconductor materials. It has a value $\xi = 1600$ nm in pure Al, $= 38$ nm in pure Nb, for example. The coherence length ξ is very small in high-T_c superconductors, it has a value of $\xi_{ab} \approx 16$ nm, and $\xi_c \approx 0.3$ nm in $La_{1.85}Sr_{0.15}CuO_4$ and $YBa_2Cu_3O_{7-\delta}$. So while the partners in the Cooper pair are far apart, the other nearest electrons (belonging to other Cooper pairs of the collective state) are only a few nanometer away. The behavior of such a fluid of correlated Cooper pairs is different from the normal electron gas. The electrons which form the pair have opposite momenta (and opposite spins), so the net momentum of the pair is zero.

1.2.1.3 Superconducting state and wave function

The Cooper pair has twice the charge of a free electron, $q = 2e$. The electrons are fermions and obey the Fermi-Dirac statistics and the Pauli exclusion principle which allows only one electron in a given quantum state. Cooper pairs are quasi-bosons, obey the Bose-Einstein statistics and are allowed to be all in the same state. In contrast to the normal metal in which each electron has its own wave function, in a superconductor, *all Cooper pairs are described*

by the single wavefunction

$$\psi(r) = \sqrt{n_s(r)}e^{i\varphi(r)} \tag{1.2.2}$$

where $n_s(r)$ can be considered as the number of superconducting electrons (Cooper pairs), $\psi(r)\psi^*(r) = n_s(r)$ and $\varphi(r)$ is a spatially varying phase. In optics, a beam of photons, being all in the same state, i.e., traveling with the same velocity, can be described by a plane wave, $exp(ikr - iwt)$ and the gradient of the phase is related to the momentum of the particle by the de-Broglie relation, $P = \hbar k$, or $v = \frac{\hbar}{m}\nabla\varphi$. As all Cooper pairs are in the same state, we have an analogous situation and the gradient of the phase becomes a macroscopic quantity, a quantity proportional to the current flowing in the superconductor [7].

1.3 High-temperature superconductor

The term high-temperature superconductor was initially employed to designate the new family of cuprate-perovskite ceramic materials (Most prominent materials in the high-T_c range are the so-called cuprates, i.e., YBCO (Yttrium-Barium-Copper-Oxide) and related substances [8]) discovered by J.G. Bednorz and K.A. Müller in 1986. These materials are characterized by presenting superconductivity at a higher temperature than conventional superconductors (which require temperatures a few degrees above absolute zero), and by other unconventional features [8], Comparison of conventional superconductors with HTS [9] is given in table (1.2). So-called high-temperature superconductors are generally considered to be those that demonstrate superconductivity at or above the temperature of liquid nitrogen, or -196 degrees C [‡].

Recently, other unconventional superconductors have been discovered. Some of them also have unusually high values of the critical temperature T_c see table (1.3), and hence they are sometimes also called high-temperature superconductors, although the record is still held by a cuprate perovskite material ($T_c = 138K$, that is $-135C$). Nevertheless it is widely believed that if room temperature superconductivity is ever achieved it will be in a different family of materials [10].

The story is as the following: In 1986 two scientists working for IBM in Switzerland, Georg Bednorz and Alex Müller, found that certain ceramic materials that normally are electrical insulators become superconducting at low temperatures. The materials they first experimented with were made from copper oxide, lanthanum, and barium. The greatest surprise of all was the temperature at which these materials became superconducting, 30 K (-243^{0}C), which was higher than for any metallic superconductor. The importance of this discovery can be judged by the fact that Bednorz and Müller were awarded the Nobel Prize in physics just a year later [11].

Müller had decided to study oxide ceramics to see if they could become superconductive. The idea that ceramics could become superconductive was rather strange considering that ceramics are usually not very good conductors of electricity. Müller was interested in a group of ceramics called pervoskites. This group of ceramics were a compound of oxygen and other metals. Many scientist believed that oxides could not be superconductors. The reason he

[‡]Despite its name, high-temperature superconductivity still occurs at cryogenic temperatures. The main difference from low-temperature superconductivity is usually that 'high-T_c' superconductors can use liquid nitrogen (at 77 K) as a coolant while low-temperature superconductors always need liquid helium (4.2 K) temperatures and below [8]

	Conventional	High T_c
Resistivity	$\rho \sim T^2$	$\rho \sim T$
Quasiparticle lifetime,$1/\tau(T,\omega)$	$aT^2 + b\omega^2$	$aT + b\omega$
Spin excitation spectrum	Flat	Peaked at $Q_i \sim (\pi/a, \pi/a)$
Maximum strength of spin excitations	$\sim$1 state$/eV$	$20 - 300$ states$/eV$
Characteristic spin excitation energy	$\sim E_f$	$\omega_{ef} \sim T << E_f$
AF correlations	None	strong, with $\xi_{AF} \geq 2a$
Uniform susceptibility, $\chi_0(T)$	Flat	varies with temperature, possesses a maximum at $T_0 > T_c$ for magnetic underdoped systems

Table 1.2: Comparison of conventional superconductors with HTS [9].

researched oxide ceramics was because the lab he worked in had researched oxides for quite a while, and scientists at the University of Caen in France had found traces that a ceramic compound of copper, oxygen, lanthanum, and barium had electrical conduction.

It took many years of work and experiments for Bednorz and Mller to find a metallic oxide superconductor. This ceramic superconductor was so odd that they kept their discovery a secret for a while. They published their finding in the September 1986 issue of the German journal Zeitschrift fr Physik[§]. It took some time for people to pay attention to the news.

The University of Tokyo in Japan was the first to take Bednorz and Müllers discovery seriously; they repeated and confirmed the results. Other groups, such as AT&T and Bell Labs, were soon doing the same. They were all in a race to produce a higher temperature superconductor.

The 1-2-3 Superconductor: At the University of Houston in Texas Paul C. W. Chu lead a group to find a higher temperature superconductor than Bednorz and Müllers superconductor. On February 16, 1987 Paul Chu, supported by the National Science Foundation, created a superconductor with a record high critical temperature of 93K. The compound was made up of oxygen, barium, copper, and yttrium. This was named the 1-2-3 superconductor for its relative atomic proportions of yttrium, barium, and copper.

[§]original paper: . G. Bednorz and K. A. Müller (1986). "Possible highT_c superconductivity in the Ba-La-Cu-O system". Z. Physik, B 64: 189-193.

Chu was curious of what would happen if an oxide superconductor was put under high pressure. He discovered that the higher the pressure, the higher the critical temperature.

In 1988 Paul Chu made a compound of bismuth, strontium, calcium, oxygen, and aluminum which had a critical temperature of 120K [12].

In 2001 Jun Akimitsu of Aoyama Gakuin University in Tokyo and coworkers discovered that the common, simple compound magnesium diboride is a superconductor at temperatures as high as 39 K (-234^{0}C), which is considerably higher than the ordinary BCS superconductors, but not quite as high as the ceramic high-temperature superconductors. So far, the record critical temperature is from mercury-thallium-barium-calcium-copper-oxygen that becomes superconducting at 138 K (-135^{o}C) [11].

Many scientist believe that an entire periodic table will have to be put together to make a room temperature superconductor [12], see also [13].

1.3.1 $\mathbf{YBa_2Cu_3O_{7-\delta}}$

In this section first the most important properties of the $YBa_2Cu_3O_{7-\delta}$ superconductor will be discussed, initially from a materials and subsequently from a physics point of view.

i **High-T_c oxides are highly anisotropic, layered structures**: Except for some materials (like $Ba_{1-x}K_xBiO_3$), most high-T_c superconducting oxides are cuprate compounds. One of their characteristics is the presence of CuO_2 layers which dominate most of the properties. A look at the schematic structure of $YBa_2Cu_3O_{7-\delta}$ presented in Fig. 1.7, shows that it is highly anisotropic. The unit cell is developed from that of a tetragonal perovskite tripled along the c-axis and it consists of a sequence of copper-oxygen layers. The dimensions of the unit cell are approximately 1.2 nm and 0.4 nm in the c and a or b-axis directions respectively. The fact that the unit cell consists of layers of copper oxides will be one of great importance for understanding the physical properties.

ii **Metallic oxides**: The second important characteristic of these oxides is their metallic behavior, as shown in Fig.(1.5). While most oxides are insulating materials, HTSC oxides exhibit a metal-like conductivity. The room temperature conductivities in a- or b-axis direction of the cuprate crystal are of the same order of magnitude as the conductivities of some disordered metallic alloys. Only the conductivity perpendicular to CuO_2-planes is much smaller.

iii **Ceramic materials**: The original materials, $La_{1.85}Sr_{0.15}CuO_4$ and $YBa_2Cu_3O_{7-\delta}$, were synthesized as ceramic pellets. One mixes the correct ratio of constituent oxides, grinds and sinters them, makes a pellet, and following a calcining procedure at annealing temperature of $T_a \approx 950^0C$ and cools it down in oxygen. As typical ceramics, high-T_c superconducting oxides also contain grains, grain boundaries, twins, and other imperfections. Even some of the best thin films may consist of grains a few microns in diameter; all these are mostly detrimental to high critical current densities that are required for applications. It is important to emphasize that even the best single crystals of HTSC oxides often contain various defects and imperfections like oxygen vacancies, twins and impurities. These imperfections are not only very relevant to their physical properties but possibly even essential for their basic thermodynamic stability. It may

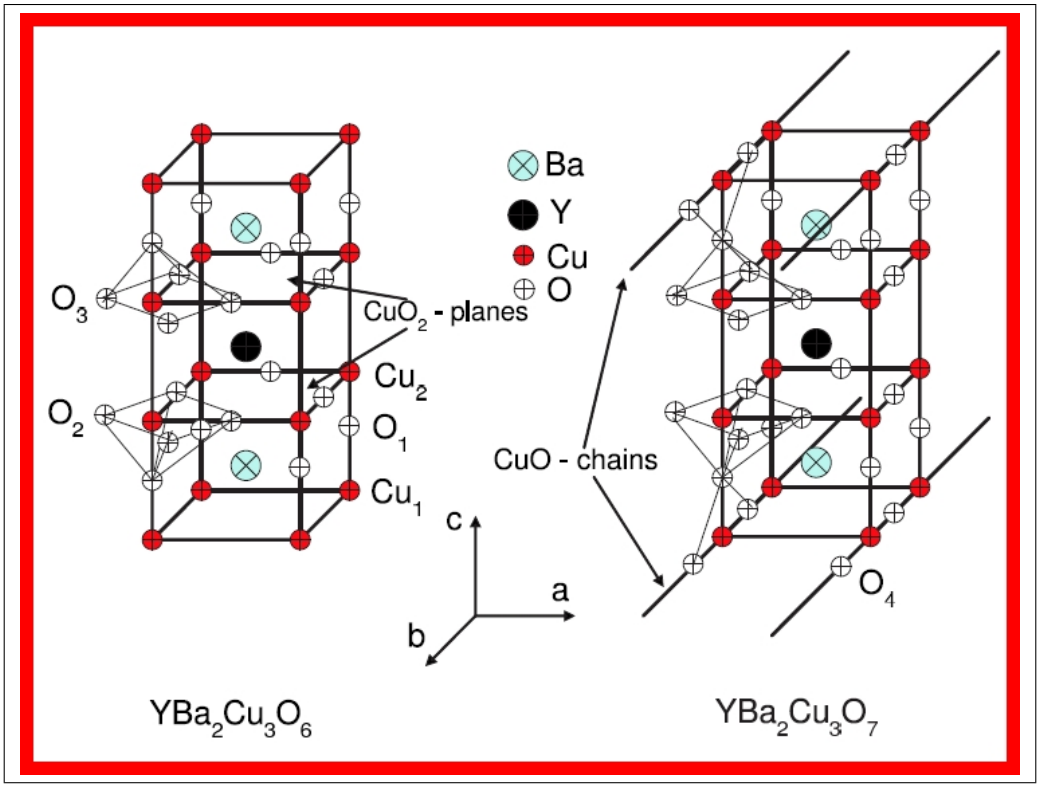

Figure 1.7: Schematic diagrams of $YBa_2Cu_3O_6$ (left) an insulator and $YBa_2Cu_3O_7$ (right) a superconducting oxide.

well turn out that various imperfections found in HTSC crystals are intrinsic to these materials. In general, it is important to understand that the materials science of HTSC oxides is a non-trivial pursuit and that the understanding of phase diagrams (especially around the pseudogap temperature T*), crystal chemistry, preparation and stability of these oxides is still not completely understood [7].

1.3.1.1 The phase diagram of $YBa_2Cu_3O_{7-\delta}$

The schematic structure of $YBa_2Cu_3O_6$, given in Fig.(1.7), represents an insulator. It has to be doped to gradually become a hole-doped metallic conductor and a superconductor below some critical temperature, as shown in Fig.(1.5). The doping is achieved by adding additional oxygen which forms CuO chains. These oxygen ions attract electrons from the CuO_2-planes which therefore become metallic (see Fig.(1.8)). Note, that the correct formula for YBCO material is $YBa_2Cu_3O_{6+x}$, where x corresponds to partial oxygen content:

* for $0.0 < x < 0.4$, $YBa_2Cu_3O_{6+x}$ is an insulator.

* for $0.4 < x < 1.0$, $YBa_2Cu_3O_{6+x}$ is a superconductor.

The schematic phase diagram of a cuprate high-T_c superconductor is given in Fig.(1.8), as a function of temperature and x the density of doped holes per CuO_2-plane. The solid lines represent phase transitions into the antiferromagnetic (AFM) and superconducting (SC) states. The dashed line marks the opening of a pseudogap (PG) around the temperature T*. The latter crossover is not sharply defined and there is still a debate on its position and the

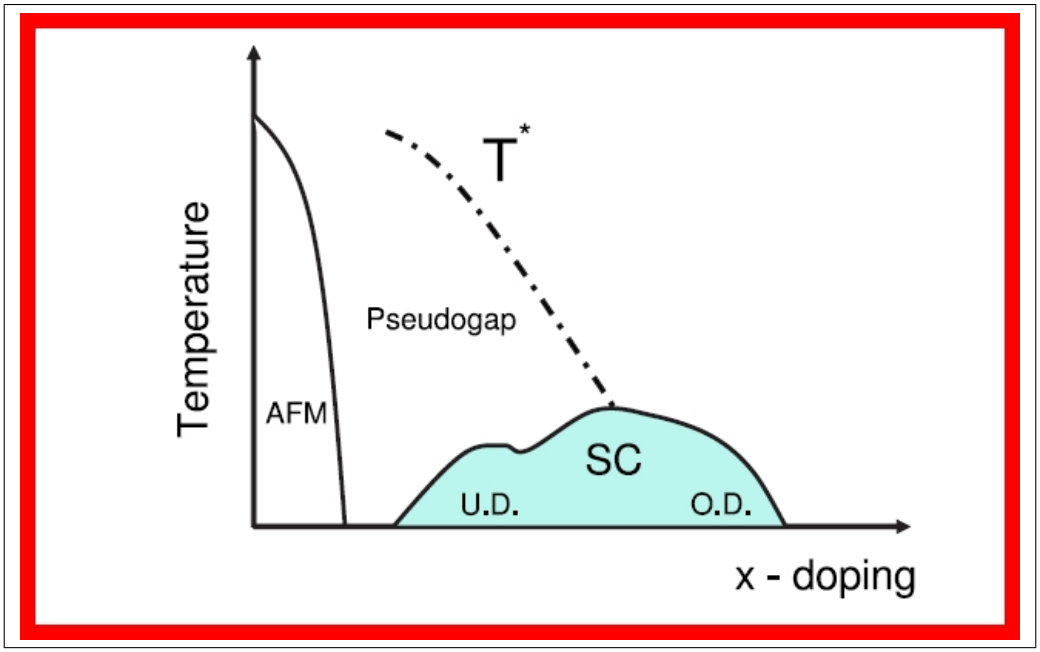

Figure 1.8: Schematic phase diagram of YBCO as a function of temperature and x the density of doped holes per CuO_2-plane. The solid lines represent phase transitions into the antiferromagnetic (AFM) and superconducting (SC) states. The dashed line marks the opening of a pseudogap (PG) around the temperature T^*.

physics behind.

The parent state of each family of HTSC is an antiferromagnetic Mott-insulator with one hole (and spin 1/2) per CuO_2-plane. These insulators are transformed into superconductors by introducing a concentration, x, of doped holes into the CuO_2-planes. As a function of increasing x, the antiferromagnetic transition temperature is rapidly suppressed to zero, then the superconducting transition temperature rises from zero to a maximum and then drops down again (see Fig.(1.8)). Where T_c is an increasing function of x, the materials are underdoped (U.D.). They are optimally doped where T_c reaches its maximum, and they are overdoped (O.D.) for larger x. In the underdoped regime there are a variety of crossover phenomena observed at temperatures above T_c . These phenomena are associated with the opening of a pseudogap. There are various families of high temperature superconductors, all of them have the same nearly square shaped copper-oxide planes, but different structures in the regions between the planes. One characteristic that seems to have a fairly direct connection with T_c is the number of copper-oxide planes that are close enough to each other that interplane coupling may be significant; T_c seems generally to increase with the number of planes within a homologous series, at least as one progresses from single layer to bilayers, to trilayers materials, see Table (1.3). The following comments concerning the phase diagram of YBCO hold in a similar way also for the all HTSC families listed in Table (1.3):

- **Oxygen content**: The oxygen content can be changed reversibly from 6.0 to 7.0 simply by pumping oxygen in/out of the parallel chains of CuO running along the b-axis of Fig.(1.7). YBa2Cu3O6 is an insulating antiferromagnet (I-AFM). Increasing the oxygen from YBCO6:4 makes the crystal metallic, nonmagnetic and superconducting, $T_c = 0+$ for $YBCO_{6.64}$.

Compound	$T_c(K)$
$La_{2-x}M_xCuO_{4-y}$	38
M=Ba, Sr, Ca	
$x \sim 0.15, y$ small	
$Nd_{2-x}Ce_xCuO_{4-y}$ (electron doped)	30
$Ba_{1-x}K_xBiO_3$ (isotropic, cubic)	30
$Pb_2Sr_2Y_{1-x}Ca_xCu_3O_8$	70
$R_1Ba_2Cu-2+mO_{6+m}$	
R: Y, La, Nd, Sm, Eu, Ho, Er, Tm, Lu	
$m = 1(123)$	93
$m = 1.5(247)$	95
$m = 2(124)$	82
$Bi_2Sr_2Ca_{n-1}Cu_nO_{2n+4}$	
$n = 1(2201)$	10
$n = 2(2212)$	85
$n = 3(2223)$	110
$Tl_2Ba_2Ca_{n-1}Cu_nO_{2n+4}$	
$n = 1(2201)$	85
$n = 2(2212)$	105
$n = 3(2223)$	125
$HgBa_2Ca_{n-1}Cu_nO_{2n+2+\delta}$	
$n = 1(1201)$	95
$n = 2(1212)$	125
$n = 3(1223)$	133
$n = 4(1234)$	127
$n = 5(1245)$	110
$n = 6(1256)$	91
$n = 7(1267)$	85

Table 1.3: Critical temperatures of some HTSC compound.

- **Higher T_c** : The order of magnitude of T_c of YBCO or all HTSC oxides [listed in Table (1.3)] are much higher compared to T_c of the classical superconductor materials T_c for Nb_3Ge is only 23 K, the critical temperature corresponds to the binding energy k_BT_c needed to hold Cooper pairs together in the superconducting state. The fact that $T_c \gg 100K$, i.e., $2\Delta = 60meV$, as compared with $< 1meV$ in conventional superconductors, surprise theorists interested in the microscopic mechanism of high-T_c superconductivity. The critical temperatures of the most extensively studied high-T_c oxide superconductors (HTSC) are shown in Table (1.3).

- **Short coherence length** ξ: Very short coherence length,$\xi = 1.0$nm. If we recall the BCS-derived formula, $\xi \sim v_F k_B T_c$, we can immediately expect somewhat shorter coherence lengths in HTSC oxides due to their higher T_cs. However, due to the low density of carriers in HTSC oxides? The Fermi velocity in these ionic metals is also lower than in normal metals. This results in a very short coherence length, $\xi = 1.0$nm, which is comparable to the size of the unit cell, and it has profound consequences for the physics of HTSC oxides. Actually, the coherence length is different for different crystallographic directions and it was experimentally found in $YBa_2Cu_3O_{7-\delta}$ that ξ_{ab} and ξ_c are 1.5 nm

and 0.4 nm, respectively. The ξ_c is roughly equal to the interlayer distance and shorter than the corresponding unit cell length, which clearly poses some conceptual problems. As we shall see, these remarkably short coherence lengths dominate all material-related properties and cause a rather complex mixed state. Short coherence length also implies that HTSC oxides are type-II superconductors with very high upper critical fields B_{c2}[7].

1.4 The pseudogap temperature T^*

The pseudogap is one of the most prominent, and most discussed features of the cuprate superconductors. It is widely observed in underdoped cuprates and, to various extents, in optimally and even slightly overdoped materials or below Tc in case of electron doped cuprates. Among the experimental probes which are used to locate the pseudogap temperature in different materials are:

1) **Angle-resolved photoelectron spectroscopy (ARPES) and c-axis tunneling**: There is a suppression of the low energy single particle spectral weight at temperatures above T_c as detected, primarily, in c-axis tunneling and ARPES experiments. The scale of energies and the momentum dependence of this suppression are very reminiscent of the d-wave superconducting gap observed in the same materials at temperatures well below T_c. This is highly suggestive of an identification between the pseudogap and some form of local superconducting pairing.

2) **Cu-NMR**: There is a suppression of low energy spin fluctuations as detected primarily in Cu-NMR. In some cases, two rather different temperature scales are deduced from these experiments. An upper crossover temperature, at which a peak occurs in the real part of the uniform spin susceptibility (i.e. the Knight shift), and a lower crossover temperature.

3) **Resistivity**: There is a significant deviation of the resistivity in the ab-plane from the linear temperature dependence which is universally observed at high temperatures. A pseudogap temperature is then identified as the point below which $d\rho/dT$ deviates significantly from its high temperature value. In some cases, a similar temperature scale can be inferred from a scaling analysis of the Hall resistance, as well. The pseudogap also appears in c-axis resistivity, although in a somewhat different manner. In this direction, the pseudogap results in a strong increase in resistivity, reminiscent of the behavior of a narrow gap semiconductor. If we imagine that the c-axis transport is dominated by tunneling events between neighboring planes, it is reasonable that a bulk measurement of ρ_c will identify the pseudogap in the same way as the c-axis tunneling does.

4) **Specific heat**: There is a suppression of the expected electronic specific heat. Above the pseudogap scale, the specific heat is generally found to be linear in temperature, $CV = \gamma T$, but below the pseudogap temperature, $CV = T$ begins to decrease with decreasing temperature. Interestingly, since the value of above the pseudogap temperature appears to be roughly doping independent.

5) **Infrared conductivity**: There is an anomalous motion of infrared spectral weight to low energies. The pseudogap is most clearly identified by plotting the frequency dependent

scattering rate, defined either as

$$\frac{1}{\tau(\omega)} = \frac{\omega_p^2}{4\pi} Re \frac{1}{\sigma(\omega)} \tag{1.4.1}$$

where ω_P is the plasma frequency; the pseudogap is rather harder to pick out from the in-plane conductivity σ_{ab} itself. At large ω_P , one generally sees $\frac{1}{\tau(\omega)}$ where $A \geq 1$ in underdoped materials and ≈ 1 in optimally doped ones. And it then drops to much smaller values, $\frac{1}{\tau} \ll \omega$ below a characteristic pseudogap frequency. While in optimally doped materials, this manifestation of a pseudogap is only observed at temperatures less than T_c , in underdoped materials persist well above T_c , and indeed to be not strongly temperature dependent [7].

1.4.1 Theories of the pseudogap

The experimental evidence of the pseudogap does not yet provide a single view, neither do the available theoretical models. A few selected models are described below. Several of the models described below involve preformed pairs at $T*$ without phase coherence. The theoretical models seem to explain the pseudogap are summarized in the following:

Spincharge separation: One scenario which has received considerable attention involves spincharge separation. This idea was first proposed by Anderson in his as the resonating valence bond (RVB) theory. Nagaosa and Lee produced a GinzburgLandau theory of the spincharge separated system calculating various transport properties in the pseudogap state. Spincharge separation creates holons with zero spin and spinons which are zero charge, spin$1/2$ fermions. The spinons pair to form a gap in the spin excitations, identified as the pseudogap. The holons Bosecondense at T_c to form the superconducting state. At present it is believed that even though it is the holons which Bosecondense, gauge field fluctuations lead to a strong coupling between the spinons and holons. A gauge theory of the normal state, including the pseudogap, has been developed by Lee and Nagaosa. Experimental results suggest that T^* is related to the occurrence of a spingap in the high-T_c materials.

Phase fluctuations: It is proposed that superconductors with a low carrier density are characterized by a relatively small phase stiffness and thus, the poor screening implies a significant role of phasefluctuations. Emery and Kivelson have developed a preformed pair model of the pseudogap based on microstripes. Phase separation takes place on a microscopic scale generating dynamical charged stripes separated by insulating antiferromagnetic (AFM) stripes. These microstripes form at the upper crossover temperature $T \gg T^*$. Above this temperature the charge is uniformly distributed. Below T^* charge is confined to the metallic stripes forming a 1D electron gas (1DEG). Spin and charge are separated as spin resides in the AFM stripes. As the temperature is lowered, AFM correlations build up. At the lower crossover temperature T^* pairing behavior emerges. Pairing is a result of a spin gap in the AFM stripes. This is manifested in the 1DEG via pair hopping between the 1DEG and AFM stripes. Emery and Kivelson describe this as a magnetic proximity effect. At this point there are only 1D superconducting correlations. The pseudogap is associated with this spin gap. At T_c Josephson coupling between the metallic stripes becomes large enough to yield global phase coherence. Note that the pairing correlations below T^* are not giving rise to real space pairing; the pairing correlations are dynamical. The phasefluctuation scenario explains quite natural the strongly enhanced Nernst signal above the critical transition temperature T_c in the underdoped HTSC materials.

Interlayer exchange coupling: Millis and Monien proposed that the pseudogap in bilayer compounds was due to interlayer exchange coupling. Further work have produced a model with interlayer pairing of holons producing a spin pseudogap. The authors claim that the pseudogap crossover temperature $T*$ for single layer materials, namely La1:85Sr0:15CuO4 , is just slightly above T_c. Interlayer coupling enhances T^* to temperatures well above T_c . Recent data on other single layer compounds throws this scenario into to be uncertain. The single layer mercury compound shows a crossover temperature well above T_c. Spin-polarized quasiparticle injection (SPQI) is a sensitive tool for detecting the opening of a spin-gap, as proposed by Si. A major point of this thesis is the influence of SPQI on the normal state resistivity of YBCO around the pseudogap temperature T^*. It is proposed that the experimental data allow to distinguish between the suggested models of spin-charge separation and phase fluctuations[7], see ref. [14; 15] for great details about pseudogap.

1.5 Superconductors that work at room temperature:

TINY tubes of carbon may conduct electricity without any resistance, at temperatures stretching up past the boiling point of water. The tubes would be the first superconductors to work at room temperature. Guo-meng Zhao and Yong Sheng Wang of the University of Houston in Texas found subtle signs of superconductivity. It wasn't zero resistance, but it's the closest anyone's got so far. "I think all the experimental results are consistent with superconductivity," Zhao says. "But I cannot rule out other explanations." At the moment no superconductor will work above about 130 kelvin (-143 C). But if a material could carry current with no resistance at room temperature, no energy would be lost as heat, meaning faster, lower-power electronics. And electricity could be carried long distances with 100 per cent efficiency.

Zhao and Wang studied the effects of magnetic fields on hollow fibres of carbon known as "multiwall carbon nanotubes". Each nanotube is typically a millionth of a metre long, several billionths of a metre in diameter and with walls a few atoms thick. The nanotubes cling together in oblong bundles about a millimetre in length. The researchers did not see zero resistance in their bundles. They think this is because the connections between the tiny tubes never become superconducting. But they did see more subtle signs of superconductivity within the tubes themselves. For example, when the researchers put a magnetic field across a bundle at temperatures up to 400 kelvin (127 C), the bundle generated its own weak, opposing magnetic field. Such a reaction can be a sign of superconductivity. And when the team cooled the bundles from even higher temperatures then turned the external field off, they stayed magnetised. A current running around within the tubes could generate this lingering field if there wasn't any resistance to make it fade away.

While each effect could have a more prosaic explanation, they varied in similar ways as the temperature of the bundles changed. The correlation suggests superconductivity was responsible, Zhao and Wang argue in a paper to be published in Philosophical Magazine B. However, their argument doesn't convince Paul Grant, a physicist with the Electric Power Research Institute in Palo Alto, California. "Generally, superconductivity is such a dominating effect that when it occurs it just shouts out at you," Grant says. "It doesn't appear in these indirect ways." Superconductivity theories do not forbid the phenomenon at very high temperatures, says Sasha Alexandrov, a theoretical physicist at Britain's Loughborough

University. A material becomes superconducting when its electrons pair up. Normally such negatively charged particles would repel each other, but in a positively charged crystal structure, vibrations called phonons help them get together. In carbon nanotubes, the frequency of these vibrations is very high, which, in theory at least, means superconductivity at higher temperatures. "The results on the magnetic response are very intriguing, and favour the explanation they present," Alexandrov says "It's certainly possible," agrees David Caplin, head of the Center for High Temperature Superconductivity at Imperial College, London.

To decide whether or not the nanotubes really are superconductors, you need to measure the resistance through a single tube, Alexandrov says. "To be convinced, I'd like to see zero resistance" [16].

1.6 Applications of Superconductors

Soon after Kamerlingh Onnes discovered superconductivity, scientists began dreaming up practical applications for this strange new phenomenon [2; 3]. Applications of superconductivity can be divided into two categories: *large-scale* and *small-scale*.
The large-scale applications generally exploit the loss of electrical resistance.

The small-scale applications are generally electronic applications that often depend upon properties of the material that can only be explained by quantum mechanics. *The small-scale applications* are primarily in electronic sensors and circuit components. Superconductive integrated circuits would be extremely fast and permit very dense packaging because there is no resistive heating. Instrumentation of unparalleled sensitivity can be made from superconductors using properties that can only be explained by quantum physics.

When powerful electromagnets are constructed from normal electrical conductors, large amounts of electrical power are required to continuously make up for heat losses. Superconducting magnets have no such losses and require no power at all once they have been energized [6].

Powerful new superconducting magnets could be made much smaller than a resistive magnet,because the windings could carry large currents with no energy loss. Generators wound with superconductors could generate the same amount of electricity with smaller equipment and less energy. Once the electricity was generated it could be distributed through superconducting wires. Energy could be stored in superconducting coils for long periods of time without significant loss.
The recent discovery of high temperature superconductors brings us a giant step closer to the dream of early scientists. Applications currently being explored are mostly extensions of current technology used with the low temperature superconductors.

Current applications of high temperature superconductors include (Fig.(1.11)); magnetic shielding devices, medical imaging systems, superconducting quantum interference devices (SQUIDS), infrared sensors, analog signal processing devices, and microwave devices. As our understanding of the properties of superconducting material increases, applications such as; power transmission, superconducting magnets in generators, energy storage devices, particle accelerators, levitated vehicle transportation, rotating machinery, and magnetic separators

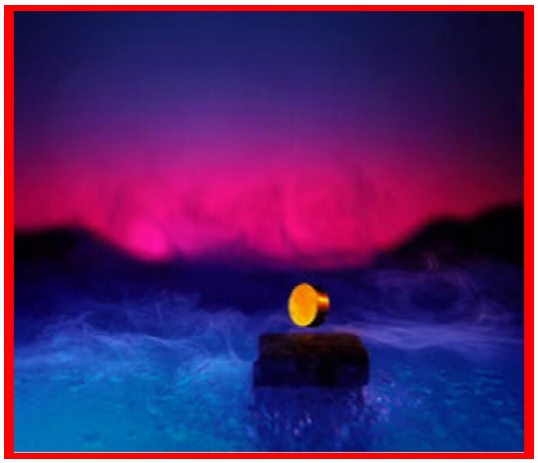

Figure 1.9: A magnet levitating above a "high-temperature" superconductor (100.37 K) with boiling liquid nitrogen underneath demonstrates the Meissner effect, taken from ref. [17]

Figure 1.10: The superconducting Maglev high-speed vehicles have been fitted with aerodynamic brake panels, taken from ref. [18]

will become more practical. The ability of superconductors to conduct electricity with zero resistance can be exploited in the use of electrical transmission lines. Currently, a substantial fraction of electricity is lost as heat through resistance associated with traditional conductors such as copper or aluminum. A large scale shift to superconductivity technology depends on whether wires can be prepared from the brittle ceramics that retain their superconductivity at 77 K while supporting large current densities.

The field of electronics holds great promise for practical applications of superconductors. The miniaturization and increased speed of computer chips are limited by the generation of heat and the charging time of capacitors due to the resistance of the interconnecting metal films. The use of new superconductive films may result in more densely packed chips which could transmit information more rapidly by several orders of magnitude. Superconducting electronics have achieved impressive accomplishments in the field of digital electronics. Logic delays of 13 picoseconds and switching times of 9 picoseconds have been experimentally demonstrated. Through the use of basic Josephson junctions scientists are able to make very sensitive microwave detectors, magnetometers, SQUIDs and very stable voltage sources.

The use of superconductors for transportation has already been established using liquid helium as a refrigerant. Prototype levitated trains have been constructed in Japan by using superconducting magnets, see Figs.(1.9 and 1.10).
Superconducting magnets are already crucial components of several technologies. Magnetic resonance imaging (MRI) is playing an ever increasing role in diagnostic medicine. The intense magnetic fields that are needed for these instruments are a perfect application of superconductors. Similarly, particle accelerators used in high-energy physics studies are very dependant on high-field superconducting magnets. The recent controversy surrounding the continued funding for the Superconducting Super Collider (SSC) illustrates the political ramifications of the applications of new technologies.

Figure 1.11: taken from ref.[19]

New applications of superconductors will increase with critical temperature. Liquid nitrogen based superconductors has provided industry more flexibility to utilize superconductivity as compared to liquid helium superconductors. The possible discovery of room temperature superconductors has the potential to bring superconducting devices into our every-day lives.

High-temperature superconductors are recent innovations from scientific research laboratories. New commercial innovations begin with the existing technological knowledge generated by the research scientist. The work of commercialization centers on the development of new products and the engineering needed to implement the new technology. Superconductivity has had a long history as a specialized field of physics. Through the collaborative efforts of government funded research, independent research groups and commercial industries, applications of new high-temperature superconductors will be in the not so distant future. Time lags however, between new discoveries and practical applications are often great. The discovery of the laser in the early 60's has only recently been appreciated today through applications such as laser surgery, laser optical communication, and compact disc players. The rapid progress in the field of superconductivity leads one to believe that applications of superconductors is limited only by one's imagination and time [2; 3].

1.7 BCS Theory of Superconductivity

The properties of Type I superconductors were modeled successfully by the efforts of John Bardeen, Leon Cooper, and Robert Schrieffer in what is commonly called the BCS theory. A key conceptual element in this theory is the pairing of electrons close to the Fermi level into Cooper pairs through interaction with the crystal lattice (see section 1.2). The electron pairs have a slightly lower energy and leave an energy gap above them on the order of .001 eV which inhibits the kind of collision interactions which lead to ordinary resistivity. For temperatures such that the thermal energy is less than the band gap, the material exhibits zero resistivity [21].

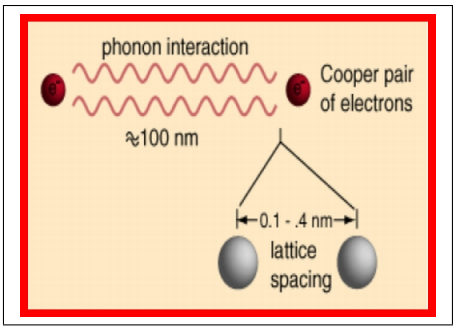

Figure 1.12: Cooper pairs of electrons, taken from ref.[20]

In more detail: BCS theory starts from the assumption that there is some attraction between electrons, which can overcome the Coulomb repulsion. In most materials (in low temperature superconductors), this attraction is brought about indirectly by the coupling of electrons to the crystal lattice (as explained above). However, the results of BCS theory do not depend on the origin of the attractive interaction. Note that the original results of BCS (discussed below) were describing an "s-wave" superconducting state, which is the rule among low-temperature superconductors but is not realized in many "unconventional superconductors", such as the "d-wave" high-temperature superconductors. Extensions of BCS theory exist to describe these other cases, although they are insufficient to completely describe the observed features of high-temperature superconductivity.

BCS were able to give an approximation for the quantum-mechanical state of the system of (attractively interacting) electrons inside the metal. This state is now known as the "BCS state". Whereas in the normal metal electrons move independently, in the BCS state they are bound into "Cooper pairs" by the attractive interaction, fig.(1.7).

BCS have derived several important theoretical predictions that are independent of the details of the interaction (note that the quantitative predictions mentioned below hold only for sufficiently weak attraction between the electrons, which is however fulfilled for many low temperature superconductors - the so-called "weak-coupling case"). These have been confirmed in numerous experiments:

- Since the electrons are bound into Cooper pairs, a finite amount of energy is needed to break these apart into two independent electrons. This means there is an "energy gap" for "single-particle excitation", unlike in the normal metal (where the state of an electron can be changed by adding an arbitrarily small amount of energy). This energy gap is highest at low temperatures but vanishes at the transition temperature when superconductivity ceases to exist. BCS theory correctly predicts the variation of this gap with temperature. It also gives an expression that shows how the gap grows with the strength of the attractive interaction and the (normal phase) "density of states" at the Fermi energy. Furthermore, it describes how the "density of states" is changed on entering the superconducting state, where there are no electronic states any more at the Fermi energy. The energy gap is most directly observed in tunneling experiments and in reflection of microwaves from the superconductor.

- The ratio between the value of the energy gap at zero temperature and the value of the superconducting transition temperature (expressed in energy units) takes the universal value

of 3.5, independent of material.

- Due to the energy gap, the specific heat of the superconductor is suppressed strongly (exponentially) at low temperatures, there being no thermal excitations left. However, before reaching the transition temperature, the specific heat of the superconductor becomes even higher than that of the normal conductor (measured immediately above the transition) and the ratio of these two values is found to be universally given by 2.5.

BCS theory correctly predicts the Meissner effect, i.e. the expulsion of a magnetic field from the superconductor and the variation of the penetration depth (the extent of the screening currents flowing below the metal's surface) with temperature. It also describes the variation of the critical magnetic field (above which the superconductor can no longer expel the field but becomes normalconducting) with temperature.

BCS theory relates the value of the critical field at zero temperature to the value of the transition temperature and the density of states at the Fermi energy [20]¶.

1.8 Ginzburg-Landau (GL)Theory

‖ In physics, Ginzburg-Landau theory is a mathematical theory used to model superconductivity. It does not purport to explain the microscopic mechanisms giving rise to superconductivity. Instead, it examines the macroscopic properties of a superconductor with the aid of general thermodynamic arguments[22].

In 1959, Gor'kov was able to show that the GL theory was, in fact, a limiting form of the microscopic theory of BCS (suitably generalized to deal with spatially varying situations), valid near T_c, in which ψ is directly proportional to the gap parameter Δ. More physically, ψ can be thought of as the wavefunction of the center-of-mass motion of the Cooper pairs. The GL theory is now universally accepted as a masterstroke of physical intuition which embodies in a simple way the macroscopic quantum-mechanical nature of the superconducting state that is crucial for understanding its unique electrodynamic[23].

Based on Landau's previously-established theory of second-order phase transitions, Landau and Ginzburg argued that the free energy F of a superconductor near the superconducting transition can be expressed in terms of a complex order parameter ψ, which describes how deep into the superconducting phase the system is. The free energy has the form

$$F = F_n + \alpha|\psi|^2 + \frac{\beta}{2}|\psi|^4 + \frac{1}{2m}|(-i\hbar\nabla - 2e\mathbf{A})\psi|^2 + \frac{|\mathbf{H}|^2}{2\mu_0}$$

where F_n is the free energy in the normal phase, α and β are phenomenological parameters, $\mathbf{A}$ is the electromagnetic vector potential, and $\mathbf{H}$ is the magnetic field. By minimizing the free energy with respect to fluctuations in the order parameter and the vector potential, one

¶Original reference: J. Bardeen, L. N. Cooper, and J. R. Schrieffer, "Theory of Superconductivity", Phys. Rev. 108 (5), 1175 (1957).

‖Original reference: V.L. Ginzburg and L.D. Landau, Zh. Eksp. Teor. Fiz. 20, 1064 (1950)

arrives at the **Ginzburg-Landau equations**

$$\alpha\psi + \beta|\psi|^2\psi + \frac{1}{2m}(-i\hbar\nabla - 2e\mathbf{A})^2\psi = 0$$
$$\mathbf{J} = \frac{2e}{m}(\psi^\star(-i\hbar\nabla - 2e\mathbf{A})\psi)$$

where **J** denotes the electrical current. The first equation, which bears interesting similarities to the time-independent Schrdinger equation, determines the order parameter ψ based on the applied magnetic field. The second equation then provides the superconducting current.

The Ginzburg-Landau equations produce many interesting and valid results. Perhaps the most important of these is its prediction of the existence of two characteristic lengths in a superconductor. The first is a **coherence length** ξ, given by

$$\xi = \sqrt{\frac{\hbar^2}{2m|\alpha|}}$$

which describes the size of thermodynamic fluctuations in the superconducting phase. The second is the **penetration depth** λ, given by

$$\lambda = \sqrt{\frac{m}{4\mu_0 e^2 \psi_0^2}}$$

where ψ_0 is the equilibrium value of the order parameter in the absence of an electromagnetic field. The penetration depth describes the depth to which an external magnetic field can penetrate the superconductor.

The ratio $\kappa = \lambda/\xi$ is known as the Ginzburg-Landau Parameter. It has been shown that Type I superconductors are those with $\kappa < 1/\sqrt{2}$, and Type II superconductors those with $\kappa > 1/\sqrt{2}$. For Type II superconductors, the phase transition from the normal state is of second order, for Type I superconductors it is of first order. This is proved by deriving a dual Ginzburg-Landau theory for the superconductor.

The most important finding from Ginzburg-Landau theory was made by Alexei Abrikosov in 1957. In a type-II superconductor in a high magnetic field - the field penetrates in quantized tubes of flux, which are most commonly arranged in a hexagonal arrangement[22], see also [23].

1.9 Literature Review

Takashi Yanagisawa and Hajime Shibata [24] wrote that the optical conductivity measurements give a powerful tool to investigate the nature of the superconducting gap for conventional and unconventional superconductors. They shown that the behavior of optical conductivity is consistent with an anisotropic gap and is well explained by the formula for d-wave pairing in the far-infrared region. The optical properties of the multiband superconductor MgB_2, in which the existence of superconductivity with relatively high-T_c (39K) was recently announced, is also examined to determine the symmetry of superconducting gaps.

Philip B. Allen [25] reported that Gtze and Wlfle (GW) wrote the conductivity in terms of a memory function $M(\omega)$ as $\sigma(\omega) = (ine2/m)(\omega + M(\omega))^{-1}$, where $M(\omega) = i/\tau$ in the Drude limit. The analytic properties of $-M(\omega)$ are the same as those of the self-energy of a retarded Green's function.

The results of a systematic study of the optical properties of the $YBa_2Cu_3O_{6+x}$-based insulators and superconductors are reported.**J. Orenstein** *et al.* [26] have presented measurements and analysis of the optical reflectivity R of a series of $YBa_2Cu_3O_{6+x}$ crystals in the frequency range from 30 to 20 000 cm^{-1} (4 meV to 2.5 eV), and temperature range from 10 to 270 K. From R they obtained the real part of the frequency-dependent optical conductivity $\sigma(\omega)$ by Kramers-Kronig analysis. In their discussion, they emphasized the development of structure and spectral weight in $\sigma(\omega)$ as the compounds change from insulators to high-T_c superconductors with varying O content or Al doping.

A.V. Balatsky [27] pointed out that impurity scattering in the unitary limit produces low energy quasiparticles with anisotropic spectrum in a two-dimensional d-wave superconductor. A. V. Balatsky described a new quasi-one-dimensional limit of the quasiparticle scattering, which might occur in a superconductor with short coherence length and with finite impurity potential range. The dc conductivity in a d-wave superconductor is predicted to be proportional to the normal state scattering rate and is impurity-dependent. Balatsky showed that quasi-one-dimensional regime might occur in high-T_c superconductors with Zn impurities at low temperatures $T \leq 10K$.

A. J. Berlinsky *et al.* [28] have used the self-consistent T-matrix approximation for impurity scattering in unconventional superconductors to interpret recent measurements of the temperature and frequency dependence of the microwave conductivity of $YBa_2Cu_3O_{6.993}$ crystals below 20 K. In the theory, the conductivity is expressed in terms of a frequency dependent single particle self-energy, determined by the impurity scattering phase shift which is small for weak (Born) scattering and approaches $\pi/2$ for unitary scattering. They reported that by inverting this process, microwave conductivity data are used to extract an effective single-particle self energy and obtain insight into the nature of the operative scattering processes. It is found that the effective self energy is well approximated by a constant plus a linear term in frequency with a small positive slope for thermal quasiparticle energies below 20 K. Possible physical origins of this form of self energy are discussed.

Durst and Lee [29] have showed that recent microwave conductivity measurements of detwinned, high-purity, slightly overdoped $YBa_2Cu_3O_{6.993}$ crystals reveal a linear temper-

ature dependence and a near-Drude lineshape for temperatures between 1 and 20 K and frequencies ranging from 1 to 75 GHz. Prior theoretical work has shown that simple models of scattering by point defects (impurities) in d-wave superconductors are inconsistent with these results. It has therefore been suggested that scattering by extended defects such as twin boundary remnants, left over from the detwinning process, may also be important. They calculate the self-energy and microwave conductivity in the self-consistent Born approximation (including vertex corrections) for a d-wave superconductor in the presence of scattering from extended linear defects. We find that in the experimentally relevant limit (Ω, $1/\tau \ll T \ll \Delta_0$), the resulting microwave conductivity has a linear temperature dependence and a near-Drude frequency dependence that agrees well with experiment.

Durst and Lee [30] have reported that due to the node structure of the gap in a d-wave superconductor, the presence of impurities generates a finite density of quasiparticle excitations at zero temperature. Since these impurity-induced quasiparticles are both generated and scattered by impurities, prior calculations indicate a universal limit($\Omega \rightarrow 0$,$T \rightarrow 0$) where the transport coefficients obtain scattering-independent values, depending only on the velocity anisotropy v_f/v_2. They improved upon prior results, including the contributions of vertex corrections and Fermi liquid corrections in their calculations of universal limit electrical, thermal, and spin conductivity. They found that while vertex corrections modify electrical conductivity and Fermi liquid corrections renormalize both electrical and spin conductivity, only thermal conductivity maintains its universal value, independent of impurity scattering or Fermi liquid interactions. Hence, low temperature thermal conductivity measurements provide the most direct means of obtaining the velocity anisotropy for high T_c cuprate superconductors.

Y. H. Yang *et al.* [31] reported that based on the self-consistent T-matrix approximation, the quantum interference (QI) effect is studied with the diagrammatic technique in weakly-disordered two-dimensional crystals with nearly half-filled bands. In addition to the usual 0-mode cooperon and diffusion, there exist π-mode cooperon and diffusion in the unitary limit due to the particle-hole symmetry. The diffusive π-modes are gapped by the deviation from the exactly-nested Fermi surface. The conductivity diagrams with the gapped π-mode cooperon or diffusion are found to give rise to unconventional features of the QI effect. Besides the inelastic scattering, the thermal fluctuation is shown to be also an important dephasing mechanism in the QI processes related with the diffusive π-modes. In the proximity of the nesting case, a power-law anti-localization effect appears due to the π-mode diffusion. For large deviation from the nested Fermi surface, this anti-localization effect is suppressed, and the conductivity remains to have the usual logarithmic weak-localization correction contributed by the 0-mode cooperon. As a result, the dc conductivity in the unitary limit becomes a non-monotonic function of the temperature or the sample size, which is quite different from the prediction of the usual weak-localization theory.

Byers *et al.* [32] have examined the effect of an impurity on the nearby tunneling conductance in an anisotropically gapped superconductor. They reported that the variation of the conductance has pronounced spatial dependence which depends strongly on the Fermi surface location of gap extrema. In particular, different gap symmetries produce profoundly different spatial features in the conductance. These effects may be detectable with a scanning-tunneling- microscope study of the surface of a high-temperature superconductor.

R. J. Radtke and M. R. Norman [33] pointed out that recent angle-resolved photoemission (ARPES) experiments have indicated that the electronic dispersion in some of the cuprates possesses an extended saddle point near the Fermi level which gives rise to a density of states that diverges like a power law instead of the weaker logarithmic divergence usually considered. Using band structures extracted from ARPES measurements, they demonstrate that, while the weak-coupling solutions suggest a strong influence of the strength of the Van Hove singularity on T_c, strong-coupling solutions show less sensitivity to the singularity strength and do not support the hypothesis that band-structure effects alone can account for either the large T_c's or the different T_c's within the copper oxide family. This conclusion is supported when the results are plotted as a function of the physically relevant self-consistent coupling constant, which shows universal behavior at very strong coupling.

Qiang-Hua Wang and Dung-Hai Lee [34] have proposed that the energy-dependent spatial modulation of the local density of states seen by Hoffman *et al.* [Science **297**, 1148(2002)] is due to the scattering interference of quasiparticles. They presented the general theoretical basis for such an interpretation and lay out the underlying assumptions. As an example, they performed an exact T-matrix calculation for the scattering due to a single impurity. The results of the calculation was used to check the assumptions, and to demonstrate that quasiparticle scattering interference can indeed produce patterns similar to those observed by Hoffman *et al.*.

L. Zhu *et al.* [35] have investigated the effect of elastic forward scattering on the ARPES spectrum of the cuprate superconductors. In the normal state, small angle scattering from out-of-plane impurities is thought to broaden the ARPES spectral response with minimal effect on the resistivity or the superconducting transition temperature T_c. Here they explore how such forward scattering affects the ARPES spectrum in the d-wave superconducting state. Away from the nodal direction, the one-electron impurity scattering rate is found to be suppressed as ω approaches the gap edge by a cancellation between normal and anomalous scattering processes, leading to a square-root-like feature in the spectral weight as ω approaches Δ_k from below. For momenta away from the Fermi surface, the analysis suggests that a dirty optimally or overdoped system will still display a sharp but nondisspersive peak which could be confused with a quasiparticle spectral feature. Only in cleaner samples should the true dispersing quasiparticle peak become visible. At the nodal point on the Fermi surface, the contribution of the anomalous scattering vanishes and the spectral weight exhibits a Lorentzian quasiparticle peak in both energy and momentum. Their analysis, including a treatment of unitary scatterers and inelastic spin fluctuation scattering, suggests explanations for the some- times mysterious lineshapes and temperature dependences of the peak structures observed in the $Bi_2Sr_2CaCu_2O_8$ system.

Y. H. Yang *et al.* [36] has mentioned that the quantum interference effect on the quasiparticle density of states (DOS) is studied with the diagrammatic technique in two-dimensional d-wave superconductors with dilute nonmagnetic impurities both near the Born and near the unitary limits. They derive in details the expressions of the Goldstone modes (cooperon and diffusion) for quasiparticle diffusion. They mentioned also that the DOS for generic Fermi surfaces is shown to be subject to a quantum interference correction of logarithmic suppression, but with various renormalization factors for the Born and unitary limits. Upon approaching the combined limit of unitarity and nested Fermi surface, the DOS correction is found to become a δ-function of the energy, which can be used to account for the

resonant peak found by the numerical studies.

S. Haas and K. Maki [37] have reported that Zn and Ni impurities in the hole-doped high-temperature superconductors are known to have strong effects on thermodynamic and transport properties. A recent scanning tunneling microscope study of Zn-doped Bi2212 (Pan *et al.*., Nature 403, 746 (2000)) has provided high-resolution images of the local density of states around non-magnetic impurities in $d_{x^2-y^2}$-wave superconductors. These pictures contain detailed information about the spinor wave functions u(r) and v(r) of bound states with energy $E_0 \sim \Delta/30$, centered at the from the solutions of the Bogoliubov-de Gennes equations for $d_{x^2-y^2}$-wave superconductors.

A. Ghosal *et al.* [38], have studied a short coherence length d-wave superconductor with finite density of unitary scatterers using the Bogoliubov-deGennes technique. They found that the low-energy density of states is reduced, the superfluid stiffness is significantly larger and off-diagonal long range order is more robust than the self-consistent T- matrix prediction. They concluded that these results are a consequence of the inhomogeneous pairing amplitude in the ground state and of the low-lying excitations formed by hybridized impurity resonances. These features, with their nontrivial spatial structure, cannot be adequately described within the conventional T-matrix approach.

Jian-Xin Zhu *et al.* [39] have written that an extensive numerical study is reported on disorder effect in two-dimensional d-wave superconductors with random impurities in the unitary limit. It is found that a sharp resonant peak shows up in the density of states at zero energy and correspondingly the finite-size spin conductance is strongly enhanced which results in a non-universal feature in one-parameter scaling. However, all quasiparticle states remain localized, indicating that the resonant density peak alone is not sufficient to induce delocalization. In the weak disorder limit, the localization length is so long that the spin conductance at small sample size is close to the universal value predicted by Lee.

W. A. Atkinson *et al.* [40] demonstrated that discrepancies between predicted low-energy quasiparticle properties in disordered 2D d-wave superconductors occur because of the unanticipated importance of disorder model details and normal-state particle-hole symmetry. This conclusion follows from numerically exact evaluations of the quasiparticle density-of-states predicted by the Bogoliubov-de Gennes (BdG) mean field equations for both binary alloy and random site energy disorder models. For the realistic case, which is best described by a binary alloy model without particle-hole symmetry, they predicted density of states suppression below an energy scale which appears to be correlated with the corresponding single-impurity resonance.

U. Michelucci *et al.* [41] investigated, employing an impurity position averaging scheme for the DOS that does not neglect these interference effects, as the commonly used T-matrix approaches do, the mutual influence of impurities in two-dimensional d-wave superconductors involving self-consistent solutions of the Bogoliubov-de Gennes equations. The local order parameter suppression, the local density of states (LDOS) as well as the interference of impurity-induced structures were analyzed.

The low-energy quasiparticle states of a disordered d-wave superconductor were investigated theoretically. A class of such states, formed via tunneling between the Andreev bound

states that are localized around extended impurities (and result from scattering between pair-potential lobes that differ in sign) was identified. **Adagideli** *et al.* [42] determined its (divergent) contribution to the total density of states by taking advantage of connections with certain one-dimensional random tight-binding models. The states under discussion should be distinguished from those associated with nodes in the pair potential.

W. A. Atkinson *et al.* [43] studied the local density of states around potential scatterers in d-wave superconductors, and showed that quantum interference between impurity states is not negligible for experimentally relevant impurity concentrations. The two impurity model was used as a paradigm to understand these effects analytically and in interpreting numerical solutions of the Bogoliubov-de Gennes equations on fully disordered systems. They said that they focused primarily on the globally particle-hole symmetric model which has been the subject of considerable controversy, and give evidence that a zero-energy delta function exists in the DOS. They concluded the anomalous spectral weight at zero energy is seen to arise from resonant impurity states belonging to a particular sublattice, exactly as in the 2-impurity version of this model.

The quasiparticle resonant states around a single nonmagnetic impurity with unitary scattering in a d-wave superconductor was studied by **Jian-Xin Zhu** *et al.* [44] by solving the Bogoliubov-de Gennes equations based on a t-J model. Both the spatial variation of the order parameter and the local density of states (LDOS) around the impurity have been investigated. they found:

i A particle-hole symmetric system has a single symmetric zero-energy peak in the LDOS regardless of the size of the superconducting coherence length ξ_0;

ii For the particle-hole asymmetric case, an asymmetric splitting of the zero- energy peak is intrinsic to a system with a small value of $k_F\xi_0$.

L. Zhu *et al.* [45] studied the problem of two local potential scatterers in a d-wave superconductor, and showed how quasiparticle bound state wave functions interfere. Each single-impurity electron and hole resonance energy is in general split in the presence of a second impurity into two, corresponding to one even parity and one odd parity state. They calculated the local density of states (LDOS), and argued that scanning tunneling microscopy (STM) measurements of 2-impurity configurations should provide more robust information about the superconducting state than 1-impurity LDOS patterns, and question whether truly isolated impurities can ever be observed. In some configurations highly localized, long-lived states were predicted. They discussed the effects of realistic band structures, and how 2-impurity STM measurements could help distinguish between current explanations of LDOS impurity spectra in the BSCCO-2212 system.

G. G. N. Angilella *et al.* [46] reported that imaging the effects of an impurity like Zn in high-T_c superconductors [see, e.g., S. H. Pan et al., Nature 61 (2000) 746] has rekindled interest in defect problems in the superconducting phase. They told that this has prompted them to re-examine the early work of March and Murray [Phys. Rev. 120 (1960) 830] on the linear response function in an initially translationally invariant Fermi gas. In particular, they present corresponding results for a superconductor at zero temperature, both in the s- and in the d-wave case, and mention their direct physical relevance in the case when the

impurpotential is highly localized.

E. Z. Kuchinskii and M. V. Sadovskii [47] presented the results of theoretical analysis of normal impurities effects in superconductors with the gap being an odd function of $k - k_F$. This model proposed by Mila and Abrahams leads to the possibility of pairing in the presence of an arbitrarily strong short-range repulsion between electrons and may be applied to high-T_c oxides. However, they demonstrated that normal impurities lead to rather strong suppression of this type of pairing, which is actually stronger than in the case of magnetic impurities in traditional superconductors. Relative stability of high-T_c cuprates to disordering makes this model a rather unlikely candidate for the pairing mechanism in these systems.

T. V. Ramakrishnan [48] reported that the interaction between planar quasiparticles in a $d_{x^2-y^2}$ superconductor and quantized vortices associated with a magnetic field perpendicular to the plane is shown to induce a pair potential with d_{xy} symmetry, out a phase with $d_{x^2-y^2}$ order. A microscopic calculation of a process involving quasiparticle scattering by the supercurrent around a vortex and Andreev reflection from its core is presented. Other processes also leading to an id_{xy} pair potential are discussed. They argued that such a fully gapped state may be the high field low temperature phase observed by Krishana, Ong *et al.*in magnetothermal conductivity measurements of superconducting single crystal Bi-2212.

H. Ghosh [49] derived a pair potential from tight binding further neighbours attraction that leads to superconducting gap symmetry similar to that of the phenomenological spin fluctuation theory of high temperature superconductors (Monthoux, Balatsky, Pines, Phys. Rev. Lett. 67, 3448). They showed that higher anisotropic d-wave than the simpliest d-wave symmetry is one of the important ingredients responsible for higher BCS characteristic ratio.

H.V. Kruis *et al.* [50] predicted a resonance impurity state generated by the substitution of one Cu atom with a nonmagnetic atom, such as Zn, in the pseudogap state of a high-T_c superconductor. They said that the precise microscopic origin of the pseudogap is not important for this state to be formed, in particular this resonance will be present even in the absence of superconducting fluctuations in the normal state. In the presence of superconducting fluctuations, Kruis *et al.* predict the existence of a counterpart impurity peak on a symmetric bias. The nature of impurity resonance is similar to the previously studied resonance in the d-wave superconducting state.

S. Haas and K. Maki [51] studied the evolution with temperature of quasiparticle bound states around non-magnetic impurities in $d_{x^2-y^2}$-wave superconductors. The associated local density of states has a fourfold symmetry which has recently been observed in Zn-doped Bi2212 using scanning tunneling microscopy (STM). From the corresponding Bogoliubov-de Gennes equation they found that with increasing temperature the magnitude of the bound state energy increases and the amplitude of the fourfold contribution to the spinor wave functions decreases. In the pseudogap regime above T_c the fourfold angular dependence of the local tunneling conductance persists as long as the superconducting fluctuations are sufficiently strong to support a finite local order parameter. Once the gap function vanishes completely, the angular structure of the bound state wave function becomes featureless. they concluded that these effects should be observable in STM studies of impurity doped high-temperature superconductors.

Jian-Xin Zhu *et al.* [52] studied, in accordance with the work of **Chakravarty** et al. that proposed an ordered d-density wave (DDW) state as an explanation of the pseudogap phase in underdoped high-temperature cuprates, the competition between the DDW and superconducting ordering based on an effective mean-field Hamiltonian. They were mainly concerned with the effect of the DDW ordering on the electronic state around a single nonmagnetic impurity. They found that a single subgap resonance peak appears in the local density of state around the impurity. In the unitary limit, the position of this resonance peak is always located at $E_r = -$ with respect to the Fermi energy. This result is dramatically different from the case of the pure superconducting state for which the impurity resonant energy is approximately pinned at the Fermi level. So they proposed that this can be used to probe the existence of the DDW ordering in cuprates.

D. K. Morr [53] studied the electronic structure near impurities in the d-density-wave (DDW) state, a possible candidate phase for the pseudo-gap region of the high-temperature superconductors. He showed that the local DOS near a non-magnetic impurity in the DDW state is qualitatively different from that in a superconductor with $d_{x^2-y^2}$-symmetry. He proposed since this result is a robust feature of the DDW phase, it can help to identify the nature of the two different phases recently observed by scanning tunneling microscopy experiments in the superconducting state of underdoped Bi-2212 compounds.

C. Ṕepin and P. A. Lee [54] presented a method to compute the exact density of states induced by N nonmagnetic impurities in a system of two dimensional Dirac fermions in the unitarity limit. they reviewed the case of the y-flux phase of the Heisenberg model and also treat the disordered d-wave superconductor. In both case they found additional states in the gap with $\delta\rho(\omega) \simeq n_i/|\omega(\ln^2|\omega/\Delta_0| + (\pi^2/2)^2)|$.

Using scanning tunneling spectroscopy,**M. Kugler** *et al.* [55] have investigated the temperature dependence of the quasiparticle density of states of overdoped $Bi_2Sr_2CuO_{6+d}$ between 275 mK and 82 K. Below $T_c = 10$K, the spectra show a gap with well-defined coherence peaks at $\pm\Delta_\rho = 12$ meV, which disappear at T_c. Above T_c, the spectra display a clear pseudogap of the same magnitude, gradually filling up and vanishing at $T* = 68$K. By the comparison with $Bi_2Sr_2CaCu_2O_{8+d}$ they concluded that the pseudogap and the superconducting gap scale with each other, providing strong evidence that they have a common origin.

Using cluster perturbation theory, it is shown that the spectral weight and pseudogap observed at the Fermi energy in recent angle resolved photoemission spectroscopy of both electron- and hole-doped high-temperature superconductors find their natural explanation within the t-t'-t"-U Hubbard model in two dimensions.**David Sénéchal and A. M. S. Tremblay** [56] have reported that the value of the interaction U needed to explain the experiments for electron-doped systems at optimal doping is in the weak to intermediate coupling regime where the t-J model is inappropriate. At strong coupling, short-range correlations suffice to create a pseudogap, but at weak coupling long correlation lengths associated with the antiferromagnetic wave vector are necessary.

Je Huan Koo and Guangsup Cho [57] have investigated the spin-gap in high T_c superconductivity. They obtained the effective exchange integral in the presence of conduction in the ab-plane from the interaction U_{sd}, where the electron-electron interaction is mediated

by the localized spin flips. They choose the exchange interaction along the c-axis from the superexchange-type interaction, U^c_{sd}. They found the spin-gap from the conducting spin- 12 ladder corresponding to the structure of high T_c superconductors.

E. Z. Kuchinskii *et al.* [58] have analyzed the anomalies of superconducting state in the model of pseudogap state induced by fluctuations of short range order of dielectric (AFM (SDW) or CDW) type, and based on the scenario of hot spots formation on the Fermi surface, with the account of all Feynman graphs for electron interaction with pseudogap fluctuations, leading to strong scattering around the hot spots. They determined the dependence of superconducting critical temperature T_c on the effective width of the pseudogap, correlation length of shortrange order and concentration of nonmagnetic impurities.

We hope to take part in such efforts to solve the mystery of High T_c superconductors.

Chapter 2

Main Tools For Our Work

According to their importance in the field of theoretical physics, we are going to mention- either in brief or in some detail- some of the useful tools, the Fourier transform, Hilbert transform, and the more important one - at least for us- the Green's functions, etc. We will do modifications only when needed, and try to keep the main source as it is.

2.1 Fourier Transform Tools

These are some of the most important and powerful tools not only in physics but in science as a whole.

2.1.1 Fourier Series

A Fourier series is an expansion of a periodic function* $f(x)$ in terms of an infinite sum of sines and cosines.

Fourier series of a function $f(x)$ is given by

$$f(x) = \frac{1}{2}a_0 + \sum_{n=1}^{\infty}(a_n \cos nx + b_n \sin nx) \tag{2.1.1}$$

where

$$a_0 = \frac{1}{\pi}\int_{-\pi}^{\pi} f(x)dx \tag{2.1.2}$$

$$a_n = \frac{1}{\pi}\int_{-\pi}^{\pi} f(x)\cos(nx)dx \tag{2.1.3}$$

$$b_n = \frac{1}{\pi}\int_{-\pi}^{\pi} f(x)sin(nx)dx \tag{2.1.4}$$

and $n == 1, 2, 3, \ldots$. Note that the coefficient of the constant term a_0 has been written in a special form in order to preserve symmetry with the definitions of a_n and b_n.
Fourier series with complex coefficients:

*A function $f(x)$ is said to be periodic with period p if $f(x) = f(x + np)$ for $n = 1, 2, \ldots$. For example, the sine function $\sin x$, is periodic with the period 2π (as well as with period $-2\pi, 4\pi, 6\pi$, etc.).

The notion of a Fourier series can also be extended to complex coefficients. Consider a real-valued function $f(x)$. Write

$$f(x) = \sum_{n=-\infty}^{\infty} A_n e^{inx}, \tag{2.1.5}$$

with

$$A_n = \frac{1}{2\pi} \int_{-\pi}^{\pi} f(x) e^{-inx} dx.$$

For a function periodic in $[-L/2, L/2]$, these relations are generalized to [59]

$$f(x) = \sum_{n=-\infty}^{\infty} A_n e^{i(2\pi nx/L)} \tag{2.1.6}$$

$$A_n = 1/L \int_{-L/2}^{L/2} f(x) e^{-i(2\pi nx/L)} dx. \tag{2.1.7}$$

2.1.2 Fourier Transform

The Fourier transform is a generalization of the complex Fourier series in the limit as $L \to \infty$. Replace the discrete A_n with the continuous $F(\nu)d\nu$ while letting $n/L \to \nu$. Then change the sum to an integral, and the equations become [60]

$$F(\nu) = \int_{-\infty}^{\infty} f(t) e^{-2\pi i\nu t} dt \tag{2.1.8}$$

$$f(t) = \int_{-\infty}^{\infty} F(\nu) e^{2\pi i\nu t} d\nu \tag{2.1.9}$$

Fourier Transform Conventions

The conventions in physics, electrical engineering, and statistics are often different and vary from country to country.

Fourier Transform in Physics

As the fundamental unit of angle is the radian and of frequency radians/second, the Fourier transform used in physics uses the *minus* omega convention, $-\omega$, given by

$$F(\omega) = \int_{-\infty}^{\infty} f(t) e^{-i\omega t}\, dt \tag{2.1.10}$$

The inverse transform used here is given by

$$f(t) = \frac{1}{2\pi} \int_{-\infty}^{\infty} F(\omega) e^{+i\omega t}\, d\omega \tag{2.1.11}$$

The $1/2\pi$ in (2.1.11) is the result of the fact that $d\nu = d\omega/2\pi$ [61].

To restore the symmetry of the transforms, the convention

$$F(\omega) = \frac{1}{\sqrt{(2\pi)}} \int_{-\infty}^{\infty} f(t) e^{-i\omega t} dt \tag{2.1.12}$$

$$f(t) = \frac{1}{\sqrt{(2\pi)}} \int_{-\infty}^{\infty} F(\omega) e^{i\omega t} d\omega \tag{2.1.13}$$

is sometimes used [60].

Fourier transform for 2v function

For a given two variable function $f(\mathbf{r}, t)$ which is continuous and integrable, and $F(\mathbf{k}, \omega)$ is integrable. The Fourier transform is [62; 63]:

$$F(\mathbf{k}, \omega) = \iint_{-\infty}^{\infty} f(\mathbf{r}, t) e^{-i(\mathbf{k}\cdot\mathbf{r}+\omega t)} d\mathbf{r}\, dt, \tag{2.1.14}$$

$$f(\mathbf{r}, t) = \frac{1}{(2\pi)^2} \iint_{-\infty}^{\infty} F(\mathbf{k}, \omega) e^{i(\mathbf{k}\cdot\mathbf{r}+\omega t)} d\mathbf{k}\, d\omega \tag{2.1.15}$$

or, as discussed above

$$F(\mathbf{k}, \omega) = \frac{1}{2\pi} \iint_{-\infty}^{\infty} f(\mathbf{r}, t) e^{-i(\mathbf{k}\cdot\mathbf{r}+\omega t)} d\mathbf{r}\, dt, \tag{2.1.16}$$

$$f(\mathbf{r}, t) = \frac{1}{2\pi} \iint_{-\infty}^{\infty} F(\mathbf{k}, \omega) e^{i(\mathbf{k}\cdot\mathbf{r}+\omega t)} d\mathbf{k}\, d\omega \tag{2.1.17}$$

2.1.3 Convolution Theorem

A convolution is an integral that expresses the amount of overlap of one function g as it is shifted over another function f. It therefore "blends" one function with another.
Convolution over an infinite range is given by,

$$F(\tau) = f_1 * f_2 \equiv \frac{1}{\sqrt{2\pi}} \int_{-\infty}^{\infty} f_1(t) f_2(\tau - t) dt = \int_{-\infty}^{\infty} f_2(t) f_1(\tau - t) d\tau \tag{2.1.18}$$

The convolution theorem states that

$$F(\tau) = f_1 * f_2 \equiv \frac{1}{\sqrt{2\pi}} \int_{-\infty}^{\infty} g_1(\omega) g_2(\omega) e^{i\omega\tau} d\omega, \tag{2.1.19}$$

where $g_1(\omega)$ and $g_2(\omega)$ are the Fourier transform of $f_1(\tau)$ and $f_2(\tau)$.

By taking the Fourier transform of this last equation, and thus solving for the product $g_1(\omega)g_2(\omega)$, we see that the convolution theorem may also be expressed as follows: The Fourier transform of the convolution of two functions is the product of the Fourier transforms of these two functions. Denoting the Fourier transform of $F(\tau)$ by $G(\omega)$[64] this may be written

$$G(\omega) = g_1(\omega) g_2(\omega).$$

2.2 Hilbert Transforms

It is often the case that in the study of some physical system one has to deal with complex-valued functions (indices of refraction, susceptibilities, scattering amplitudes, impedances, etc.) which have a physical meaning only when the argument of the function (which might, for example, be a frequency or an energy) takes on *real* values. In many cases it is possible to obtain, from the laws governing the system, information about the general properties of such functions when the argument is *complex*; for example, it may be that the function is *analytic* in some region of the complex plane. Since experimental data can only be obtained for real values of the argument. It is of interest to see whether we can use general properties such as analyticity to deduce relations between real quantities of direct physical significance. The key to such a program can be found in the study of Hilbert transform pairs.

Here we go, consider a function $f(z)$, which is analytic in the upper half of the complex plane, and which is such that $|f(z)| \to 0$ as $|z| \to \infty$ in the upper half-plane (Note that the only function which can satisfy these conditions in the entire plane is $f \equiv 0$). We have

$$\mathcal{P}\int_{-\infty}^{\infty} \frac{f(x)}{x-\alpha}dx = i\pi f(\alpha), \tag{2.2.1}$$

where $f(x)$ is a complex-valued function of a real variable. We may write it as

$$f(x) \equiv f_R(\alpha) + if_I(\alpha).$$

Equating real and imaginary parts in Eq.(2.2.1), we get

$$f_R(\alpha) = \frac{1}{\pi}\mathcal{P}\int_{-\infty}^{\infty} \frac{f_I(x)}{x-\alpha}dx, \tag{2.2.2a}$$

$$f_I(\alpha) = -\frac{1}{\pi}\mathcal{P}\int_{-\infty}^{\infty} \frac{f_R(x)}{x-\alpha}dx, \tag{2.2.2b}$$

any pair of functions which satisfy Eqs.(2.2.2a) and (2.2.2b) is called a *Hilbert transform pair*. Note that these equations tell us that if $f_I(x) \equiv 0$, then $f_R(x) \equiv 0$ [65; 66].

2.3 Kramers-Krönig Analysis for Conductivity

We wish to establish formal relations between real and imaginary parts of certain physical quantities; these are termed "Kramers-Krönig relations". We shall describe the analysis for the electrical conductivity, because it appears for this quantity in its simplest form, and because this particular application of the Kramers-Krönig relations is of considerable importance.

We begin our discussion by noting that the Fourier components of electric field and current are related by

$$\boldsymbol{J}(\omega) = \sigma(\omega)\boldsymbol{\mathcal{E}}(\omega)$$

In this equation we allow all three functions to be complex-in particular

$$\sigma = \sigma_1 + i\sigma_2 \tag{2.3.1}$$

where σ_1 and σ_2 are real. On the other hand, this complex nature is purely formal and the actual current

$$J(t) = (1/2\pi)\int_{-\infty}^{\infty}\sigma(\omega)e^{-i\omega t}\mathcal{E}(\omega)d\omega \tag{2.3.2}$$

must be real on the application of a real electric field; thus in the conduction of this expression

$$J(t) = \int_{-\infty}^{\infty}\sigma(t-t')\mathcal{E}(t')dt' \tag{2.3.3}$$

the quantity

$$\sigma(t) = (1/2\pi)\int_{-\infty}^{\infty}\sigma(\omega)e^{-i\omega t}d\omega \tag{2.3.4}$$

must be real. This implies that

$$\sigma(-\omega) = \sigma^*(\omega) \tag{2.3.5}$$

1.e

$$\sigma_1(-\omega) = \sigma_1(\omega), \qquad \sigma_2(-\omega) = -\sigma_2(\omega). \tag{2.3.6}$$

We come now to the crucial point in obtaining the Kramers-Krönig relations: by the"causality principle" (section2.6.4) $J(t)$ can not depend on $\mathcal{E}(t')$ if $t < t'$. This implies

$$\sigma(t) = 0 \text{ if } t < 0 \tag{2.3.7}$$

and so we can write the inverse Fourier transform of $\sigma(t)$ as

$$\sigma(\omega) = \int_{0}^{\infty}\sigma(t)e^{i\omega t}dt. \tag{2.3.8}$$

we may note from Eq.(2.3.3) that if $\mathcal{E}(t)$ is a delta-function impulse, $J(t) = \sigma(t)$, 1.e, $\sigma(t)$ is the current produced by a"unit impulse" of electric field at t=0. This establishes, on physical grounds, that $\sigma(t)$is "well behaved". We shall also use the result that

$$\lim_{\omega\to\infty}\sigma(\omega) = 0. \tag{2.3.9}$$

The good behaviour of $\sigma(t)$ has the consequence that, admitting complex values of ω $\sigma(\omega)$has no zeros or singularities in the upper half of the complex-plane, and since Eq.(2.3.9) holds, $\sigma(\omega)$ vanishes over the semi-circle at infinity in this plane. Consider therefore the contour C shown in Fig.(2.1) and the integral

$$\int_c \frac{\sigma(\omega_0)}{\omega_0-\omega}d\omega_0 = 0. \tag{2.3.10}$$

The integral is zero since the contour contains no poles and, since the integrand vanishes over the semi-circle at infinity, can also be written (Eq.(2.2.1))

$$\mathcal{P}\int \frac{\sigma(\omega_0)}{\omega_0-\omega}d\omega_0 - i\pi\sigma(\omega) = 0, \tag{2.3.11}$$

the second term on the left-hand side being the contribution to the integral over the infinitesimal semi-circle about the simple pole at $\omega_0 = \omega$, and $\mathcal{P}$ is the *Cauchy* principle value

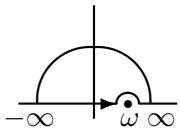

Figure 2.1: Form of contour in integral 2.3.10

(sections 2.1.2 & 2.1.3). Taking real and imaginary parts of equation (2.3.11) we immediately find

$$\sigma_1(\omega) = \frac{\mathcal{P}}{\pi}\int_{-\infty}^{\infty}\frac{\sigma_2(\omega_0)}{\omega_0-\omega}d\omega_0, \tag{2.3.12}$$

$$\sigma_2(\omega) = -\frac{\mathcal{P}}{\pi}\int_{-\infty}^{\infty}\frac{\sigma_1(\omega_0)}{\omega_0-\omega}d\omega_0 \tag{2.3.13}$$

these are the Kramers-Krönig relation, often rewritten as

$$\sigma_1(\omega) = \frac{2\mathcal{P}}{\pi}\int_{0}^{\infty}\frac{\omega_0\sigma_2(\omega_0)}{\omega_0^2-\omega^2}d\omega_0, \tag{2.3.14}$$

$$\sigma_2(\omega) = -\frac{2\omega\mathcal{P}}{\pi}\int_{0}^{\infty}\frac{\sigma_1(\omega_0)}{\omega_0^2-\omega^2}d\omega_0 \tag{2.3.15}$$

which forms are easily obtained from (2.3.12) by using the fact that $\sigma_1(\omega)$ is even and $\sigma_2(\omega)$ is odd [67].

2.4 Residue Theorem

The coefficient a_{-1} in Laurent's expansion of

$$f(z) = \sum_{n=-\infty}^{\infty} a_n(z-z_0)^n, \tag{2.4.1}$$

$$= \cdots + a_{-2}(z-z_0)^{-2} + a_{-1}(z-z_0)^{-1} + a_0 + a_1(z-z_0) + \cdots \tag{2.4.2}$$

is called the residue of $f(z)$ at $z = z_0$; it is denoted as follows

$$a_{-1} = Res f(z)_{z=z_0}.$$

From the integral of $(z-z_0)^n$ we have

$$\oint f(z)dz = 2\pi i a_{-1} = 2\pi i Res f(z)_{z=z_0}, \tag{2.4.3}$$

for any contour enclosing $z = z_0$ but no other singularity of $f(z)$ [68].

If the closed contour C encloses several singularities, we can let it shrink to enclose each singularity separately, as shown in Fig.(2.4). Cauchy's integral theorem leads to

$$\oint_c f(z)dz + \oint_{c_0} f(z)dz + \oint_{c_1} f(z)dz +$$
$$\oint_{c_2} f(z)dz + \cdots = 0. \tag{2.4.4}$$

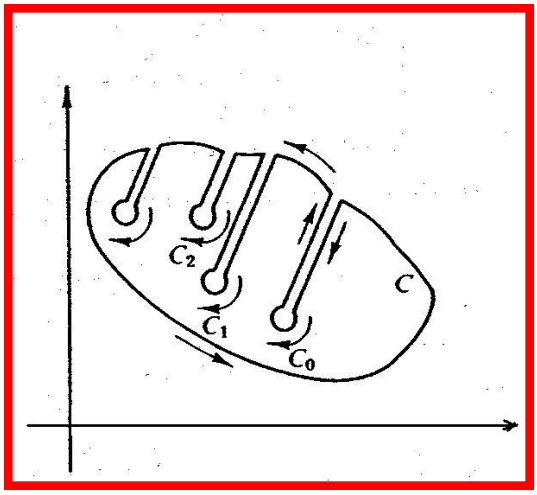

Figure 2.2: Contour of integration

but the circular integral around any given singular point is given by

$$\oint_{c_i} f(z)dz = -2\pi i a_{-1\ z_i} = -2\pi i\, Res f(z)_{z=z_{0i}} \tag{2.4.5}$$

assuming a Laurent expansion about the singular point, $z = z_i$.
Combining the last two Eqs., we have

$$\begin{aligned}\oint_c f(z)dz =& -2\pi i(a_{-1z_{00}} + (a_{-1z_{01}} + (a_{-1z_{02}} + \cdots)\\ =& 2\pi i \sum Res f(z).\end{aligned} \tag{2.4.6}$$

This is the residue theorem [69].

2.4.1 Evaluation of definite integrals

Consider an integral of the form

$$I = \int_0^{2\pi} f(\cos\theta, \sin\theta)d\theta \tag{2.4.7}$$

where f is finite and also single-valued for all values of θ.

Let $z = e^{i\theta}$, $dz = ie^{i\theta}d\theta$. From this

$$d\theta = -i\frac{dz}{z}, \sin\theta = \frac{z - z^{-1}}{2i}, \cos\theta = \frac{z + z^{-1}}{2}$$

then

$$I = -i \oint_{\text{unit circle}} f(\frac{z - z^{-1}}{2i}, \quad \frac{z + z^{-1}}{2}) \quad \frac{dz}{z} \tag{2.4.8}$$

By residue theorem [69]

$$I = (-i)2\pi i \sum \text{residues within the unit circle} \tag{2.4.9}$$

2.5 Second Quantization

In many-body theories, the method of second quantization is a powerful tool. Second quantization was originally introduced in order to deal with relativistic quantum mechanics, realizing that a consistent way of formulating a relativistic field theory had to go beyond first quantization. In our case, we stay in the realms of nonrelativistic quantum mechanics, but second quantization will allow us to describe a many-body system in a transparent way, on the basis of the occupation-number states [70; 71].

2.5.1 Occupation Number Space

Occupation number, or *Fock space*, is an abstract mathematical space in which complete sets of basis states are enumerated by indicating the number of particles in single particle states with (sets of) quantum numbers λ. A basis vector in occupation number space has the form

$$|\Psi >= |n_1, n_2, \dots, n_\lambda, \dots > \tag{2.5.1}$$

where n_λ is the number of particles in each single particle state [72].

For bosons, n_λ must be a non-negative integer; for fermions, the Pauli exclusion principle restricts n_λ to be either 0 or 1. A feature of the Fock space is that the total number of particles is not a fixed parameter, but rather is a dynamical variable associated with a total number operator

$$N = \sum_{\lambda=0}^{\infty} n_\lambda \tag{2.5.2}$$

This state vector $|\Psi >$ has the following properties.

- For given N, it corresponds to the fully symmetrized or antisymmetrized product of N single particle wave function in the Schrdinger picture.
- It is a complete description of the N-body system.
- It is not a function of any particular set of coordinates.
- It is part of a set that forms a complete orthogonal basis, that is,

$$\begin{aligned} < \Psi|\Psi' >&= < n_1, n_2, \dots, n_\lambda, \dots |n'_1, n'_2, \dots, n'_\lambda, \dots > \\ &= \prod_{\lambda=1}^{\infty} \delta_{n_\lambda n'_\lambda} \end{aligned} \tag{2.5.3}$$

The vacuum state $|0 >$ is the state that has zero particles in every slot:

$$|0 >= |0, 0, \dots, 0, \dots >$$

A single particle states is [72; 73]:

$$|\lambda >= |0, 0, \dots, n_\lambda = 1, 0, \dots >\equiv |0_1, 0_2, \dots, 0_{\lambda-1}, 1_\lambda, 0_{\lambda+1}, \dots >$$

2.5.2 Construction of States

The basic building element in Fock space the destruction or annihilation operator c_λ that removes one particle from state λ. Its adjoint $c_\lambda^\dagger$ is a creation operator that places one additional particle into the state λ [72].

Fermionic operators. We define the two operators, c_λ and $c_\lambda^\dagger$, by

$$c_\lambda^\dagger|\psi> = c_\lambda^\dagger|\cdots, n_\lambda, \cdots> = (\pm 1)^{(\sum_{\lambda'}^{\lambda'<\lambda} n_{\lambda'})}(1-n_\lambda)^{\frac{1}{2}}|\cdots, n_{\lambda+1}, \cdots>, \tag{2.5.4}$$

$$c_\lambda|\psi> = c_\lambda|\cdots, n_\lambda, \cdots> = (\pm 1)^{(\sum_{\lambda'}^{\lambda'<\lambda} n_{\lambda'})}(n_\lambda)^{\frac{1}{2}}|\cdots, n_{\lambda-1}, \cdots>, \tag{2.5.5}$$

where the (+) corresponds to Bosons and the (-) corresponds to Fermions[†]. To fully specify the operators we must also specify their commutation relations.

The Fermions commutation relations are:

$$c_\lambda c_{\lambda'}^\dagger + c_{\lambda'}^\dagger c_\lambda = \delta_{\lambda\lambda'} \tag{2.5.6}$$

$$c_{\lambda'}^\dagger c_\lambda^\dagger + c_\lambda^\dagger c_{\lambda'}^\dagger = 0 \tag{2.5.7}$$

$$c_{\lambda'} c_\lambda + c_\lambda c_{\lambda'} = 0 \tag{2.5.8}$$

The field operators: We now define the field operators, $\psi_\sigma^\dagger(r)$ and $\psi_\sigma(r)$, by

$$\psi_\sigma^\dagger(\mathbf{r}) = \sum_\lambda c_\lambda^\dagger \phi_\lambda^*(\mathbf{r}) \tag{2.5.9}$$

$$\psi_\sigma(\mathbf{r}) = \sum_\lambda c_\lambda \phi_\lambda(\mathbf{r}) \tag{2.5.10}$$

where $\phi_\lambda(\mathbf{r})$ is the wave function of a particle in the state λ at the position $\mathbf{r}$. $\psi_\sigma^\dagger(\mathbf{r})$ creates a particle with spin σ at position $\mathbf{r}$ and $\psi_\sigma(\mathbf{r})$ annihilates a particle with spin σ at position $\mathbf{r}$.

We can use the field operators to define composite operators. For example the density operator:

$$\rho_\sigma(\mathbf{r}) = m\psi_\sigma^\dagger(\mathbf{r})\psi_\sigma(\mathbf{r}) \tag{2.5.11}$$

the expectation value of which is the density in the state $|\Psi_0>$:

$$\rho_\sigma(\mathbf{r}) = m < \psi_0|\psi_\sigma^\dagger(\mathbf{r})\psi_\sigma(\mathbf{r})|\psi_0> \tag{2.5.12}$$

or the (particle) current operator:

$$\mathbf{j}_\sigma(\mathbf{r}) = \psi_\sigma^\dagger(\mathbf{r})\frac{\nabla}{im}\psi_\sigma(\mathbf{r}) + h.c., \tag{2.5.13}$$

where h.c. indicates the Hermitian conjugate, the expectation value of which is the (particle) current :

$$\mathbf{j}_\sigma(\mathbf{r}) =< \psi_0|\psi_\sigma^\dagger(\mathbf{r})\frac{\nabla}{im}\psi_\sigma(\mathbf{r}) + h.c.|\psi_0> . \tag{2.5.14}$$

[†] we shall consider throughout the thesis the fermions only.

In terms of the field operators, the single particle Hamiltonian, H_0, is given by

$$H_0 = \sum_{\sigma} \int d\mathbf{r} \psi^{\dagger}_{\sigma}(\mathbf{r}) \Big(-\frac{\nabla^2}{2m} + V^{ext}(\mathbf{r}) \Big) \psi_{\sigma}(\mathbf{r}) \tag{2.5.15}$$

For two body interactions the Hamiltonian [74], H', is

$$H' = \frac{1}{2} \sum_{\sigma\sigma'} \int d\mathbf{r} \int d\mathbf{r}' \psi^{\dagger}_{\sigma}(\mathbf{r}) \psi^{\dagger}_{\sigma'}(\mathbf{r}') V(|\mathbf{r} - \mathbf{r}'|) \psi_{\sigma'}(\mathbf{r}') \psi_{\sigma}(\mathbf{r}). \tag{2.5.16}$$

2.5.3 The tight binding Hamiltonian

We will now derive the tight binding Hamiltonian from Eq.(2.5.15). We begin by substituting Eq.(2.5.9) and Eq.(2.5.10) into the single particle Hamiltonian. This gives

$$H_0 = \sum_{\mathbf{k}\sigma} \int d\mathbf{r} c^{\dagger}_{\mathbf{k}\sigma} \phi^{*}_{\mathbf{k}\sigma}(\mathbf{r}) \Big(-\frac{\nabla^2}{2m} + V^{ext}(\mathbf{r}) \Big) \phi_{\mathbf{k}\sigma}(\mathbf{r}) c_{\mathbf{k}\sigma}. \tag{2.5.17}$$

where we have identified k and σ as the state labels λ, and $\phi_{\mathbf{k}\sigma}(\mathbf{r})$ is the solution of the single particle **TISE** so

$$\Big(-\frac{\nabla^2}{2m} + V^{ext}(\mathbf{r}) \Big) \phi_{\mathbf{k}\sigma}(\mathbf{r}) = \varepsilon_{\mathbf{k}\sigma} \phi_{\mathbf{k}\sigma}(\mathbf{r}) \tag{2.5.18}$$

Substituting this into Eq.(2.5.17) we find that

$$H_0 = \sum_{\mathbf{k}\sigma} \varepsilon_{\mathbf{k}\sigma} c^{\dagger}_{\mathbf{k}\sigma} c_{\mathbf{k}\sigma}. \tag{2.5.19}$$

The number operator simply counts the number of particles in the state $|\mathrm{k}\sigma>$. The single particle Hamiltonian then becomes

$$H_0 = \sum_{\mathbf{k}\sigma} \varepsilon_{\mathbf{k}\sigma} N_{\mathbf{k}\sigma}. \tag{2.5.20}$$

Thus the energy of the non-interacting system is given by the product of the energy of a single particle state and the number of particles in the that state summed over all states.

We now introduce the (lattice) Fourier transformations of the second quantization operators.

$$c_{n\sigma} = \frac{1}{\sqrt{N}} \sum_{\mathbf{k}} e^{i\mathbf{k}\cdot\mathbf{R}_n} c_{\mathbf{k}\sigma} \tag{2.5.21}$$

$$c^{\dagger}_{n\sigma} = \frac{1}{\sqrt{N}} \sum_{\mathbf{k}} e^{-i\mathbf{k}\cdot\mathbf{R}_n} c^{\dagger}_{\mathbf{k}\sigma} \tag{2.5.22}$$

where the sum is over the states of the system at the wave vector k in the first Brillouin zone. $c^{\dagger}_{n\sigma}$ annihilates (creates) a particle in an orbital centered on the lattice site n. Substituting the inverse Fourier transforms into Eq.(2.5.19) we find that

$$H_0 = \sum_{nm\sigma} t_{nm} c^{\dagger}_{n\sigma} c_{m\sigma}. \tag{2.5.23}$$

where the hopping integral, t_{nm} , S3.1, is the Fourier transform of the state energy, $\varepsilon_{\mathbf{k}\sigma}$. Thus

$$\varepsilon_{\mathbf{k}\sigma} = \sum_m t_{nm} e^{i\mathbf{k}\cdot(\mathbf{R}_n - \mathbf{R}_m)} \tag{2.5.24}$$

If we assume a simple cubic lattice with on site and nearest neighbour hopping only [74], we find that

$$\varepsilon_{\mathbf{k}\sigma} = t_0 + at'\big(\cos(k_x a) + \cos(k_y a) + \cos(k_z a)\big) \tag{2.5.25}$$

2.6 Green's Function

2.6.1 Introduction and Definition of Green's Functions

Due to their great importance in our field of interest, we will discuss Green's function in some detail. Green's function (GF) is a basic solution to a linear differential equation, a building block that can be used to construct many useful solutions. The exact form of the GF depends on the differential equation, the body shape, and the type of boundary conditions present. Green functions are named in honor of English mathematician and physicist *George Green* (1793-1841) [75]. In its basic definition it is much more complex function than the "simple" Green's function, familiar from the theory of partial differential equations, but many of its properties do bear a very close relationship to the simple function.

Suppose we start with the ground state of an N particle system($|$N>), then add a particle of spin σ to the system at $\boldsymbol{r}, t$ by applying a creation operator $\psi^{\dagger}_{\sigma}(\boldsymbol{r}, t)$ in the Heisenberg picture (Appendix A.2). The new state will be $\psi^{\dagger}_{\sigma}(\boldsymbol{r}, t)|N>$. We can construct a type of Green's function by considering the propagation of the extra particle. If we remove a particle of spin σ' at $\boldsymbol{r}', t'$ from the new state, then the overlap with the ground state should tell us something about the probability that the system is left undisturb, or alternatively, the probability that the particle propagated from $\boldsymbol{r}, t$ to $\boldsymbol{r}', t'$ with a change of spin from σ to σ' on the way, see Fig.(2.3). That is, we envisage the following train of events.

1. $|N>$: ground state of system,
2. $\psi^{\dagger}_{\sigma}(\boldsymbol{r}, t)|N>$, system with particle added at $\boldsymbol{r}, t$ with spin σ,
3. $\psi_{\sigma'}(\boldsymbol{r}', t')\psi^{\dagger}_{\sigma}(\boldsymbol{r}, t)|N>$: particle removed at $\boldsymbol{r}', t'$ with spin σ' from $N+1$ state, and
4. $< N|\psi_{\sigma'}(\boldsymbol{r}', t')\psi^{\dagger}_{\sigma}(\boldsymbol{r}, t)|N>$: overlap of system after perturbation with the original ground state.

Alternatively, we consider the propagation of a hole, described by the following train of events:

1. $|N>$,
2. $\psi_{\sigma}(\boldsymbol{r}, t)|N>$,
3. $\psi^{\dagger}_{\sigma'}(\boldsymbol{r}', t')\psi_{\sigma}(\boldsymbol{r}, t)|N>$, and
4. $< N|\psi^{\dagger}_{\sigma'}(\boldsymbol{r}', t')\psi_{\sigma}(\boldsymbol{r}, t)|N>$.

Now we define a time-ordering operator T such that

$$T[\psi_{\sigma}(\boldsymbol{r}, t)\psi^{\dagger}_{\sigma'}(\boldsymbol{r}', t')] = \begin{cases} \psi_{\sigma}(\boldsymbol{r}, t)\psi^{\dagger}_{\sigma'}(\boldsymbol{r}', t'), & t > t' \\ -\psi^{\dagger}_{\sigma'}(\boldsymbol{r}', t')\psi_{\sigma}(\boldsymbol{r}, t), & t < t' \end{cases} \tag{2.6.1}$$

The -ve sign means fermions and is designed to take care of the anti-commutators. Now both of the above sequence can be combined in a single expression for our definition of Green's function [77].

$$G_{\sigma\sigma'} = -i < N|T[\psi_{\sigma}(\boldsymbol{r}, t)\psi^{\dagger}_{\sigma'}(\boldsymbol{r}', t')]|N> \tag{2.6.2}$$

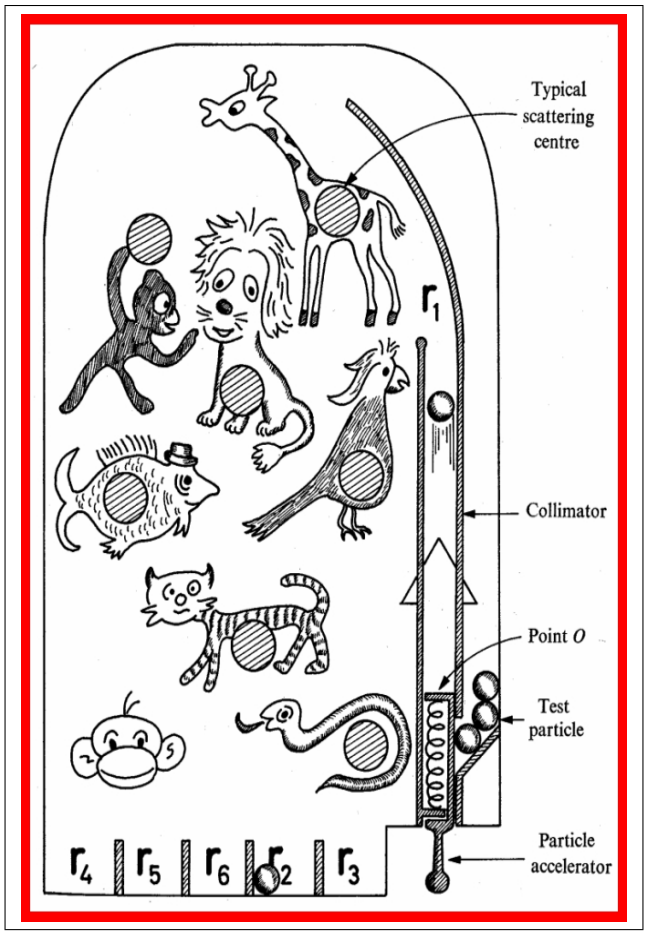

Figure 2.3: Classical analogue machine to illustrate the single-particle propagator and the vacuum amplitude [76].

Since we are interested in temperature effects. We therefor define the Green's function, as an average over all possible configurations of the system. Taking the average with respect to the grand canonical ensemble, which is particularly useful for a description of the superconducting state, the Green's function for an electron system reads[‡]

$$G(\mathbf{r}t, \mathbf{r}'t') = -i < T[\psi(\boldsymbol{r}, t)\psi^{\dagger}(\boldsymbol{r}', t')] > \tag{2.6.3}$$

$$= \frac{-i\, Tr e^{-\beta K}\Big[T\{\psi(\mathbf{r}, t)\psi^{\dagger}(\mathbf{r}', t')\}\Big]}{Tr\, e^{-\beta K}} \tag{2.6.4}$$

Where $\beta = 1/k_B T$, and $K = H - \mu N$ and K is the grand canonical Hamiltonian.

According to Mahan[78] and Economu[79] one can define six different Green's functions. The six functions are advanced G_A, retarded G_R, time-ordered G_t, anti-time-ordered $G_{\bar{t}}$, and

[‡]From here to the end we shall omit the spin symbol, unless it is required.

$G^<,\ G^>$ which have no name :

$$\begin{aligned}
G^>(\mathbf{r}t;\mathbf{r}'t') &= -i < \psi(\mathbf{r},t)\psi^\dagger(\mathbf{r}',t') > \\
G^<(\mathbf{r}t;\mathbf{r}'t') &= i < \psi^\dagger(\mathbf{r}',t')\psi(\mathbf{r},t) > \\
G_t(\mathbf{r}t;\mathbf{r}'t') &= \Theta(t-t')\ G^>(\mathbf{r}t;\mathbf{r}'t') + \Theta(t'-t)G^<(\mathbf{r}t;\mathbf{r}'t') \\
G_{\bar{t}}(\mathbf{r}t;\mathbf{r}'t') &= \Theta(t'-t)\ G^>(\mathbf{r}t;\mathbf{r}'t') + \Theta(t-t')G^<(\mathbf{r}t;\mathbf{r}'t') \\
G_R(\mathbf{r}t;\mathbf{r}'t') &= G_t - G^< = G^> - G_{\bar{t}} \\
G_A(\mathbf{r}t;\mathbf{r}'t') &= G_t - G^> = G^< - G_{\bar{t}}
\end{aligned} \tag{2.6.5}$$

The Green's functions can be written in terms of the eigenfunctions $\phi_\lambda(\mathbf{r})$ by expanding the field operators in terms of these eigenfunctions and creation $C^\dagger_\lambda$ and destruction (annihilation) C_λ operators [cf section 2.5, and Appx.A.2.1]:

$$\begin{aligned}
\psi(\mathbf{r},t) &= \sum_\lambda c_\lambda \phi_\lambda(\mathbf{r})\, e^{-i\varepsilon_\lambda t} \\
\psi^\dagger(\mathbf{r}',t') &= \sum_\lambda c^\dagger_\lambda \phi^*_\lambda(\mathbf{r}')\, e^{i\varepsilon_\lambda t'}
\end{aligned} \tag{2.6.6}$$

The Green's functions in (2.6.5) are evaluated with the occupation factor $n_\lambda =< c^\dagger_\lambda c_\lambda >$. At zero temperature[§] $n_\lambda = \Theta(-\xi_\lambda)$ is a step function that is zero or one depending upon whether $\xi_\lambda = \varepsilon_\lambda - \mu$ is positive or negative:

$$\begin{aligned}
G^>(\mathbf{r}t,\mathbf{r}'t') &= -i\sum_\lambda (1-n_\lambda)\,\phi_\lambda(\mathbf{r})\phi^*_\lambda(\mathbf{r}')e^{-i\varepsilon_\lambda(t-t')} \\
G^<(\mathbf{r}t,\mathbf{r}'t') &= i\sum_\lambda n_\lambda\phi_\lambda(\mathbf{r})\phi^*_\lambda(\mathbf{r}')e^{-i\varepsilon_\lambda(t-t')} \\
G_t(\mathbf{r}t,\mathbf{r}'t') &= -i\sum_\lambda [\Theta(t-t')-n_\lambda]\phi_\lambda(\mathbf{r})\phi^*_\lambda(\mathbf{r}')e^{-i\varepsilon_\lambda(t-t')} \\
G_{\bar{t}}(\mathbf{r}t,\mathbf{r}'t') &= -i\sum_\lambda [\Theta(t'-t)-n_\lambda]\phi_\lambda(\mathbf{r})\phi^*_\lambda(\mathbf{r}')e^{-i\varepsilon_\lambda(t-t')} \\
G_R(\mathbf{r}t,\mathbf{r}'t') &= -i\Theta(t-t')\sum_\lambda \phi_\lambda(\mathbf{r})\phi^*_\lambda(\mathbf{r}')e^{-i\varepsilon_\lambda(t-t')} \\
G_A(\mathbf{r}t,\mathbf{r}'t') &= i\Theta(t'-t)\sum_\lambda \phi_\lambda(\mathbf{r})\phi^*_\lambda(\mathbf{r}')e^{-i\varepsilon_\lambda(t-t')}.
\end{aligned} \tag{2.6.7}$$

The starting point for any calculation, at least conceptually, is the behaviour of the Green's functions for systems without interactions. Then the wave functions are those for plane wave or noninteracting Bloch states, if such can be defined. The quantum number λ becomes the wave vector $\mathbf{k}$, and a spin index σ, which is usually not written as we mentioned. The eigenvalue combination is $\phi_k(\mathbf{r}_1)\phi^\dagger_k(\mathbf{r}_2) = exp[i\mathbf{k}\cdot(\mathbf{r}_1-\mathbf{r}_2)]/\nu$. Fourier-transforming the $\mathbf{r}$-variable to $\mathbf{k}$ (section 2.1.2) gives the free particle Green's functions $G^{(0)}(\mathbf{k},t)$[¶]. For Fermions

[§]They are also valid in equilibrium at finite temperatures if $n_\lambda = 1/[exp(\beta\xi_\lambda)+1]$ is the thermodynamic average of the occupation number.

[¶]The superscript"0" or the subscript "0" on the Green's functions means to use those for a noninteracting system in equilibrium.

of band energy ε_k and occupation number $n_k = n_F(\varepsilon_k)$ they are

$$\begin{aligned} G_t^0(\mathbf{k},t) &= -i\,[\Theta(t-t') - n_{\mathbf{k}}]e^{-i\varepsilon_{\mathbf{k}}(t-t')} \\ G_{\bar{t}}^0(\mathbf{k},t) &= -i\,[\Theta(t'-t) - n_{\mathbf{k}}]e^{-i\varepsilon_{\mathbf{k}}(t-t')} \\ G_0^<(\mathbf{k},t) &= i\,n_{\mathbf{k}}\,e^{-i\varepsilon_{\mathbf{k}}(t-t')} \\ G_0^>(\mathbf{k},t) &= -i\,(1-n_{\mathbf{k}})\,e^{-i\varepsilon_{\mathbf{k}}(t-t')} \\ G_R^0(\mathbf{k},t) &= -i\,\Theta(t-t')\,e^{-i\varepsilon_{\mathbf{k}}(t-t')} \\ G_A^0(\mathbf{k},t) &= i\,\Theta(t'-t)\,e^{-i\varepsilon_{\mathbf{k}}(t-t')} \end{aligned} \tag{2.6.8}$$

The t variable can be Fourier transformed, which gives the noninteracting Green's function of frequency; the quantity δ (the convergence parameter) is infinitesimal:

$$\begin{aligned} G_R^0(\mathbf{k},\omega) &= \frac{1}{\omega - \varepsilon_{\mathbf{k}} + i\delta} \\ G_A^0(\mathbf{k},\omega) &= \frac{1}{\omega - \varepsilon_{\mathbf{k}} - i\delta} \\ G_0^<(\mathbf{k},\omega) &= 2\pi\,i\,n_{\mathbf{k}}\,\delta(\omega - \varepsilon_{\mathbf{k}}) \\ G_0^>(\mathbf{k},\omega) &= -2\pi\,i\,(1-n_{\mathbf{k}})\,\delta(\omega - \varepsilon_{\mathbf{k}}) \\ G_t^0(\mathbf{k},\omega) &= G_R + G_0^< = \frac{1}{\omega - \varepsilon_{\mathbf{k}} + i\delta_{\mathbf{k}}} \\ G_{\bar{t}}^0(\mathbf{k},\omega) &= -G_A + G_0^< = \frac{-1}{\omega - \varepsilon_{\mathbf{k}} - i\delta_{\mathbf{k}}} \end{aligned} \tag{2.6.9}$$

N.B:
-the two kinds of δ is always positive, while δ_k is positive for $k > k_F$ and negative for $k < k_F$.
-the retarded functions always have a positive δ,
-the retarded and advanced Green's functions could differ as soon as interactions are introduced, since they have different self-energy functions in degenerate Fermi systems.
-Also the expressions such $G_R = G_t - G^<$ are obeyed for interacting and noninteracting functions. They are obeyed for both cases of arguments $(\mathbf{k},t)$ and $(\mathbf{k},\omega)$.

2.6.2 Imaginary Time Green's Functions

Imaginary time is a concept derived from quantum mechanics and is essential in connecting quantum mechanics with statistical mechanics. Imaginary time τ is obtained from real time via a Wick rotation by $\pi/2$: $\tau = it$ [80].

Just for orientation, assume $t > t'$ and let us use the cyclic property of a trace (that it is unchanged by a cyclic permutation of the operators). Recalling Eq.(2.6.4) we find that

$$\begin{aligned} \bar{G}(\mathbf{r}t,\mathbf{r}'t') &= -\frac{i\,Tr[\,e^{(-\beta K)}T\{\psi(\mathbf{r},t)\psi^\dagger(\mathbf{r}',t')\}]}{Tr\;e^{(-\beta K)}} \\ &= -\frac{i\,Tr\;e^{-(\beta - it)K}\;\psi(\mathbf{r})\;e^{-i(t-t')K}\psi(\mathbf{r}')\;e^{-it'K}}{Tr\;e^{(-\beta K)}} \\ &= -\frac{i\,Tr\;e^{-\beta K}[e^{(\beta+it')K}\psi^\dagger(\mathbf{r}')\;e^{-(\beta+it')K}]\;[e^{itK}\psi(\mathbf{r})e^{-itK}]}{Tr\;e^{(-\beta K)}} \\ &= -\;G(\mathbf{r}t,\mathbf{r}'t' - i\,\beta) \end{aligned} \tag{2.6.10}$$

if in some sense we could say that $t - i\,\beta > t$. This suggests one of two possible procedures:

1. We could let $\beta \to i\gamma(1-i\eta)$, γ real, consider Green functions for imaginary temperature, and having calculated them, continue analytically to real temperature. This is essentially the procedure followed by Martin and Schwinger.

2. Alternatively, we could let $it = \tau$ and $it' = \tau'$ understanding the T product to be ordered acording to the relative sizes of τ and τ'. Then eventually we would have to continue analytically to real times (or real time differences). This is the procedure of Abrikosov *et al.* and the one we shall follow.

To be systematic, we introduce still another Green function defined most conveniently directly in terms of imaginary times[‖]:

$$\mathcal{G}(\mathbf{r}\,\tau, \mathbf{r}'\tau') = -\frac{Tr\,[e^{(-\beta K)}T\{\psi(\mathbf{r}\tau)\psi^{\dagger}(\mathbf{r}'\tau')\}]}{tr\;e^{(-\beta K)}} \tag{2.6.11}$$

Consider homogeneous time-independent systems (this is not necessary but simplifies the discussion). Then just as for (2.6.10), it is show

$$\mathcal{G}(\mathbf{r}-\mathbf{r}', \tau-\tau') = \begin{cases} -\mathcal{G}(\mathbf{r}-\mathbf{r}', \tau-\tau'-\beta) & \text{if } \tau-\tau' > 0 \text{ and } \tau-\tau'-\beta < 0, \\ -\mathcal{G}(\mathbf{r}-\mathbf{r}', \tau-\tau'+\beta) & \text{if } \tau-\tau' < 0 \text{ and } \tau-\tau'+\beta > 0. \end{cases} \tag{2.6.12}$$

Letting $\mathbf{r}-\mathbf{r}' \to \mathbf{r}$ and $\tau-\tau' \to \tau$ these are rewritten

$$\mathcal{G}(\mathbf{r}, \tau) = \begin{cases} -\mathcal{G}(\mathbf{r}, \tau-\beta) & \text{if } \tau > 0 \text{ and } \tau-\beta < 0, \\ -\mathcal{G}(\mathbf{r}, \tau+\beta) & \text{if } \tau < 0 \text{ and } \tau+\beta > 0. \end{cases} \tag{2.6.13}$$

Given $\mathcal{G}$ for $-\beta < \tau < 0$, we thus define $\mathcal{G}$ for $0 < \tau < \beta$. It is convenient to define $\mathcal{G}$ outside the interval $(-\beta, \beta)$ by requiring it to be periodic with period 2β. Expanding $\mathcal{G}(\mathbf{r}, \tau)$ in a Fourier series

$$\mathcal{G}(\mathbf{r}, \tau) = \frac{1}{\beta} \sum_{n=-\infty}^{\infty} e^{(-i\omega_n\tau)}\mathcal{G}(\mathbf{r}, \omega_n), \tag{2.6.14}$$

we must require for Matsubara frequencies ω_n that

$$\omega_n = \frac{(2n+1)\pi}{\beta}, \tag{2.6.15}$$

so that $\mathcal{G}(\mathbf{r}, \tau)$ is periodic in τ with period 2β and therefore it satisfies (2.6.13).

The expansion coefficients $\mathcal{G}(\mathbf{r}, \omega_n)$ are the analogue of the function $G(\mathbf{r}, \omega)$ at absolute zero. Inverting (2.6.14), we have

$$\mathcal{G}(\mathbf{r}, \omega_n) = \frac{1}{2} \int_{-\beta}^{\beta} \mathcal{G}(\mathbf{r}, \tau)\, e^{(i\omega_n\tau)}\, d\tau. \tag{2.6.16}$$

If we divide the integral (2.6.16) into its negative and positive regions,

$$\mathcal{G}(\omega_n) = \frac{1}{2} \Big[\int_0^{\beta} \mathcal{G}(\tau)\, e^{i\omega_n\tau}\, d\tau + \int_{-\beta}^{0} \mathcal{G}(\tau)\, e^{i\omega_n\tau}\, d\tau\Big] \tag{2.6.17}$$

[‖]To describe the Green's function at finite temperature we must introduce two new concepts. The first of these is imaginary time, $\tau = it$. Secondly we introduce the 'Heisenberg' field operators[74]

and change the variables in the second term from τ to $\tau + \beta$ this gives

$$\mathcal{G}(\omega_n) = \frac{1}{2}\,(1 - e^{i\omega_n\beta}) \int_0^\beta \mathcal{G}(\tau)\, e^{i\omega_n\tau}\, d\tau. \tag{2.6.18}$$

We get for Fermions[78]

$$\mathcal{G}(\omega_n) = \int_0^\beta \mathcal{G}(\tau)\, e^{i\omega_n\tau}\, d\tau \tag{2.6.19}$$

The momentum Green functions for noninteracting particles are[81] readily calculated (Eq.(2.6.8)) and they are

$$\begin{aligned} \mathcal{G}_0(\mathbf{k},\tau) = &\quad \frac{e^{-\varepsilon_0(\mathbf{k})\tau}}{1 + e^{-\beta\varepsilon_0(\mathbf{k})}}, \quad \beta > \tau > 0 \\ = &- \frac{e^{-\varepsilon_0(\mathbf{k})\tau}}{1 + e^{\beta\varepsilon_0(\mathbf{k})}}, \quad -\beta < \tau < 0 \end{aligned} \tag{2.6.20}$$

and

$$\mathcal{G}_0(\mathbf{k},\omega_n) = \frac{1}{i\omega_n - \{\varepsilon_0(\mathbf{k})\}}. \tag{2.6.21}$$

The connection between the functions $\mathcal{G}_0(\omega_n)$ and $G_R^{(0)}(\omega)$:

Comparing Eq.(2.6.21) and Eq.(2.6.9), we see that $i\omega_n$ in $\mathcal{G}_0(\omega_n)$ is equivalent to $\omega + i\delta$ in $G_R^{(0)}(\omega)$, so we can obtain the retarded Green's function from $\mathcal{G}_0(\omega_n)$ just by replacing $i\omega_n$ everywhere by $\omega + i\delta$. This called analytical continuation.

2.6.3 Spectral Function

Another quantity of great importance is the *spectral function* $A(\mathbf{k},\omega)$, which is also called the *spectral density function*. The retarded G_R^0 and advanced Green's functions G_A^0 are given by Eq.(2.6.9) and they are

$$\underset{A}{G_R^0} = \frac{1}{\Big(\omega - \varepsilon_k \pm i\delta\Big)} \tag{2.6.22}$$

By subtracting, we obtain

$$[G_R^0 - G_A^0] = \lim_{\delta\to 0}\Big[\frac{1}{\omega - \varepsilon_k + i\delta} - \frac{1}{\omega - \varepsilon_k - i\delta}\Big] \tag{2.6.23}$$

Now recall the Dirac relation

$$\lim_{\delta\to 0}\frac{1}{r \pm i\delta} = \mathcal{P}\Big(\frac{1}{r}\Big) \mp i\pi\delta(r) \tag{2.6.24}$$

where $\mathcal{P}$ denotes principle part. Employing this relation in Eq.(2.6.23) gives

$$A(\mathbf{k},\omega) \equiv i[G_R^0 - G_A^0] = 2\pi\delta\Big(\omega - \varepsilon_k\Big) \equiv -2Im\, G_R^0 \tag{2.6.25}$$

This form is generally known as the *spectral function* as it displays the dispersion relation of ω and k [78; 82].

Features of the Spectral function:

1. $A(\mathbf{k},\omega) \geq 0$
   This positiveness is an important feature, since we shall interpret $A(\mathbf{k},\omega)$ as a probability function.

2. Another important feature of the electron spectral function is obtained by integrating overall frequencies [78]:
$$1 = \int_{-\infty}^{\infty} \frac{d\omega}{2\pi} A(\mathbf{k},\omega)$$

2.6.4 Causal Green's Functions

Causality in general is that the effect cannot precede the cause. A scattered wave cannot be emitted by the scattering center before the incident wave has arrived. For linear systems the most general relation between an input function D (the cause) and an output function Y (the effect) may be written as
$$Y(t) = \int_{-\infty}^{\infty} I(t-t')D(t') \tag{2.6.26}$$
Causality is imposed by requiring that [69]
$$I(t-t') = 0 \qquad \text{for } \; t-t' < 0. \tag{2.6.27}$$
A causal Greens function is zero when $t-t' \leq 0$. From (2.6.7) we see that the retarded Green's function $G_R(\mathbf{r}t,\mathbf{r}'t')$ is the causal Green's function. Causality also shows up as a property in the complex plane. If the Fourier transform with respect to time is denoted by $G_R(\omega)$, then we have
$$G_R(t-t') = \frac{1}{2\pi}\int_{-\infty}^{\infty} e^{-i\omega(t-t')} G_R(\omega) d\omega. \tag{2.6.28}$$
For $t-t' > 0$ we can perform the Fourier transform by closing the contour in the upper half plane (Fig.(2.1)),
$$G_R(t-t') = i\sum \text{residues in upper half plane..} \tag{2.6.29}$$
Thus we see that Green's functions that are analytic in the upper half plane are causal. In contrast to causal, or retarded Greens functions, there are advanced Greens functions which are zero for $t-t' > 0$ and non-zero for $t-t' < 0$. These functions are analytic on the lower half plane [66].

2.6.5 Equation of Motion for Green's Functions

Suppose we measure the one-particle energies from the energy μ [81], then the Hamiltonian will be
$$\begin{aligned} K = &\int d^3r\, \psi^\dagger(\mathbf{r})\Big(-\frac{\nabla^2}{2m} - \mu + u(\mathbf{r})\Big)\psi(\mathbf{r}) + \\ &\frac{1}{2}\int d^3r\, d^3r' \psi^\dagger(\mathbf{r}')\psi^\dagger(\mathbf{r}) V(|\mathbf{r}'-\mathbf{r}|)\psi(\mathbf{r})\psi(\mathbf{r}') \qquad (2.6.30) \\ =&(H_0 - \mu N) + H' \qquad (2.6.31) \end{aligned}$$
Where $u(\mathbf{r})$ is the one-particle potential (external potential).

Using the equations of motion for the Heisenberg operator, as seen in Appendix A.2, one can derive the equations of motion for the Green's functions. We start with the equation of motion for the Heisenberg operator ψ[**]:

$$\frac{\partial}{\partial\tau}\psi(\boldsymbol{r},\tau)+\Big(\frac{\nabla^2}{2m}+\mu-u(\mathbf{r})\Big)\psi(\boldsymbol{r},\tau)=[\psi(\boldsymbol{r},\tau),H'], \tag{2.6.32}$$

If the interaction H' is independent of the spin variable and is given by

$$H'=\frac{1}{2}\int d^3r\,d^3r'\psi^\dagger(r')\psi^\dagger(r)V(|r'-r|)\psi(r)\psi(r'), \tag{2.5.16}$$

then

$$[\psi,H']=\int d^3r'\,V(|r'-r|)\psi^\dagger(r')\psi(r')\psi(r) \tag{2.6.33}$$

Therefore

$$\frac{\partial}{\partial\tau}\psi(\boldsymbol{r},\tau)+\Big(\frac{\nabla^2}{2m}+\mu\Big)\psi(\boldsymbol{r},\tau)=\int d^3r'\,V(|r'-r|)\psi^\dagger(r')\psi(r')\psi(r). \tag{2.6.34}$$

Rewriting the term $<\cdots>$ in Eq.(2.6.4) in an explicit form, we have

$$\begin{aligned}<T\psi(\boldsymbol{r},\tau)\psi^\dagger(\boldsymbol{r}',0)>=&<\psi(\boldsymbol{r},\tau)\psi^\dagger(\boldsymbol{r}',0)>\Theta(\tau)\\&-<\psi^\dagger(\boldsymbol{r}',0)\psi(\boldsymbol{r},\tau)>\Theta(-\tau),\end{aligned} \tag{2.6.35}$$

where $\Theta(\tau)=1$ for $\tau>0$ and $\Theta(\tau)=0$ for $\tau<0$. Differentiating Eq.(2.6.35) w.r.to time [70], we find

$$\begin{aligned}\frac{\partial}{\partial\tau}G(\boldsymbol{r},\boldsymbol{r}',\tau)=&\frac{\partial}{\partial\tau}[-<\psi(\boldsymbol{r},\tau)\psi^\dagger(\boldsymbol{r}',0)>\Theta(\tau)+<\psi^\dagger(\boldsymbol{r}',0)\psi(\boldsymbol{r},\tau)>\Theta(-\tau)]\\=&-\big\langle\frac{\partial}{\partial\tau}\psi(\boldsymbol{r},\tau)\psi^\dagger(\boldsymbol{r}',0)\big\rangle\Theta(\tau)+\big\langle\psi^\dagger(\boldsymbol{r}',0)\frac{\partial}{\partial\tau}\psi(\boldsymbol{r},\tau)\big\rangle\Theta(-\tau)\\&-<\psi(\boldsymbol{r},\tau)\psi^\dagger(\boldsymbol{r}',0)>\delta(\tau)-<\psi^\dagger(\boldsymbol{r}',0)\psi(\boldsymbol{r},\tau)]>\delta(\tau)\\=&-\big\langle T\big(\frac{\partial}{\partial\tau}\psi(\boldsymbol{r},\tau)\psi^\dagger(\boldsymbol{r}',0)\big)\big\rangle-\underbrace{<\{\psi(\boldsymbol{r}),\psi(\boldsymbol{r}')\}>}_{\delta(\boldsymbol{r}-\boldsymbol{r}')}\delta(\tau)\end{aligned} \tag{2.6.36}$$

Thus

$$[\frac{\partial}{\partial\tau}+\frac{\nabla^2}{2m}+\mu-u(\mathbf{r})]G(\boldsymbol{r},\boldsymbol{r}',\tau)]=\delta(\boldsymbol{r}-\boldsymbol{r}')\delta(\tau)-i<T[\psi(\boldsymbol{r},\tau),H']\psi^\dagger(\boldsymbol{r}',0)> \tag{2.6.37}$$

A statistical average over 4-field operators appears [83].

$$G(1234)=<T(\psi(1)\psi(2)\psi^\dagger(3)\psi^\dagger(4))>,$$

where 1,2 etc. represent $(\mathbf{r},t),(\mathbf{r}',t')$, etc. Eq.(2.6.37) becomes

$$\begin{aligned}[\frac{\partial}{\partial\tau}+\frac{\nabla^2}{2m}+\mu-u(\mathbf{r})]G(\boldsymbol{r},\boldsymbol{r}',\tau)]=&\delta(\boldsymbol{r}-\boldsymbol{r}')\delta(\tau)\\&-i\int dr''V(|r-r'|)K(r''\tau,r\tau,r'\tau,r''\tau_+)\end{aligned} \tag{2.6.38}$$

[**] ψ will be written in Heisenberg picture

Thus, as we see the Green's functions form a hierarchy of equations: In order to determine the one-particle Green's function, one needs the two-particle Green's function, and so on [70; 83]. Omit the two-particle interaction, we find

$$[\frac{\partial}{\partial\tau}+\frac{\nabla^2}{2m}+\mu-u(\mathbf{r})]G(\boldsymbol{r},\boldsymbol{r}',\tau)=\delta(\boldsymbol{r}-\boldsymbol{r}')\delta(\tau) \tag{2.6.39}$$

Fourier transform the last equation with respect to τ, we get

$$[i\omega_n+\frac{\nabla^2}{2m}+\mu-u(\boldsymbol{r})]G(\boldsymbol{r}-\boldsymbol{r}')=\delta(\boldsymbol{r}-\boldsymbol{r}') \tag{2.6.40}$$

Consider the simpler case where $u(\mathbf{r})=0$

$$[i\omega_n+\frac{\nabla^2}{2m}+\mu]G^0(\boldsymbol{r}-\boldsymbol{r}')=\delta(\boldsymbol{r}-\boldsymbol{r}') \tag{2.6.41}$$

G^0 can be used to rewrite the equation for G in the form of an integral equation [83]:

$$G(\boldsymbol{r},\boldsymbol{r}'',\omega_n)=G^0(\boldsymbol{r}-\boldsymbol{r}'',\omega_n)+\int dr'G^0(\boldsymbol{r}-\boldsymbol{r}',\omega_n)V(\boldsymbol{r}')G(\boldsymbol{r}',\boldsymbol{r}'',\omega_n). \tag{2.6.42}$$

As will be shown in section (2.7) on scattering.

2.7 Scattering Theory In Language Of Bloch Function And Green's Function

The time-independent Schrödinger equation

$$[H_0(\mathbf{r}) + V(\mathbf{r})]\psi_{n,\mathbf{k}}(\mathbf{r}) = \varepsilon_{n,\mathbf{k}}\psi_{n,\mathbf{k}}(\mathbf{r})$$

for a particle scattered by some random defect potential $V(\mathbf{r})$ can be transformed to an integral equation

$$\psi_{n,\mathbf{k}}(\mathbf{r}) = \phi_{n,\mathbf{k}}(\mathbf{r}) + \int d^D r'\, G^0_{n,\mathbf{k}}(\mathbf{r},\mathbf{r}')V(\mathbf{r}')\psi_{n,\mathbf{k}}(\mathbf{r}') \tag{2.7.1}$$

with the help of the Green function for the clean system

$$[\varepsilon_{n,\mathbf{k}} - H_0(\mathbf{r})]\, G^0_{n,\mathbf{k}}(\mathbf{r},\mathbf{r}') = \delta(\mathbf{r}-\mathbf{r}'). \tag{2.7.2}$$

We have allowed for the possibility that a periodic lattice potential is incorporated in H_0. The eigenfunctions of H_0 are Bloch functions $\phi_{n,\mathbf{k}}(\mathbf{r})$ n is the band index and k the quasi-momentum from the 1st Brillouin zone.
Eq. (2.7.2) is solved by

$$G^0_{n,\mathbf{k}}(\mathbf{r},\mathbf{r}') = \sum_m \int \frac{d^D p}{(2\pi)^D}\, \phi_{m,\mathbf{p}}(\mathbf{r})\phi^*_{m,\mathbf{p}}(\mathbf{r}')G^0_{n,\mathbf{k}}(m,\mathbf{p}) \tag{2.7.3a}$$

with

$$G^0_{n,\mathbf{k}}(m,\mathbf{p}) = \frac{1}{\varepsilon_{n,\mathbf{k}} - \varepsilon_{m,\mathbf{p}}} \tag{2.7.3b}$$

When this representation of the Green's function is inserted in (2.7.1) we obtain

$$\psi_{n,\mathbf{k}}(\mathbf{r}) = \phi_{n,\mathbf{k}}(\mathbf{r}) + \sum_m \int \frac{d^D p}{(2\pi)^D}\, \phi_{m,\mathbf{p}}(\mathbf{r})G^0_{n,\mathbf{k}}(m,\mathbf{p})T(m,\mathbf{p};n,\mathbf{k}). \tag{2.7.4}$$

Here we have defined the T-matrix

$$T_{m,n}(\mathbf{p},\mathbf{k}) = \int d^D r'\, \phi^*_{m,\mathbf{p}}V(\mathbf{r}')\psi_{n,\mathbf{k}}(\mathbf{r}'). \tag{2.7.5}$$

The Lippmann-Schwinger equation, from which the T-matrix can be calculated, is obtained by multiplying (2.7.4) by $\phi_{n',\mathbf{k}'}(\mathbf{r})V(\mathbf{r})$ and then integrating with respect to $d^D r$:

$$T_{n',n}(\mathbf{k}',\mathbf{k}) = V_{n',n}(\mathbf{k}',\mathbf{k}) + \sum_m \int \frac{d^D p}{(2\pi)^D}\, V_{n',m}(\mathbf{k}',\mathbf{p})G^0_{n,\mathbf{k}}(m,\mathbf{p})T_{m,n}(\mathbf{p},\mathbf{k}). \tag{2.7.6}$$

$V_{n',n}(\mathbf{k}',\mathbf{k})$ is the matrix element

$$V_{n',n}(\mathbf{k}',\mathbf{k}) = \int d^D r'\, \phi^*_{n',\mathbf{k}'}V(\mathbf{r}')\phi_{n,\mathbf{k}}(\mathbf{r}'). \tag{2.7.7}$$

of the scattering potential with respect to Bloch functions.

The set of equations ((2.7.4),(2.7.6)) gives the exact solution for the wave function of a particle propagating in a crystal lattice which contains random defects. In analogy to (2.7.3) these wave functions can be used to construct the Green function for the system containing defects:

$$G_\varepsilon(\mathbf{r},\mathbf{r}') = \sum_m \int \frac{d^D p}{(2\pi)^D} \frac{\psi_{m,\mathbf{p}}(\mathbf{r}')\psi_{m,\mathbf{p}}(\mathbf{r}')}{\varepsilon + i\delta - \varepsilon_{m,\mathbf{p}}} \tag{2.7.8}$$

Taking the imaginary part essentially gives the local density of states.
Alternatively, the equation of motion for Green function leads to

$$G_\varepsilon(\mathbf{r},\mathbf{r}') = G^0_\varepsilon(\mathbf{r},\mathbf{r}') + \int d^D\rho\, G^0_\varepsilon(\mathbf{r},\boldsymbol{\rho})V(\boldsymbol{\rho})G_\varepsilon(\boldsymbol{\rho},\mathbf{r}') \tag{2.7.9a}$$

which we rewrite as

$$G_\varepsilon(\mathbf{r},\mathbf{r}') = G^0_\varepsilon(\mathbf{r},\mathbf{r}') + \int d^D\rho \int d^D\rho'\, G^0_\varepsilon(\mathbf{r},\rho)T^\varepsilon(\rho,\rho')G_\varepsilon(\rho,\mathbf{r}'), \tag{2.7.9b}$$

defining a generalized T-matrix. An equation for this quantity can be derived by operating with $\varepsilon - H_0(\mathbf{r}) - V(\mathbf{r})$ on both sides of (2.7.9b) and using (2.7.2):

$$T^\varepsilon(\mathbf{r},\mathbf{r}') = V(\mathbf{r})\delta(\mathbf{r}-\mathbf{r}') + V(\mathbf{r}) \int d^D\rho\, G^0_\varepsilon(\mathbf{r},\rho)T^\varepsilon(\rho,\mathbf{r}') \tag{2.7.10}$$

Defining

$$T^\varepsilon_{n',n}(\mathbf{k}',\mathbf{k}) = \int d^D\, r \int d^D\, r'\, \phi^*_{n',\mathbf{k}'}(\mathbf{r})T(\mathbf{r},\mathbf{r}')\phi_{n,\mathbf{k}}(\mathbf{r}') \tag{2.7.11}$$

we arrive at

$$T^\varepsilon_{n',n}(\mathbf{k}',\mathbf{k}) = V_{n',n}(\mathbf{k}',\mathbf{k}) + \sum_m \int \frac{d^D p}{(2\pi)^D}\, V_{n',m}(\mathbf{k}',\mathbf{p})G^0_\varepsilon(m,\mathbf{p})T^\varepsilon_{m,n}(\mathbf{p},\mathbf{k}). \tag{2.7.12}$$

Comparison with (2.7.6) shows that this generalized T-matrix reduces to the T-matrix used in scattering theory when $\varepsilon = \varepsilon_{n,\mathbf{k}}$.
With (2.7.3) and the definition (2.7.11) we can rewrite the equation (2.7.9b) for the Green function as

$$G_\varepsilon(\mathbf{r},\mathbf{r}') = G^0_\varepsilon(\mathbf{r},\mathbf{r}') + \sum_{m,n}\int \frac{d^D k}{(2\pi)^D} \int \frac{d^D k'}{(2\pi)^D}\phi_{m,\mathbf{k}}(\mathbf{r})G^0_\varepsilon(m,\mathbf{k})T^\varepsilon_{m,n}(\mathbf{k},\mathbf{k}')G^0_\varepsilon(n,\mathbf{k}')\phi^*_{m,\mathbf{k}'}(\mathbf{r}'). \tag{2.7.13}$$

From this, the LDOS near a single impurity could also be obtained [83].

SCTMA
Empty lattice

We shall restrict our discussion to the empty lattice so that the undisturbed wave functions are plane waves and the energy $\varepsilon_\mathbf{k}$ of the elastically scattered particle is

$$\varepsilon_\mathbf{k} = \frac{k^2}{2\mu} \tag{2.7.14}$$

independent of the direction of $\mathbf{k}$. The range of momenta is unrestricted and the band index is redundant. The solution for the Green's function thus reads

$$G_k^0(\mathbf{r},\mathbf{r}') = \int \frac{d^D p}{(2\pi)^D} \frac{e^{i\mathbf{p}\cdot(\mathbf{r}-\mathbf{r}')}}{\frac{k^2}{2\mu} - \frac{p^2}{2\mu}} \tag{2.7.15}$$

The wave function of the scattered particle is given by

$$\psi_{\mathbf{k}}(\mathbf{r}) = e^{i\mathbf{k}\cdot\mathbf{r}} + \int d^D r'\, G_{\mathbf{k}}^0(\mathbf{r},\mathbf{r}') V(\mathbf{r}') \psi_{\mathbf{k}}(\mathbf{r}') \tag{2.7.16a}$$

$$= e^{i\mathbf{k}\cdot\mathbf{r}} + \int \frac{d^D\, p}{(2\pi)^D} e^{i\mathbf{p}\cdot\mathbf{r}} G_{\mathbf{k}}^0(p) T(\mathbf{p},\mathbf{k}) \tag{2.7.16b}$$

and the Lippmann-Schwinger equation reduces to

$$T(\mathbf{k}',\mathbf{k}) = V(\mathbf{k}'-\mathbf{k}) + \int \frac{d^D p}{(2\pi)^D} V(\mathbf{k}'-\mathbf{p}) G_k^0(p) T(\mathbf{p},\mathbf{k}) \tag{2.7.17}$$

The only difference to the previous form of this equation is that the matrix element of the scattering potential is a function of $\mathbf{k}'-\mathbf{k}$.

Solving (2.7.17) can be simplified if only a single defect, described by a spherically symmetric potential $v(r)$ is considered. Then the T-matrix can only depend on the moduli of $\mathbf{p}$ and $\mathbf{k}$ and the angle between them, even when these vectors belong to different energies. In the case of two dimensions, which is of primary interest here, (2.7.17) can thus be rewritten as

$$\begin{aligned} T(k',k,\cos\varphi) = {} & v(k',k,\cos\varphi) + \\ & \int_0^\infty \frac{dp\, p}{2\pi} \int_0^{2\pi} \frac{d\theta}{(2\pi)} v(k',p,\cos(\varphi-\theta)) G_k^0(p) T(p,k,\cos\theta) \end{aligned} \tag{2.7.18}$$

Expanding T and v into Fourier series

$$T(k',k,\cos\varphi) = T_0(k',k) + 2\sum_{m=1}^{\infty} T_m(k',k)\cos m\varphi \tag{2.7.19}$$

leads to a set of decoupled one-dimensional integral equations for the Fourier coefficients [83]

$$T_m(k',k) = v_m(k',k) + \int_0^\infty \frac{dp\, p}{2\pi} v_m(k',p) G_k^0(p) T_m(p,k). \tag{2.7.20}$$

Solution of the T-matrix equation: δ-function potential

The most widely used model for a single, spherically symmetric defect is $v(r) = \bar{v}\delta(r)$. Note that $\bar{v}$ is the maximum of the potential times some effective area. The Fourier transform $\bar{v}$ of $v(r)$ is constant and, in particular, independent of the scattering angle. Hence, only the zeroth Fourier coefficient T_0 is different from zero which corresponds to pure s-wave scattering, as expected. However, the assumption $v_0(k',k) = \bar{v}$ also renders $T_0(k',k)$ independent of the first variable so that (2.7.20) is no longer an integral equation. One immediately arrives at the solution

$$T_0(k) = \frac{1}{\frac{1}{\bar{v}} - \int_0^\infty \frac{dp\, p}{2\pi} G_k^0(p)} \tag{2.7.21}$$

The remaining k-dependence of T_0, usually written in terms of an energy $\omega = \frac{k^2}{2m} - \varepsilon_F$ relative to the chemical potential, is absolutely essential in the theory of superconductivity. The remaining integral in Eq.(2.7.21) is divided into real and imaginary parts [83]:

$$\int_0^\infty \frac{dp\,p}{2\pi} G_k^0(p) = \mathcal{P}\int_0^\infty \frac{dp\,p}{2\pi} ReG_k^0(p) - i\pi N(\varepsilon(k)) \tag{2.7.22}$$

Eq.(2.7.22) will be being used in chapter3 to get both the density of states $(N(\omega))$ and its Hilbert transform $F(\omega)(= ReG_k^0(p))$.

2.8 Dynamics correlation and response functions

Much of what we observe in nature is either time- or frequency-dependent. We will introduce a language to describe time- and frequency-dependent phenomena in condensed matter systems near thermal equilibrium. We will focus on linear response to time-dependent external fields. These functions (dynamics correlation and response functions) contain information about the nature of dynamical modes, e.g., the imaginary part of the response function is a measure of the rate of dissipation of energy of external forces. The possibility of this linear expansion implies, of course, an inherent stability in the system being tested [84]

A knowledge of the equations of motion in the presence of external forces is sufficient to determine dynamical response functions[85].

2.8.1 Linear Response Theory

As mentioned above we drive the system with an external field and measures the response of the system. The external field couples to the system via some operator B and we measure the *average value* of some other operator A of the system, as schematically illustrated in Fig.2.4.

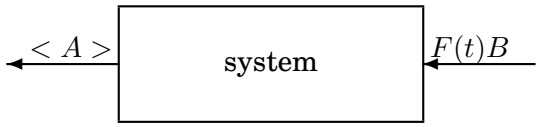

Figure 2.4: The driven response of a system

Typical examples are the application of a frequency-dependent electric field and measuring the induced electric moment, which gives the polarisability, or when we determine the frequency-dependent magnetic susceptibility by measuring the induced moment when applying an external magnetic field.

We wish to calculate the forced motion of some dynamical variable A. The total *Hamiltonian* of the system is

$$H(t) = H_0 + H'(t), \tag{2.8.1}$$

we shall consider the case where the perturbation has the form[86]

$$H'(t) = -\int d^3r B(\boldsymbol{r}')F(\boldsymbol{r}', t) \tag{2.8.2}$$

where $F(\boldsymbol{r}', t)$ is a real or complex function, e.g, a component of the vector potential $\mathbf{A}(\mathbf{r}', t)$.

We consider the average

$$< A >= Tr(\rho A). \tag{2.8.3}$$

over a statistical distribution given by a density matrix

$$\rho = \sum_n P_n |n >< n|. \tag{2.8.4}$$

The statistical weights P_n are assumed to be time-independent while the state vectors $|n>$ evolve according to the Schrödinger equation. This leads to (see AppendixA.4)

$$i\frac{\partial\rho(t)}{\partial t} = [H, \rho(t)] \tag{2.8.5}$$

Transforming into the *interaction picture*, according to Appendix A.3, we get

$$i\frac{\partial\rho_I(t)}{\partial t} = [H'_I(t), \rho_I(t)] \tag{2.8.6}$$

We shall assume that the external field has been switched on adiabatically at $t = -\infty$, and this can be taken care of by multiplying F by a factor $e^{\delta t}$, δ being a positive infinitesimal. Then $H'(t)$ at $t = -\infty$ is zero so $\rho = \rho(H_0)$. So that

$$\rho_I(t)|_{t\to-\infty} = \rho_0.$$

Upon integration we thus have

$$\rho_I(t) = \rho_0 - i\int_{-\infty}^{t} dt'[H'_I(t'), \rho_I(t)] \tag{2.8.7}$$

Since we are only interested in terms linear in $H'_I(t)$ [87], we may write

$$\rho_I(t) = \rho_0 + \Delta\rho_I(t) \tag{2.8.8}$$

and drop terms like $[H'(t'), \Delta\rho]$, so that the equation for $\rho_I(t)$ becomes

$$\rho_I(t) = \rho_0 - i\int_{-\infty}^{t} dt'[H'_I(t'), \rho_0]. \tag{2.8.9}$$

The average $< A >$ in linear response is then given by:

$$\begin{aligned} < A > &= Tr[\rho A] = Tr[\rho_I(t)A_I(t)] \\ &= Tr(\rho_0 A) - Tr\Big(i\int_{-\infty}^{t} dt'[H'_I(t'), \rho_0]A_I(t)\Big) \end{aligned}$$

upon cyclic invariance of the trace

$$\begin{aligned} < A > &= Tr(\rho_0 A) - Tr\Big(i\int_{-\infty}^{t} dt'[A_I(t), H'_I(t')]\rho_0\Big) \\ &= < A >_0 - Tr\Big(i\int_{-\infty}^{t} dt'[A_I(t), H'_I(t')]\rho_0\Big). \end{aligned} \tag{2.8.10}$$

The first term in this equation is merely the equilibrium expectation value $\langle A\rangle_0$ in the absence of the external field, and the second term reflects the effects of the external potential to lowest (i.e., linear) order in $F(\mathbf{r}', t)$.

$$\begin{aligned} < A > &= < A >_0 + i\,Tr\int_{-\infty}^{t} dt' \int d^3r'\rho_0[A_I(\mathbf{r}, t), B_I(\mathbf{r}', t')]F(\mathbf{r}', t') \\ &= < A >_0 + i\int_{-\infty}^{t} dt' \int d^3r' < [A_I(\mathbf{r}, t), B_I(\mathbf{r}', t')] >_0 F(\mathbf{r}', t') \end{aligned}$$

upon cyclic invariance of the trace

$$= < A >_0 + i \int_{-\infty}^{t} dt' \int d^3r' < [A_I(\mathbf{r}, t-t'), B_I(\mathbf{r}', 0)] >_0 F(\mathbf{r}', t') \tag{2.8.11}$$

$$< A >= < A >_0 + \int_{-\infty}^{t} dt' \int d^3r' \phi_{AB}(\mathbf{r}, \mathbf{r}', t-t') F(\mathbf{r}', t') \tag{2.8.12}$$

where, $\phi_{AB}(\boldsymbol{r}, r', t-t') = i < [A_I(\boldsymbol{r}, t-t'), B_I(\boldsymbol{r}', 0)] >_0$.

In case of a uniform system, i.e. translational invariant system,

$$\begin{aligned} \phi_{AB}(\mathbf{r}, \mathbf{r}', t-t') &= i < [A_I(\boldsymbol{r}, t-t'), B_I(\boldsymbol{r}', 0)] > \\ &= \phi_{AB}(\mathbf{r} - \mathbf{r}', t-t') \end{aligned} \tag{2.8.13}$$

then

$$\Delta < A > (\boldsymbol{r}, t) = \int_{-\infty}^{t} dt' \int d^3r' \phi_{AB}(\mathbf{r} - \mathbf{r}', t-t') F(\boldsymbol{r}', t') \tag{2.8.14}$$

The integral in (2.8.14) is simply a four-dimensional convolution. Thus its Fourier transform, see section 2.1.2, is

$$\Delta < A > (\mathbf{k}, \omega) = \chi_{AB}(\mathbf{k}, \omega)\ F(\mathbf{k}, \omega) \tag{2.8.15}$$

The function χ_{AB} is called the *generalized susceptibility* [83; 88], and it is defined by

$$\chi_{AB}(\mathbf{k}, \omega) = \int_{-\infty}^{t} dt' \int d^3r'\ \phi_{AB}(\mathbf{r} - \mathbf{r}', t-t')\ e^{-i\mathbf{k}\cdot(\mathbf{r}-\mathbf{r}')} e^{i\omega(t-t')}, \tag{2.8.16}$$

using Eq.(2.8.13) into Eq.(2.8.16) $\chi_{AB}(\mathbf{k}, \omega)$ becomes

$$\chi_{AB}(\mathbf{k}, \omega) = i \int_{-\infty}^{t} dt' \int d^3r'\ < [A_I(\boldsymbol{r}, t-t'), B_I(\boldsymbol{r}', 0)] >\ e^{-i\mathbf{k}\cdot(\mathbf{r}-\mathbf{r}')} e^{i\omega(t-t')}. \tag{2.8.17}$$

Substituting $t - t' = t_1$ and omit the subscript I, $\chi_{AB}(\mathbf{k}, \omega)$ becomes

$$\chi_{AB}(\mathbf{k}, \omega) = i \int_{0}^{\infty} dt_1 \int d^3r'\ < [A(\boldsymbol{r}, t_1), B(\boldsymbol{r}', 0)] >\ e^{-i\mathbf{k}\cdot(\mathbf{r}-\mathbf{r}')} e^{i\omega t_1}, \tag{2.8.18}$$

Because of the analyticity of the function $\phi_{AB}(t_1)$ in the complex time plane. $\chi_{AB}(\mathbf{k}, \omega)$ becomes very simple when we choose for ω the complex frequency $\nu_m = 2\pi m/\beta = 2\pi m T$, $m \in \mathbb{Z}$

$$\chi_{AB}(\mathbf{k}, i\nu_m) = \int_{0}^{\frac{1}{T}} d\tau \int d^3r'\ < A(\boldsymbol{r}, \tau) B(\boldsymbol{r}', 0) >\ e^{-i\mathbf{k}\cdot(\mathbf{r}-\mathbf{r}')} e^{i\nu_m \tau} \tag{2.8.19}$$

2.8.2 Kubo Formula for Conductivity

Kubo formulas are the name applied to the correlation function which describes the linear response. There are many of them, since there are many possible perturbations and many linear responses for each perturbation. Formulas of this type were first proposed by *Green*(1952,1954) for transport in liquids. *Kubo*(1959) first derived the equations for electrical conductivity in solids [78].

The *Kubo* formula for the transverse conductivity is obtained from linear response theory, when the perturbation is an electric field which can be expressed in terms of a vector potential alone:

$$\mathcal{E} = -\frac{\partial}{\partial t}\mathbf{A}(\mathbf{r},t) \tag{2.8.20}$$

2.8.2.1 Transverse Electrical Conductivity

The classical electric current density of a set of point charges $-e$ moving with velocities $\mathbf{v}_i$ is given by

$$\mathbf{J}(\mathbf{r}) = -e\sum_i \mathbf{v}_i\,\delta(\mathbf{r}-\mathbf{r}_i) \tag{2.8.21}$$

$$\mathbf{v}_i = \frac{1}{m}(\mathbf{p}_i + e\mathbf{A}(\mathbf{r}_i,t)) \tag{2.8.22}$$

$\mathbf{v}_i$ is replaced by the operator $\frac{1}{m}(\mathbf{p}_i + e\mathbf{A}(\mathbf{r}_i,t))$. To ensure that $\mathbf{J}(\mathbf{r})$ is a hermitian operator, Eq.(2.8.21) has to be symmetrized. $\mathbf{J(r)}$ in the second quantization language is

$$\mathbf{J}(\mathbf{r}) = \frac{-e}{2m}\int d\mathbf{r}'\sum_\sigma \psi^\dagger_\sigma(\mathbf{r}')\Big[(\mathbf{p}+e\mathbf{A}(\mathbf{r}',t))\,\delta(\mathbf{r}-\mathbf{r}') + \delta(\mathbf{r}-\mathbf{r}')(\mathbf{p}+e\mathbf{A}(\mathbf{r}',t))\Big]\psi_\sigma(\mathbf{r}') \tag{2.8.23}$$

$$= -e\Big[\mathbf{j}(\mathbf{r}) + \frac{e}{m}\mathbf{A}(\mathbf{r},t)n(\mathbf{r})\Big] \tag{2.8.24}$$

with the current density operator $\mathbf{j(r)}$ given by

$$\mathbf{j}(\mathbf{r}) = \frac{1}{2mi}\sum_\sigma [\psi^\dagger_\sigma(\mathbf{r})(\nabla\psi_\sigma(\mathbf{r})) - (\nabla\psi^\dagger_\sigma(\mathbf{r}))\psi_\sigma(\mathbf{r})] \tag{2.8.25}$$

or

$$\mathbf{j}(\mathbf{r}) = \frac{1}{2mi}\sum_\sigma (\boldsymbol{\nabla}-\boldsymbol{\nabla'})\psi^\dagger_\sigma(\mathbf{r}')\psi_\sigma(\mathbf{r})|_{\mathbf{r}'=\mathbf{r}}. \tag{2.8.26}$$

The second form is useful when expressing the expectation value of the current density in terms of Green's functions. The Hamiltonian of the system in the presence of the vector potential is given by

$$H = \frac{1}{2m}\sum_i (\mathbf{p_i} + e\mathbf{A}(\mathbf{r}_i,t))^2 = \sum_i\Big[\frac{1}{2m}p_i^2 + \frac{e}{2m}(\mathbf{p}_i\cdot\mathbf{A}+\mathbf{A}\cdot\mathbf{p}_i) + \frac{e^2}{2m}\mathbf{A}\cdot\mathbf{A}\Big]$$
$$= H_0 + H'(t)$$

In addition to the kinetic energy H_0 must, at least, contain a random potential responsibile for a finite resistance and the superconducting pairing interaction. Because we are interested in linear response we neglect the term $(\mathbf{A}\cdot\mathbf{A})$, so that

$$H' = \frac{e}{2m}\sum_i (\mathbf{p}_i\cdot\mathbf{A}+\mathbf{A}\cdot\mathbf{p}_i)$$

In the second quantization form $H'(t)$ reads

$$H'(t) = e \int d\mathbf{r}' \mathbf{j}(\mathbf{r}') \cdot \mathbf{A}(\mathbf{r}', t) \tag{2.8.27}$$

This is of the form 2.8.2 when we identify $B(\mathbf{r}')$ with the negative of a cartesion coordinate of the current operator $\mathbf{j}(\mathbf{r})$ (2.8.25) or (2.8.26). Inserting $\mathbf{J}(\mathbf{r})$ from Eq.(2.8.23) into the equation (2.8.11) of linear response theory gives

$$< J_\alpha > (\mathbf{r}, t) = -\frac{e^2}{m} n_0 \, A_\alpha(\mathbf{r}, t) + e^2 \, i \int_{-\infty}^{t} dt' \int d\mathbf{r}' < [j_\alpha(\mathbf{r}, t - t'), j_\beta(\mathbf{r}', 0)] > \mathbf{A}_\beta(\mathbf{r}', t'). \tag{2.8.28}$$

When the system is homogeneous, Fourier transformation reduces this to

$$< J_\alpha > (\mathbf{k}, \omega) = \sum_\beta \sigma_{\alpha\beta}(\mathbf{k}, \omega) \mathcal{E}_\beta(\mathbf{k}, \omega) \tag{2.8.29}$$

Eq.(2.8.29) is Ohm's law with the conductivity tensor given by

$$\sigma_{\alpha\beta}(\mathbf{k}, \omega) = \frac{e^2}{i\omega} \Big(\chi_{j_\alpha j_\beta}(\mathbf{k}, \omega) - \frac{n}{m} \delta_{\alpha\beta} \Big) \tag{2.8.30}$$

If the electromagnetic response of the system is local, the current-current correlation function is proportional to $\delta(\mathbf{r} - \mathbf{r}')$. Then there is no need to take the Fourier transform with respect to spatial variables and we obtain

$$< J_\alpha > (\mathbf{r}, \omega) = \sum_\beta \sigma_{\alpha\beta}(\mathbf{r}, \omega) \mathcal{E}_\beta(\mathbf{r}, \omega). \tag{2.8.31}$$

Usually, the position dependence of the conductivity merely reflects the geometrical shape of the conductor. The conductivity itself is calculated as if the conductor filled all space and the local limit is obtained by setting the wave vector k in (2.8.29) equal to zero at some early stage in the calculations.
The response function (generalized susceptibility), defined and transformed to imaginary times in Eqs.(2.8.16) and (2.8.19) reads for this special case

$$\chi_{j_\alpha j_\beta}(\mathbf{k}, i\nu_m) = \int d\mathbf{r} \, e^{i\mathbf{k}\cdot(\mathbf{r} - \mathbf{r}'')} \int_0^{\frac{1}{T}} d\tau < j_\alpha(\mathbf{r}, \tau) j_\beta(\mathbf{r}'', 0) > e^{i\nu_m \tau} \tag{2.8.32}$$

From Eq.(2.8.26)

$$< j_\alpha(\mathbf{r}, \tau) j_\beta(\mathbf{r}'', 0) > = \sum_{\sigma\sigma'} \frac{\nabla_\alpha - \nabla'_\alpha}{2mi} \frac{\nabla''_\beta - \nabla'''_\beta}{2mi} < \psi^\dagger_\sigma(\mathbf{r}'\tau) \psi_\sigma(\mathbf{r}\tau) \psi^\dagger_{\sigma'}(\mathbf{r}''', 0) \psi_{\sigma'}(\mathbf{r}'', 0) > |_{\substack{\mathbf{r}''' \to \mathbf{r}'' \\ \mathbf{r}' \to \mathbf{r}}} \tag{2.8.33}$$

We do not consider particle-particle interactions as source of the resistivity and the superconductor pairing interaction is reduced to a single particle problem by treating it in a mean field approximation i.e., we neglect quantum fluctuation of the order parameter. Then the expectation value of four field operators can be factorized:

$$\begin{aligned} < \psi^\dagger_\sigma(\mathbf{r}'\tau) \psi_\sigma(\mathbf{r}\tau) \psi^\dagger_{\sigma'}(\mathbf{r}''', 0) \psi_{\sigma'}(\mathbf{r}'', 0) > = & < \psi^\dagger_\sigma(\mathbf{r}'\tau) \psi_\sigma(\mathbf{r}\tau) > < \psi^\dagger_{\sigma'}(\mathbf{r}''', 0) \psi_{\sigma'}(\mathbf{r}'', 0) > \\ & + < \psi^\dagger_\sigma(\mathbf{r}'\tau) \psi_{\sigma'}(\mathbf{r}'', 0) > < \psi_\sigma(\mathbf{r}\tau) \psi^\dagger_{\sigma'}(\mathbf{r}''', 0) > \\ & - < \psi^\dagger_\sigma(\mathbf{r}'\tau) \psi^\dagger_{\sigma'}(\mathbf{r}''', 0) > < \psi_\sigma(\mathbf{r}\tau) \psi_{\sigma'}(\mathbf{r}'', 0) > \end{aligned}$$

The first term is independent of τ and contributes only for $\nu_m = 0$. This term is omitted. The remaining terms can be expressed through normal and anomalous Green's functions

$$< j_\alpha(\mathbf{r},\tau) j_\beta(\mathbf{r}'',0) >= \frac{\nabla_\alpha - \nabla'_\alpha}{2mi}\frac{\nabla''_\beta - \nabla'''_\beta}{2mi} Sp\left[-G(\mathbf{r}'',\mathbf{r}',-\tau)G(\mathbf{r},\mathbf{r}'',\tau) + F(\mathbf{r}',\mathbf{r}''',\tau)F(\mathbf{r}'',\mathbf{r},-\tau)\right]. \tag{2.8.34}$$

The spur takes care of the spin summation. Expanding the imaginary time Green's function in Fourier series according to (2.6.14) and taking the Fourier transform with respect to spatial variables, assuming translational invariance, gives

$$\begin{aligned}\chi_{j_\alpha j_\beta}(\mathbf{q},\nu_m) =& Sp \int \frac{d^D p}{(2\pi)^D}\Big(\frac{(2p_\alpha + q_\alpha)(2p_\beta + q_\beta)}{(2m)^2}\Big) \\ & \times\ 2T\Sigma_{\omega_m}[G_{\omega_n}(\mathbf{p})G_{\omega_n-\nu_m}(\mathbf{p}+\mathbf{q}) + F_{\omega_n}(\mathbf{p})F_{\omega_n-\nu_m}(\mathbf{p}+\mathbf{q})] \\ \equiv& \chi^G_{j_\alpha j_\beta}(\mathbf{q},\nu_m) + \chi^F_{j_\alpha j_\beta}(\mathbf{q},\nu_m)\end{aligned} \tag{2.8.35}$$

The first term on the right hand side of Eq.2.8.35 will be used in Chapter 3 to calculate the conductivity in the local limit ($q = 0$).
The Green's functions themselves are, of course, modified through the onset of superconducting order:

$$G_{\omega_n}(\mathbf{p}) = \frac{i\omega_n + \varepsilon(\mathbf{p})}{(i\omega_n)^2 - \varepsilon^2(\mathbf{p}) - \Delta^2(\mathbf{p})} \tag{2.8.36}$$

$$F_{\omega_n}(\mathbf{p}) = \frac{\Delta(\mathbf{p})}{(i\omega_n)^2 - \varepsilon^2(\mathbf{p}) - \Delta^2(\mathbf{p})} \tag{2.8.37}$$

$\Delta(\mathbf{p})$ is the order parameter in this weak coupling approximation. The fact that $\Delta(\mathbf{p})$ depends on momentum is a generalization of the original BCS theory and suffices to describe unconventional pairing, like (spin-singlet) d-wave pairing. $\varepsilon(\mathbf{p})$ is the quasiparticle dispersion, which could be modeled by a parabolic band, or a tight-binding band.

The order in which the sum over Matsubara frequencies and the momentum integration is performed matters. This is particularly clear for the parabolic band, where the real part of the response function diverges even for 2D systems when the momentum integration is performed first while the response function vanishes in the clean limit when the frequency sum is performed first. According to (2.8.30) this leads to

$$\sigma(\omega) = -\frac{e^2}{i\omega}\frac{n}{m} \tag{2.8.38}$$

which is the correct result for an ideal conductor or a superconductor. It embodies the Meissner effect with the London penetration depth.

$$\lambda_L = \sqrt{\frac{m}{ne}} \tag{2.8.39}$$

In the presence of a random impurity potential the Green's functions are modified by self-energy corrections. Then the Green's functions no longer have isolated poles but cuts. The frequency sums can be converted into integrals along these cuts, by noting that the Fermi function has poles of the first order at every Matsubara frequency $i\omega_n = i(2n+1)\pi T$:

$$f\Big(\frac{i\omega_n}{T}\Big) = \frac{1}{1 + e^{i(2n+1)\pi}e^{\frac{\varepsilon}{T}}} = \frac{1}{1 - e^{\frac{\varepsilon}{T}}} \to \frac{-T}{\varepsilon} \quad for\ \frac{\varepsilon}{T} \ll 1. \tag{2.8.40}$$

The sum over Matsubara frequencies can thus be transformed into contour integral where the contour consists of small circles around each $i\omega_n$. This contour is then deformed into one that encloses the cut of $G_\omega(\mathbf{p})$, i.e., the real axis, and $G_{\omega - i\nu_m}(\mathbf{p})$, which is parallel to the real axis but shifted by $i\nu_m$. At this stage the analytic continuation $i\nu_m \to \omega + i\delta$ can be performed. Noting that

$$\int_{+\infty}^{-\infty} d\omega_0 \, G(\omega_0 + i\delta) + \int_{-\infty}^{+\infty} d\omega_0 \, G(\omega_0 - i\delta) = -2i \int_{-\infty}^{+\infty} d\omega_0 \, Im\, G(\omega_0 + i\delta) \tag{2.8.41}$$

We arrive at the final result

$$\begin{aligned} \chi_{j_\alpha j_\beta}(\mathbf{q}, \omega_0 + i\delta) = \int \frac{d^3p}{(2\pi)^3} \frac{(2p_\alpha + q_\alpha)(2p_\beta + q_\beta)}{(2m)^2} \int_{-\infty}^{+\infty} d\omega \, f(\frac{\omega}{T}) \\ \times \; Sp\left\{ G_A(\mathbf{p} + \mathbf{q}, \omega - \omega_0) \, Im\, G_R(\mathbf{p}, \omega) + G_R(\mathbf{p}, \omega + \omega_0) \, Im\, G_R(\mathbf{p} + \mathbf{q}, \omega) \right\} \end{aligned} \tag{2.8.42}$$

The integral with respect to frequency should be done first, but this is usually impossible analytically. The only progress in the calculation of the conductivity that can be made is evaluation of the momentum integral. When only the real part of the conductivity is of interest, the calculation is straightforward because the integrals converge. For a calculation of the imaginary part of the conductivity one has to improve the convergence by subtracting and adding the clean limit which can be calculated exactly because $Im\, G_R$ reduces to a δ-function [83].

Chapter 3

High Temperature Superconductor From Our Viewpoint

3.1 Tight Binding Approximation:

3.1.1 Introduction

The tight-binding method is perhaps the simplest approach conceptually for describing energy bands. This approach has been used in chemistry for some time under the name of *linear combination of atomic orbitals, LCAO method* for band structure calculations [89]. Depending on doping, the high temperature superconductors, which are of interest here, can be treated using this approach.

3.1.2 Assumptions

In the tight binding approximation a number of assumptions are made, and these assumptions are:

1. The energy eigenvalues and eigenfunctions are known for an electron in an isolated atom.

2. When the atoms are brought together to form a solid they remain sufficiently far apart so that each electron can be assigned to a particular atomic site.

3. The periodic potential is approximated by a superposition of atomic potentials.

4. Perturbation theory can be used to treat the difference between the actual potential and the atomic potential.

3.1.3 Formalism

For the tight binding approximation the unperturbed state is the atomic state, and the perturbation is the difference between the periodic potential and the atomic potential around which the electron is localized.

We construct the wave functions for the unperturbed problem as a linear combination of atomic functions $\phi_j(\boldsymbol{r}-\boldsymbol{R}_n)$ labeled by quantum number j

$$\psi_j(\boldsymbol{r}) = \sum_{n=1}^{N} C_{j,n}\phi_j(\boldsymbol{r}-\boldsymbol{R}_n) \tag{3.1.1}$$

and so that $\psi_j(\boldsymbol{r})$ is an eigenstate of a Hamiltonian satisfying the periodic potential of the lattice. In this treatment we assume that the tight binding wavefunctions $\psi_j(\boldsymbol{r})$ can be

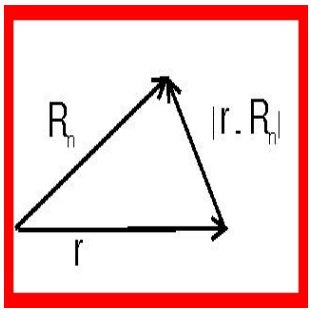

Figure 3.1: Definition of the vectors used in the tight binding approximation

identified with a single atomic state ϕ_j; this approximation must be relaxed in dealing with degenerate levels. According to Bloch's theorem $\psi_j(\boldsymbol{r})$ must satisfy the relation:

$$\psi_j(\boldsymbol{r}+\boldsymbol{R}_m) = e^{i\boldsymbol{k}\cdot\boldsymbol{R}_m}\psi_j(\boldsymbol{r}) \tag{3.1.2}$$

where $\mathbf{R}_m$ is an arbitrary lattice vector. This restriction imposes a special form on the coefficients $C_{j,n}$.
Substitution of the expansion in atomic functions $\psi_j(\mathbf{r})$ from Eq.(3.1.1) into the left side of Eq.(3.1.2) yields:

$$\begin{aligned}\psi_j(\boldsymbol{r}+\boldsymbol{R}_m) &= \sum_n C_{j,n}\ \phi_j(\mathbf{r}-\mathbf{R}_n+\mathbf{R}_m)\\ &= \sum_Q C_{j,Q+m}\ \phi_j(\mathbf{r}-\mathbf{R}_Q)\\ &= \sum_n C_{j,n+m}\ \phi(\mathbf{r}-\mathbf{R}_n)\end{aligned} \tag{3.1.3}$$

where we have utilized the substitution $\mathbf{R}_Q = \mathbf{R}_n - \mathbf{R}_m$ and the fact that Q is a dummy index. Now for the right side of the Bloch theorem (Eq.(3.1.2)) we have

$$e^{i\mathbf{k}\cdot\mathbf{R}_m}\ \psi_j(\mathbf{r}) = \sum_n C_{j,n}\ e^{i\mathbf{k}\cdot\mathbf{R}_m}\ \phi_j(\mathbf{r}-\mathbf{R}_n). \tag{3.1.4}$$

The coefficients $C_{j,n}$ which relate the actual wave function $\psi_j(\mathbf{r})$ to the atomic functions $\phi_j(\mathbf{r}-\mathbf{R}_n)$ are therefore not arbitrary but must thus satisfy:

$$C_{j,n+m} = e^{i\mathbf{k}\cdot\mathbf{R}_m}\, C_{j,n} \tag{3.1.5}$$

which can be accomplished by setting:

$$C_{j,n} = \xi_j\ e^{i\mathbf{k}\cdot\mathbf{R}_n} \tag{3.1.6}$$

where the new coefficient ξ_j is independent of n. We therefore obtain:

$$\psi_{j,\mathbf{k}}(\mathbf{r}) = \xi_j \sum_n e^{i\mathbf{k}\cdot\mathbf{R}_n}\phi_j(\mathbf{r}-\mathbf{R}_n) \tag{3.1.7}$$

one may write

$$\psi_{j,\mathbf{k}}(\mathbf{r}) = \frac{1}{\sqrt{N}} \sum_n e^{i\mathbf{k}\cdot\mathbf{R}_n}\phi_j(\mathbf{r}-\mathbf{R}_n) \tag{3.1.8}$$

where j is an index labeling the particular atomic state of degeneracy N and k is the quantum number for the translation operator and labels the Bloch state $\psi_{j,\mathbf{k}}(\mathbf{r})$. Note that the atomic wavefunctions did not overlap each other, this wavefunction would be normalized. Because they do overlap, the wavefunction as written is not accurately normalized [90].

3.1.3.1 The Dispersion Relation

Having assumed this wavefunction we may now directly compute the expectation value of the energy

$$< \varepsilon(\boldsymbol{k}) >= \frac{< \boldsymbol{k}|H|\boldsymbol{k} >}{< \boldsymbol{k}|\boldsymbol{k} >} \tag{3.1.9}$$

We write the potential as a superposition of potentials centered on the individual atoms, $V(\mathbf{r}) = \sum_j U(\mathbf{r}-\mathbf{R}_n)$, which in this case is quite consistent with our assumed wavefunctions. Furthermore we may write

$$\Big[-\frac{\nabla^2}{2m} + U(\mathbf{r}-\mathbf{R}_n)\Big]\phi_j(\mathbf{r}-\mathbf{R}_n) = \varepsilon_0\phi_j(\mathbf{r}-\mathbf{R}_n)$$

where ε_0 is the energy eigenvalue for the corresponding state in the free atom. Then

$$\Big(-\frac{\nabla^2}{2m} + V\Big)\psi_{j,\mathbf{k}}(\mathbf{r}) = \frac{1}{\sqrt{N}}\sum_n \Big[\varepsilon_0 + \sum_{m\neq n} U(\mathbf{r}-\mathbf{R}_n)\Big]\phi_j(\mathbf{r}-\mathbf{R}_n)e^{-i\mathbf{k}\cdot\mathbf{R}_n}$$

and the expectation value of the energy becomes

$$\begin{aligned} < \varepsilon(\mathbf{k}) >=& \varepsilon_0 \\ &+ \frac{1/N \ \sum_{n,l} e^{-i\mathbf{k}\cdot(\mathbf{R}_n-\mathbf{R}_l)} \ \int \phi_j^\star(\mathbf{r}-\mathbf{R}_l) \ \sum_{m\neq n} U(\mathbf{r}-\mathbf{R}_m)\phi_j(\mathbf{r}-\mathbf{R}_n)d^3r}{\int \phi_{j,\mathbf{k}}^\star\phi_{j,\mathbf{k}}d^3r} \end{aligned} \tag{3.1.10}$$

Notice that the corrections to the free-atom values will be small if the neighboring wavefunctions and potentials do not overlap greatly. In the tight-binding method we treat the overlap of the wavefunctions as a small correction. To lowest order in this overlap, then, we may set the denominator in Eq.(3.1.10) equal to 1. Furthermore it is reasonable to expect that three-center integrals will be small compared to two-center integrals and to drop them from the summation. Then we will have terms only for $l = m$ or $l = n$. This may not always

be a very good approximation but it is one customarily made in the tight-binding method.

Let us consider first the terms for which $l = n$.

$$\frac{1}{N} \sum_n \int \phi_j^\star(\mathbf{r} - \mathbf{R}_n) \sum_{m \neq n} U(\mathbf{r} - \mathbf{R}_m) \phi_j(\mathbf{r} - \mathbf{R}_n) d^3r \tag{3.1.11}$$

This is simply the expectation value (based upon our atomic wavefunctions) at each ion of the potential arising from all of the neighbors. For a perfect crystal this value will be independent of n so that the sum over n divided by N is equal to the value taken by one term

$$\int \phi_j^\star(\mathbf{r} - \mathbf{R}_n) \phi_j(\mathbf{r} - \mathbf{R}_n) \sum_{m \neq n} U(\mathbf{r} - \mathbf{R}_m) d^3r \tag{3.1.12}$$

The potential due to each atom is attractive and therefore this is a negative term which is independent of the wavenumber of the state being considered. This term contributes to the binding of the crystal and is important in that regard but has little bearing on the energy-band structure itself.

We consider next the terms for which $l = m$.

$$\frac{1}{N} \sum_{m \neq n} e^{-i\mathbf{k}\cdot(\mathbf{R}_n - \mathbf{R}_m)} \int \phi_j^\star(\mathbf{r} - \mathbf{R}_m) U(\mathbf{r} - \mathbf{R}_m) \phi_t(\mathbf{r} - \mathbf{R}_n) d^3r \tag{3.1.13}$$

Again these terms are independent of n so we can replace the sum over n by a factor of N and take our origin at a given r_n.

$$\sum_{\mathbf{R}_m \neq 0} e^{-i\mathbf{k}\cdot\mathbf{R}_m} \int \phi_j^\star(\mathbf{r} - \mathbf{R}_m) U(\mathbf{r} - \mathbf{R}_m) \phi_j(\mathbf{r}) d^3r \tag{3.1.14}$$

These are the k-dependent terms that give rise to interesting band-structure effects. In the tight-binding approximation it is frequently assumed that the nearest-neighbor contributes dominate and only these are included.

Let us consider now the simplest case, that of an energy band arising from atomic s states. Furthermore we will simplify the problem by letting the atoms lie in a simple cubic structure. We look in particular at the wavenumber-dependent terms arising from nearest-neighbor overlaps. The integral in each term is given by

$$t = \int \phi_j^\star(\mathbf{r} - \mathbf{R}_m) U(\mathbf{r} - \mathbf{R}_m) \phi_j(\mathbf{r}) d^3r \tag{3.1.15}$$

and for s states takes on the same value for all neighbors. The value of t may be obtained from atomic wavefunctions, the atomic potential, and the near-neighbor distance. Then the wavenumber-dependent correction takes the form

$$t \sum_{\substack{nearest \\ neighbors}} e^{-i\mathbf{k}\cdot\mathbf{R}_m} = 2t(\cos k_x a + \cos k_y a + \cos k_z a) \tag{3.1.16}$$

Note that if we included contributions for more distant neighbors this would give us additional corrections to the energy bands which would also be sums of cosines. The important part of the integral will ordinarily occur beyond the last node in both of the atomic wavefunctions. Thus, since the potential is attractive, t will ordinarily be negative [89].
This dispersion relation $\varepsilon(\boldsymbol{k})$ clearly satisfies three properties which characterize energy eigenvalues in typical periodic structures:

1. Periodicity in $\boldsymbol{k}$ space under translation by a reciprocal lattice vector $\boldsymbol{k} \rightarrow \boldsymbol{k} + \boldsymbol{G}$,
2. $\varepsilon(\boldsymbol{k})$ is an even function of $\boldsymbol{k}$(i.e., $\varepsilon(\mathbf{k}) = \varepsilon(-\mathbf{k})$),
3. $\frac{\partial \varepsilon}{\partial k} = 0$ at the Brillouin zone boundary [90].

3.1.4 D-wave Superconductor and The Tight Binding Approximation

We start the investigation of disorder d-wave supperconductor on a two-dimensional square lattice with a Hubbard model Hamiltonian:

$$H = \sum_{\substack{<i,j> \\ \sigma}} t_{i,j} \, (c^{\dagger}_{i\sigma} c_{j\sigma} + H.c.) + U \sum_{i} n_{i\uparrow} n_{i\downarrow} - \mu \sum_{i} (n_{i\uparrow} + n_{i\downarrow}). \tag{3.1.17}$$

It describes a single s band in a tight-binding basis, with a local electron-electron repulsion U for electrons of opposite site spin at the atomic orbital. The model is thought to be appropriate to describe the main features of electron correlations in narrow energy bands, leading to collective effects such as itinerant magnetism and metal-insulator transition, and has been often used to describe real materials exhibiting these phenomena. A detailed justification for Eq.(3.1.18) as a model for narrow-band systems has been given by Hubbard [91; 92].

In two dimensions, the Hubbard Hamiltonian with only nearest-neighbor hopping[93; 94] is given by

$$H = -t \sum_{\substack{<i,j> \\ \sigma}} (c^{\dagger}_{i\sigma} c_{j\sigma} + H.c.) + U \sum_{i} n_{i\sigma} n_{i-\sigma} - \mu \sum_{i\sigma} (n_{i\sigma}). \tag{3.1.18}$$

where the sum over i and j is done over the nearest-neighbour sites on a square lattice. The one electron hopping matrix element is t, the onsite Coulomb repulsion is U and the chemical potential μ (which is determined by the electron filling factor n) is used for controlling the electron occupation in the grand canonical ensemble. Here, $c^{\dagger}_{i\sigma}(c_{i\sigma})$ creates (annihilates) an electron of spin σ at site i and $n_{i\sigma} = c^{\dagger}_{i\sigma} c_{i\sigma}$ is the occupation number of electrons with spin σ at site i (section 2.5 on second quantization). High-temperature superconducting cuprates are known to be highly anisotropic, and the electronic band structures may be approximated by that of a two-dimensional square lattice. In the tight-binding approximation, assuming that the only relevant orbitals are $d_{x^2-y^2}$ and d_{xy}, and that the relevant interactions are the attractive nearest-neighbor and repulsive next-nearest-neighbor interactions, the dispersion relation (Eq.(3.1.16)) has the following form [95]:

$$\varepsilon(\mathbf{k}) = -2t(\cos k_x a + \cos k_y a) + 4t'(\cos k_x a \cos k_y a) - \mu; \tag{3.1.19}$$

where t and t' are nearest and next-nearest hopping integrals, and a ($a = 1$) is the lattice constant. In dimensionless units (see Appendix C).

$$\varepsilon(k_x, k_y) = \varepsilon(k) = -(\cos k_x + \cos k_y) + 2B(\cos k_x \cos k_y) - \mu, \tag{3.1.20}$$

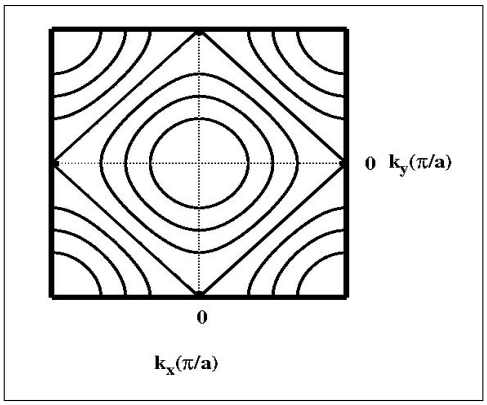

(a) The Fermi surface of a tight binding model with nearest neighbour hopping only for various fillings.

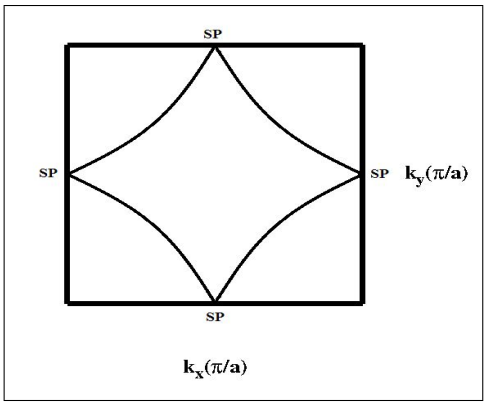

(b) The Fermi surface at van Hove filling:$B = 0.27$ and $\mu = 1.46$

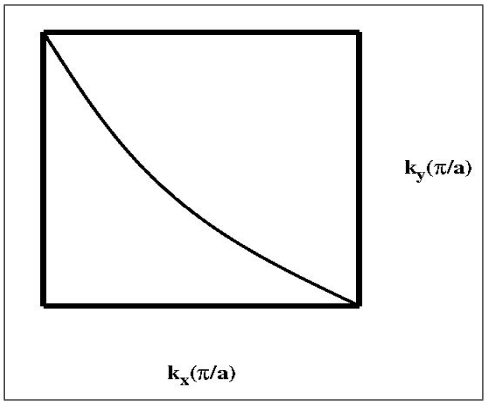

(c) The Fermi surface at van Hove filling:$B = 0.27$ and $\mu = 1.46$

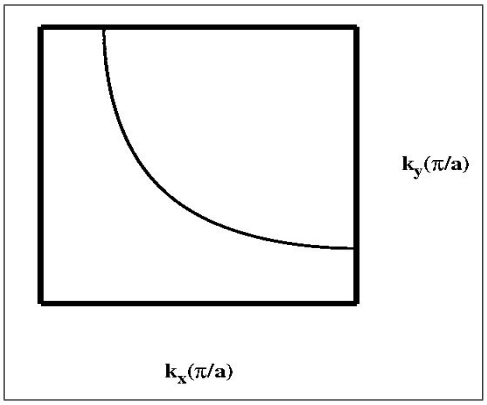

(d) $B = 0.45$ and $\mu = 1.46$

Figure 3.2: Fermi Surface at different values of B

where B is next-neighbor hopping integral in units of t. In the tight-binding approximation, the normal-state dispersion of square lattice, with nearest-neighbors hopping only, is given by

$$\varepsilon(\boldsymbol{k}) = -(\cos k_x + \cos k_y) - \mu, \tag{3.1.21}$$

For the half-filled nearest-neighbor tight-binding band, the Fermi surface is perfectly nested, which is composed of four straight lines ($k_x \pm k_y = \pi$ and $k_x \pm k_y = -\pi$), as seen in Fig.3.2(a). But with the next-nearest-neighbor hopping the Fermi surface is never perfectly nested, the Van Hove singularity is at the Fermi level for an electron doping blow one half. Another important feature of this relation is that in contrast to the nearest-neighbor tight-binding form, (3.1.21), there are pieces of the Fermi surface that are connected by the antiferromagnetic wave vector **Q** below half filling [96].

Fig.(3.3(e)) is the Fermi line for a tight-binding band given in equation (3.1.20) with B=0.45 and a chemical potential $\mu = 1.46$. It is similar but not identical to the Fermi surfaces found for both YBCO-123 and BSCCO-2212 by ARPES[45]. Fig.(3.3(f)) is the Fermi surface (for LSCO) at half filling calculated only with the nearest-neighbour hopping, and also Fermi surface including the next-nearest-neighbour hopping [97].

The above electronic dispersion is quite general for $2D$ transport in strongly correlated systems and its also suitable to describe the conduction band associated with the Cu O_2 planes in high-T_c superconductors[98]. The value $n = 0.75$ appropriate to [$YBa_2Cu_3O_7$], this value of n corresponds, with the band structure in (Eq 3.1.20), to a value $|\mu| \sim 1.46t$, these values from the ref.[99], as in see Fig 3.2(b), a finite electron hopping $0 < B < 1/2$ between next nearest neighbors has been included and the chemical potential is fine-tuned such that the Fermi surface contains the saddle points at $(\pm\pi, 0)$ and $(0, \pm\pi)$.

3.1.4.1 The effect of the hopping integral B:

From Figs.(3.2(b)) and (3.3), we see that with increasing the value of B Fermi surface begins to change until B reaches the value 0.27 at that value of B the saddle points (sp) appear, and by increasing B further we notice the appearance of what is called hot spot beside the Fermi surface changes slightly.

Conclusion:

From we mentioned above we conclude that B is responsible for the presence of hot spots, while the additives concentration (x), or the chemical potential μ, see section 3.2.1 and also [cf ref.[100]], influences the Fermi surface and in turn the hot spots and naturally superconductivity of the materials, as we shall discuss later.

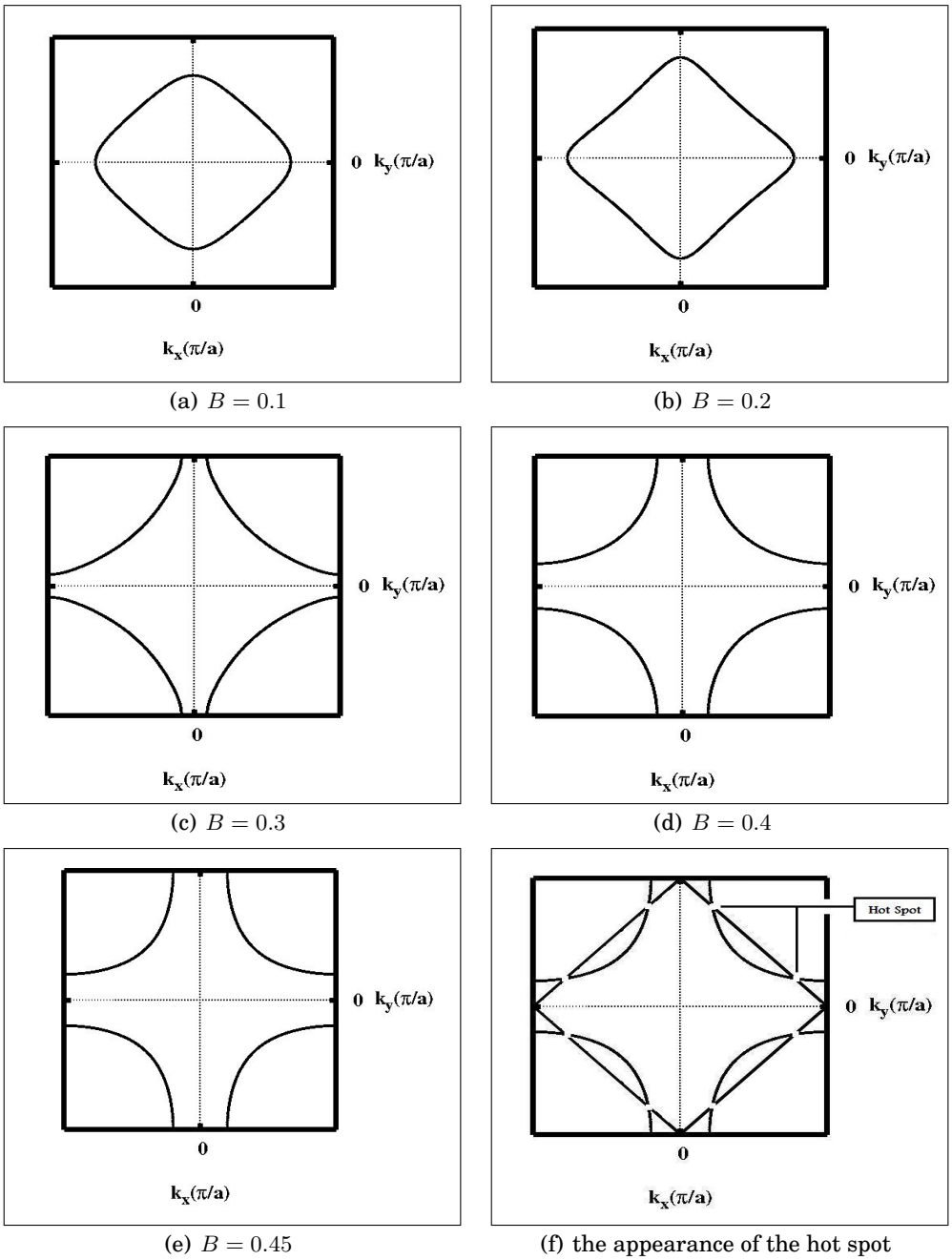

(a) $B = 0.1$ (b) $B = 0.2$

(c) $B = 0.3$ (d) $B = 0.4$

(e) $B = 0.45$ (f) the appearance of the hot spot

Figure 3.3: Fermi Surface at different values of B

3.1.5 Tight Binding Density of States

The equilibrium thermodynamics of a disordered system can be expressed entirely as a functional of the density of states or spectral density [88].

The total density of states or simply the density of states (DOS) of a system is defined as:

$$N(\varepsilon) = \sum_n \delta(\varepsilon - \varepsilon_n); \tag{3.1.22}$$

where the sum runs over all energy states ε_n of the system.

A more sophisticated and far more accurate approximation is the coherent potential approximation. The essential idea is to replace each atom by an "effective" atom so that on the average no scattering takes place on each site. To be more precise, consider a single impurity of type B at site i in an otherwise type A crystal. The Hamiltonian then is

$$H = H_A + (E_B - E_A)\, c_i^\dagger c_i = H_A + U \tag{3.1.23}$$

We now define the resolvent operator (or Green's function) $G(z)$:

$$\begin{aligned} G(z) =& (z-H)^{-1} = (z - H_A - U)^{-1} \\ =& (z-H_A)^{-1} + (z-H_A)^{-1} U (z-H)^{-1} \end{aligned} \tag{3.1.24}$$

The last equation can easily be shown to be correct by premultiplying by $(z - H_A)$ and postmultiplying by $(z - H)$. Taking matrix elements in the atomic basis and defining

$$G_{mj}(z) =< m|(z-H)^{-1}|j > \quad G^0_{mj}(z) =< m|(z-H_A)^{-1}|j >$$

we obtain, on iterating (3.1.24),

$$\begin{aligned} G_{mj}(z) &= G^0_{mj}(z) + G^0_{mi}(z) U_{ii} G_{ij}(z) \\ &= G^0_{mj}(z) + G^0_{mi}(z) U_{ii} G^0_{ij}(z) + G^0_{mi}(z) U_{ii} G^0_{ii}(z) U_{ii} G^0_{ij}(z) + \cdots \\ &= G^0_{mj}(z) + G^0_{mi} U_{ii} (1 - G^0_{ii} U_{ii})^{-1} G^0_{ij} \end{aligned} \tag{3.1.25}$$

The operator $T = U(1 - G^0 U)^{-1}$ is known as the T-matrix of the potential U and has, in the particular case of a single impurity (3.1.23), only diagonal matrix elements. The generalization of (3.1.24) and (3.1.25) for an arbitrary perturbation U is, in operator form,

$$G(z) = G^0(z) + G^0(z)\; U\; G(z) = G^0(z) + G^0(z)\; T(z)\; G^0(z) \tag{3.1.26}$$

The Green's function $G(z)$ yields the density of states, as we now show. Suppose that the eigenstates of H are $|\phi_m >$ with energies ε_m and consider

$$\begin{aligned} Tr\; G(\varepsilon + i\,\eta) &= \sum_m < \phi_m|(\varepsilon - H - i\,\eta)^{-1}|\phi_m > \\ &= \sum_m (\varepsilon - \varepsilon_m + i\,\eta)^{-1} \end{aligned} \tag{3.1.27}$$

Using

$$\lim_{\eta \to 0} \frac{1}{\varepsilon - \varepsilon_m + i\,\eta} = \mathcal{P}\frac{1}{\varepsilon - \varepsilon_m} - i\pi\delta(\varepsilon - \varepsilon_m) \tag{3.1.28}$$

we see that

$$N(\varepsilon) = \sum_m \delta(\varepsilon - \varepsilon_m) = -\frac{1}{\pi}\, Im\, Tr\, G(\varepsilon + i0^+) \tag{3.1.29}$$

Since the trace (3.1.29) can be evaluated in any basis, we are free to use our Warnnier states or the Bloch states to calculate the density of states. It is only necessary to find the diagonal matrix elements of the operator $G(z)$ [88].

DOS is just the number of energy levels between ε and $\varepsilon + d\varepsilon$ divided by the infinitesimal energy interval $d\varepsilon$

$$N(\varepsilon) = \frac{1}{d\varepsilon} \sum_{\varepsilon}^{\varepsilon + d\varepsilon} 1. \tag{3.1.30}$$

It is clear that the integral of $N(\varepsilon)$ over ε is the total number of states in the system. This concept is applicable to both finite systems, such as molecules or clusters, and infinite crystals. In the former case the energy interval $d\varepsilon$ should be chosen to be reasonably small but finite. We can even drop out the denominator in Eq.(3.1.30). Recall that the integral of $N(\varepsilon)$ over energy should always be the total number of states, so that we must introduce in this case a normalization constant. For crystals with perfectly periodic atom arrangements, (i.e., without defects) the sum in eq.(3.1.22) can be taken over wave vector k: DOS for periodic

$$N(\varepsilon) = \sum_k \delta(\varepsilon - \varepsilon(k)); \tag{3.1.31}$$

The sum runs over all possible values of k, but in actual calculations we restrict k to the first Brillouin zone [101]. Our focus will be on the density of states $N(\omega)$*, its Hilbert transform $F(\omega)$, and virtual states:

3.1.5.1 The Density of States $N(\omega)$ and Its Hilbert Transform $F(\omega)$:

The concept of density of states is extremely useful in electronic structure calculations, especially given that DOS is an experimentally measurable quantity by a variety of techniques, e.g., scanning tunneling microscopy.

DOS cannot be calculated analytically (obtained as an analytic function of energy) for two and three-dimensional systems. However, we can always integrate numerically over the Brillouin zone, although it is computationally not efficient [101]. For practical purposes, we often only require that the DOS is correct near the Fermi level.

We have numerically calculated the DOS, $N(\omega)$, for our tight binding models by direct evaluation, using the elliptical integral formalism, for the formula [cf. refs [102–104]]

$$N(\omega) = \sum_k \delta(\omega - \varepsilon(\boldsymbol{k})) \tag{((3.1.31))}$$

*for convenience, from here on, we shall use $N(\omega)$ instead of $N(\varepsilon)$

or [105]

$$N(\omega) = \int \frac{d^2k}{(2\pi)^2}\,\delta(\omega - \varepsilon(\boldsymbol{k})) \tag{3.1.32}$$

the solution of this integral, we have discussed the solution in great detail in Appendix C, is given by

$$N(\omega) = \frac{1}{2\pi^2\sqrt{1+2BE}}\,K\Big(k^2 = \frac{1-(\frac{E}{2}-B)^2}{1+2BE}\Big) \quad E>0 \tag{3.1.33}$$

$$N(\omega) = Sign[E]\frac{1}{\pi^2}\frac{1}{(\frac{E}{2}+B)}\,K\Big(\frac{(\frac{E}{2}-B)^2-1}{(\frac{E}{2}+B)^2}\Big) \quad E<0. \tag{3.1.34}$$

Where $K(k)$ is the Complete Elliptic Integral of the First Kind[106].

The well known DOS for a nearest-neighbor[104] and next-nearest-neighbors tight binding model is shown in Fig.3.4(b). Particular feature to notice is that there is a van Hove singularity at half filling (one electron per site, $E = 0$)[74], also with $B = 0.27, 0.45$ and $\mu = 1.46$ there is a van Hove singularities with a peak in the total density of states at$-0.6, -0.8$ respectively, as shown in Fig.(3.4(b)). In the same manner, see Appendix C, we solved $F(\omega)$

$$F(\omega) = Sign(E)\,\frac{1}{(\pi)}\frac{1}{\sqrt{(2BE+1)}}K\Big(\frac{(2B+E)^2}{4(1+2BE)}\Big) \quad E<2+2B \tag{3.1.35}$$

$$F(\omega) = \frac{1}{(\pi)}\frac{2}{\sqrt{(2B+E)}}\,K\Big(\frac{4(1+2BE)}{(2B+E)^2}\Big) \quad E>2+2B \tag{3.1.36}$$

Fig.3.5(a) shows the response of the function $F(\omega)$ to the energy E, the DOS and $F(\omega)$ functions are plotted in Figs. (3.4(b),3.5(a)). Note that the DOS exhibits, at both band edges a discontinuity which produces the logarithmic singularities of the $Re(G)$ at the band edges. As was mentioned before, this behavior is characteristic of the 2-dimensionality of the system (in our case $YBa_2Cu_3O_7$). Note also that the singularity at the interior of the band $(E = 0)$; the $F(\omega)$ is discontinuous there and the $N(\omega)$ has a logarithmic singularity. The singularities of $G^0(\mathrm{k})$ within the band are associated with sadle points in the function $E(k)$[79], where k is a wave vector of charge carrier, electron or hole [see section (3.2.1) on charge carriers], as shown in Fig.3.2(b).

3.1.5.2 The Impurity-Induced Virtual States:

Scattering of quasiparticle from impurity is described by a T-matrix, $T(\omega)$, which is independent of wave vector[107]. The scattering matrix can be written, [see section3.4(b) and refs.[108; 109]], as

$$T = U(1-G^0U)^{-1} = [(1/U) + F(\omega) - i\pi N(\omega)]^{-1} \tag{3.1.37}$$

Since the Green's functions in the presence of impurity scattering is $G = G^0 + G^0TG^0$, poles of the T-matrix are the new poles of G that are not poles of G^0, signifying the appearance of new states[110]. By plotting the $ImT(\omega)$ against the impurity potential $1/U$ supposing U is attractive, we got a virtual states as shown in Fig.3.5(b).

Now let us compare our work with other work, Clogston [111], also see Doniach [84] and Fistul [112], in his work used a model DOS that is an inverted parabola, $F(\omega)$ has

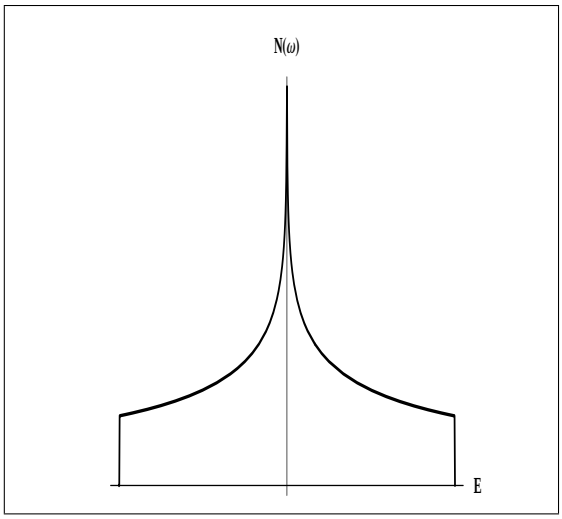

(a) The DOS for a tight binding model with nearest-neighbor hopping only in two dimensions,calculated by direct evaluation of Eq.((3.1.31)).

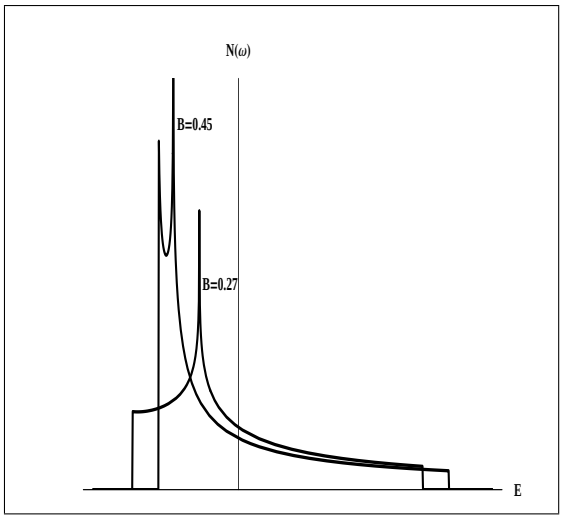

(b) The DOS for a tight binding model with nearest- and next-nearest- neighbor hopping in two dimensions,calculated by direct evaluation of Eq.((3.1.31)).

Figure 3.4: The Density of states DOS at various value of B

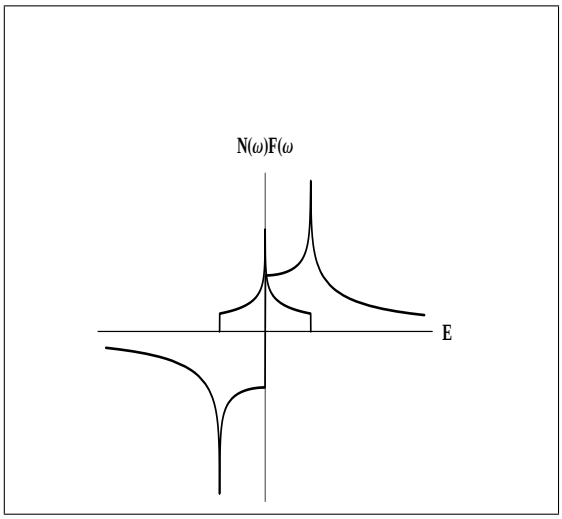

(a) the response of the functions $N(\omega)\&F(\omega)$ to the energy E

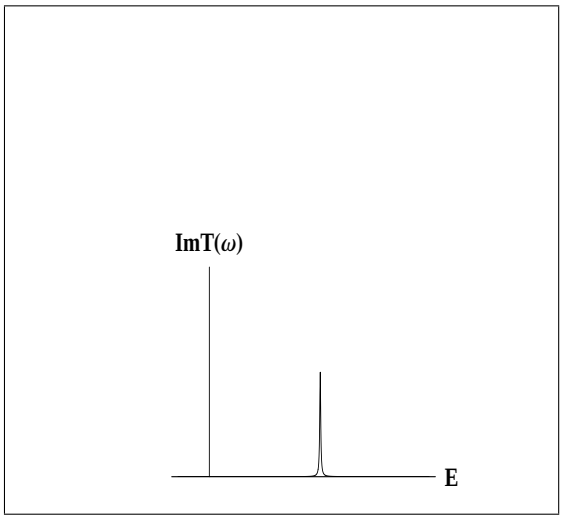

(b) the figure shows the virtual states

Figure 3.5: The figure shows N(ω), F(ω), and Im T vs. E

no singularity at the band edges, because there is no discontinuity in the DOS, and no discontinuity at $E = 0$, because there is no singularity in DOS at $E = 0$ in the band, he pointed out that if U is negative (an attractive potential) and is large enough so that $1/U$ cuts $F(\omega)$ in two points, a virtual state has been created in the vicinity of the first intersection point, E_0, it means that approximately one whole state has been brought below this energy by perturbation. The width of the virtual state is of interest. This is clearly controlled by the value of $N(\omega)$ at the point of intersection. If $N(\omega)$ is small, the state is very narrow, and vice versa.

Balatsky *et al.*[108] used another different DOS model, $F(\omega)$ has no discontinuity anywhere, they pointed out that under the condition $|2UN| > 1$ one gets a resonance states inside the band, referring that to the presence of pseudogap(PG), they also argued that by using a DOS with a quadratic dependent gap, one can obtain a similar results.

Conclusion:

From the previous one deduces that there are four quantities or parameters that control the position and the type of the additional states i mean bound, virtual, or resonance (anti-resonance) states, these quantities are $\varepsilon(k)$, $N(\omega)$, and $F(\omega)$ beside the impurity potential U, one can say by controlling U and choosing a suitable dispersion relation $\varepsilon(k)$, and suitable DOS model one can control the type and the position of the additional states.

3.1.5.3 Density of States of The Virtual States

We can also introduce the local density of states (LDOS): LDOS definition

$$N(\mathbf{r},\omega) = \sum_n |\psi_n(\mathbf{r})|^2 \delta(\omega - \varepsilon_n). \tag{3.1.38}$$

where $\psi_n(\mathbf{r}))$ is the eigenfunction of the Hamiltonian with label n. LDOS can be interpreted as the charge density resulting exclusively from states in the energy interval from ε to $\varepsilon + d\varepsilon$. For the tight-binding approximation, LDOS on atom j is

$$N(j,\omega) = \sum_n |c_j^n(\mathbf{r})|^2 \delta(\omega - \varepsilon_n); \tag{3.1.39}$$

It is obvious that if we sum LDOS over all atom in the system, we will get the total DOS because of the normalization condition on the wave function. DOS of a finite system is a discrete function of energy and, in general, it is continuous for an infinite system (except for a regions where it is zero- so called energy gaps).

We now seek to study the corrections to the local density of states due to virtual state. In the presence of impurity, the Green's function is given by

$$G(\mathbf{r},\mathbf{r}';\omega) = G^0(\mathbf{r}-\mathbf{r}';\omega) + G^0(\mathbf{r},0;\omega)T(\omega)G^0(0,\mathbf{r}';\omega) \tag{3.1.40}$$

the second term describing the local distortion due to the impurity.
By using Lehmann representation for Green's function, we get

$$G(\mathbf{r},\mathbf{r}';\omega) = \sum_n (\psi_n^*(\mathbf{r})\psi_n(\mathbf{r}))/(\omega - \varepsilon_n) \tag{3.1.41}$$

from Eqs. (3.1.40) and (3.1.41), and taking the imaginary part, see Appendix E.3

$$N(\mathbf{r},\omega) = N(\omega) + N_{\text{imp},n}(\mathbf{r},\omega)(\text{or}\delta N(\mathbf{r},\omega)) \tag{3.1.42}$$

the 1st term is the DOS of a clean superconductor, and the second is the change induced by impurity

$$N_{\text{imp}} = \sum_n (\psi^*_{\text{imp},n}(\mathbf{r})\psi_{\text{imp},n}(\mathbf{r}))\delta(\omega - \varepsilon_n) \tag{3.1.43}$$

$$= -\frac{1}{\pi} Im[G^0(\mathbf{r};\omega)T(\omega)G^0(-\mathbf{r}';\omega))] \tag{3.1.44}$$

Because $G^0(\mathbf{r}, \omega = 0)\ G^0(-\mathbf{r}', \omega = 0)$ as $\varepsilon_{\text{imp}} \to 0$ is real only the imaginary part of the T-matrix, i.e., $Im[T(\omega)]$, contributes to N_{imp}, as shown in Fig.(3.5) [107].

3.2 What HT$_c$ Superconductor Is!

3.2.1 Charge Carriers and Pairing Symmetry of the Order Parameter

In its paper and the references therein Daniela Lindner[113] has shown that for many different reasons the charge carriers in electron-doped superconductors cuprates are both electrons and holes.

Now, another important point is the pairing symmetry of the order parameter, while in hole-doped superconductors the $d_{x^2-y^2}$ type is the acceptable one. The situation is enough different in electron-doped superconductors, in one hand and in accordance with experiments some talk about s-wave type, on the other hand Khodel *et al.*[100] proposed the p-wave type, on the third hand D. Manske *et al.*[114] have shown the presence of d-wave type.

Conclusion:

We propose the presence of all mentioned types of pairing symmetry, d-wave, s-wave, and may be p-wave, of the order parameter in electron doped superconductor cuprates. The point is that the percentage of each type does depend upon the hot spots (next section) which in turn depends upon the percentage of the additives.

3.2.2 The Role of Hot Spots:

From the dispersion relation

$$\varepsilon_k = -(\cos k_x + \cos k_y) + 2B \cos k_x \cos k_y - \mu \tag{3.1.19}$$

the presence of B (see section 3.1.4.1) allows "hot spots" on the Fermi surface Fig.3.6(a) which can be connected by Q [99]. These points (hot spots) are labeled in Fig.3.6(b) by the consective numbers from 1 to 8, the superconductivity pairing potential $\Delta(P)$ has opposite signs at the

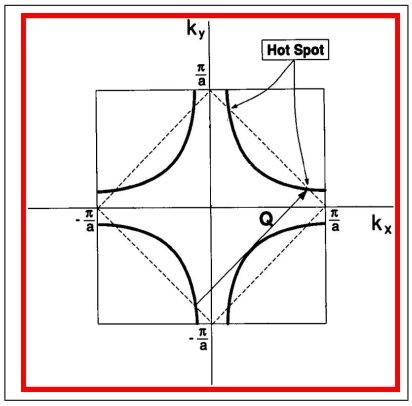

(a) Fermi surface in the first Brillouin zone. Taken from ref. [99]

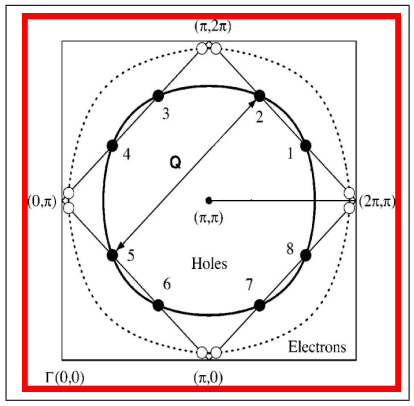

(b) Fermi surfaces of Eq.(3.1.19) for hole doping (dashed line) and electron doping (solid line). The hot spots are shown by openand solid circles. Taken from ref. [100]

Figure 3.6: hot spots

two hot spots connected by the vector **Q**:

$$\Delta(P+Q) = -\Delta(P) \tag{3.2.1}$$

Thus, the eight hot spots can be divided into four groups (1,6), (2,5), (3,8), and (4,7), with the signs of $\Delta(P)$ being opposite within each group. In Fig.(3.2.1). the dashed (encloses a large area) and solid lines show the Fermi surfaces corresponding to the hole- and electron-doped cuprates. Because the Γ point (0,0) is located at the corner of Fig.(3.2.1), the area inside the Fermi surface is occupied by holes and outside by electrons [100].

Hole-doped case:

The pairs of hot spots shown by the open circles in Fig.(3.2.1) are located close to the Van Hove points (0,π), (π,0), (2π,π), and (π,2π). Assuming that $\Delta(P)$ has the same sign within each pair of the neighbouring hot spots. This assumption, in combination with Eq.(3.2.1), immediately results in the familiar symmetry (d-wave) of the pairing potential.

The electron-doped case:

with the increase of electron doping, the Fermi surface shrinks, and the hot spots move away from the Van Hove points toward the Brillouin zone diagonals [100], see also [115]. The following pairs of the hot spots approach each other: (1,2), (3,4), (5,6), and (7,8). The d-wave pairing potential has opposite sign within each pair and vanishes at the zone diagonals. Thus, in the electron-overdoped cuprates, when hot spots get close enough, the d-wave pairing becomes suppressed. Then, a superconducting pairing of another symmetry may emerge.

Conclusion:

In case of hole-doped, and electron (under- and optimally-) doped superconductor cuprates the holes are the majority carriers, while electrons are minority. Beside the favor pairing symmetry is the $d_{x^2-y^2}$.

3.2.3 The Role of Pseudogap:

3.2.3.1 The Presence of Pseudogap:

density of states, spectral functions, and ARPES spectra calculated within DMFT+Σ_k show a pseudogap formation near the Fermi level of the quasiparticle [102], see also ref. [56].

Short note about ARPES:

Angle-resolved photoelectron spectroscopy (ARPES) probes the electronic structure (energy and momentum) of materials by measuring the energy and angle of the emitted electrons. In particular, ARPES can determine in "momentum space" the Fermi surface which represents the locus of the momenta of the highest energy occupied electron states (Fermi energy). The Fermi surface is important because electrons near the Fermi surface are responsible for many physical properties, including superconductivity. From high-resolution measurements along the Fermi surface in HTSCs, ARPES has revealed several major departures from the behavior of conventional superconductors [116; 117].

Intensive research has focused on the pseudogap regime, which is observed in high-T_c cuprates below a characteristic temperature that is higher than the transition temperature T_c. It occurs in a number of different experiments as a suppression of low-frequency spectral weight. They also proposed that there may be different pseudogap phenomena operating in different temperature and doping regimes [118].

3.2.4 Effect of Pseudogap:

It is widely believed that the peculiar normal pseudogap regime in underdoped cuprate superconductors, holds keys to unraveling the entire problem of cuprate superconductivity. In this regime, between the superconducting transition temperature T_c, and T^*, possibly hundreds of degrees higher, spectral density near the putative Fermi surface is suppressed. Evidence of this phenomenon is consistently observed most clearly in angle-resolved photoemission (ARPES), but also in c-axis tunneling, magnetic susceptibility, heat capacity, Raman scattering, neutron scattering, and NMR measurements. The variation of the pseudogap with momentum, strongest near the (π, 0) directions and weak or nonexistent near (π,π), mirrors that of the full $d_{x^2-y^2}$ superconducting gap. One potential explanation of this behavior, as suggested by Kivelson and Emery, is that local superconducting correlations (Cooper pairing) set in at T^*, but that long-range phase coherence is not established until the temperature drops below T_c. The notion is analogous to a magnetic material in which local moments form far above the temperature at which they become ordered. Nevertheless, this is not quite the same thing as pre-formed pairs [119].

3.2.5 Hot Spots and Pseudogap Together:

For high enough temperatures $2\pi T \gg \omega_{sf}$ where ω_{sf} is the frequency of spin fluctuations. Electron interaction with spin (pseudogap) fluctuations reduces then to elastic scattering. It can be seen that pseudogap fluctuations lead to significant suppression of superconductivity. This suppression of T_c is naturally due to partial dielectrization of electronic spectrum in the vicinity of hot spots. It is seen that in the presence of pseudogap fluctuations T_c suppression with the growth of disorder is faster than in the absence of the pseudogap. The effect of pseudogap fluctuations is enhanced by impurity scattering [115].

Conclusion:

We conclude that hot spots and pseudogap give a big chance for holes to be in pairs (hole pairing), and the electrons to be single electrons and a minority of electrons to be in pairs.

3.2.6 Hole Pairing:

A 'hole' is the absence of an electron, and hole carriers exist when an electronic energy band is almost full. Holes are different from electrons , as the Fig.(3.7) clearly shows. A hole in a full band has difficulty propagating due to the disruption it causes in its environment. The paired holes can propagate more easily (have a smaller effective mass) than single holes. In contrast, single electrons can move easily and so they don't pair. The reason for the increased mobility of holes upon pairing is that they 'undress' when they pair, and turn into electrons [120]. The charge distribution in superconductors is inhomogeneous, with higher concentration of negative charge near the surface. Some of this negative charge will spill out, giving rise to a negative electron layer, see also [116], right outside the surface of the superconductor, which

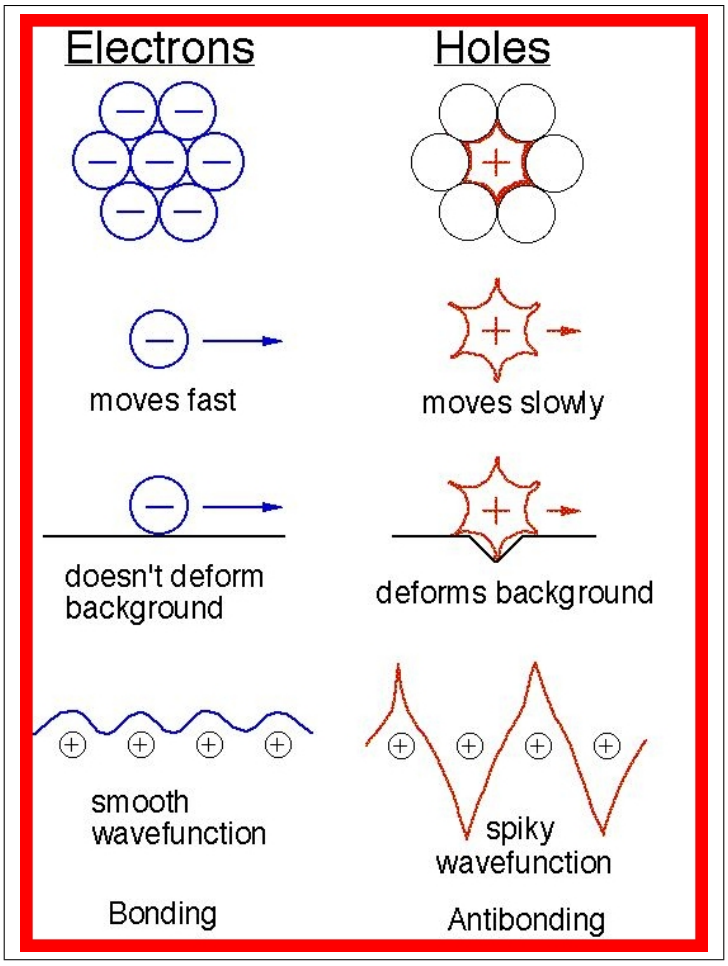

Figure 3.7: Taken from ref. [116]

should be experimentally detectable. Also superconductors should have a tendency to easily lose negative charge and become positively charged. Macroscopic spin currents are predicted to exist in superconducting bodies, giving rise to electric fields near the surface of multiply connected superconductors [121], see Fig.(3.8).

3.2.7 Short Note About Charge Stripes in High-Temperature Superconductors:

Depending on ARPES some researchers have talked about the self-assembling of charge carriers into spatially localized, one-dimensional stripes. For their ARPES experiments, the researchers studied a compound known to have stripes, $(La_{1.28}Nd_{0.6}Sr_{0.12})CuO_4$, whose "parent" compound, La_2CuO_4, is an insulator. Copper and some of the oxygen atoms are arranged on a square lattice in parallel planes with little interplanar interaction. Replacing some of the lanthanum in the insulator with strontium (strontium doping), which has one less electron for bonding, to form $(La_{2-x}Sr_x)CuO_4$ results in the generation of positively charged holes (missing electrons) that end up in the copper-oxygen planes. Over a strontium concentration range (x) from around 6 to 27 percent, the material becomes superconducting, except at 12 percent where the superconductivity is suppressed.

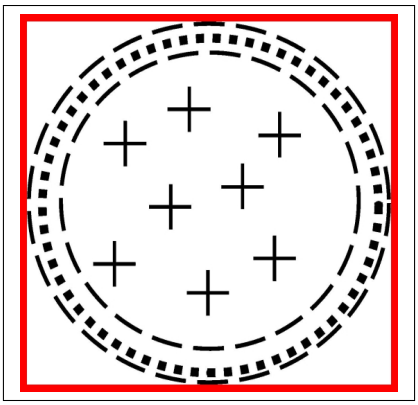

Figure 3.8: Schematic picture of a spherical superconductor. Negative charge is expelled from the bulk to the surface. The surface is denoted by the dotted line. A layer of negative charge exists outside the surface. Taken from ref. [121]

Stripes, in which holes are confined to parallel lines of copper atoms in the copper-oxygen planes separated by insulating regions without holes, were first observed at this so-called one-eighth doping, suggesting a perhaps antagonistic, but in any case intimate, relationship between superconductivity and stripe formation. The replacement of some lanthanum with neodymium stabilizes the stripes at low temperature. Stripes were later seen at other dopings and in other superconductors [116]†.

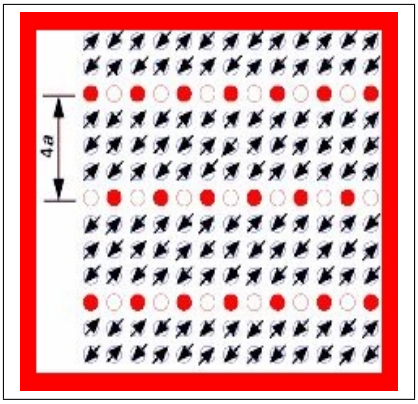

Figure 3.9: Model showing one orientation of charge stripes in the Cu-O planes. Up and down arrows represent local magnetic moments in the antiferromagnetic insulator that separates the stripes. Red circles in stripes represent holes. ,taken from ref. [116]

3.2.8 Conclusion:

From all the preceding items we see (conclude) that hole-pairing playing the major role for superconductivity, while electron-pairing play the minor role in HTSCs. One can imagine the superconductor as "Hole-pairs exist inside the core which in turn consists of stripes that contain the hole-pairs (and may be single electrons), and a minority of electron pairs outside the core".

†original work ref.[122]

3.3 Electrical Conductivity

3.3.1 Introduction

We shall study one of the major aspects of irreversible statistical mechanics: the transport coefficients that are obtained from general considerations of the linear response of a system to external forces. For irreversible statistical mechanics *Kirkwood* gave correlation function expression for the transport coefficients of dense fluids. For quantum systems, in 1956, *Nakano* developed a linear response theory and derived a correlation function expression for the electrical conductivity. These and other important aspects of response functions were summrized by *Kubo* in 1957 (cf. see Isihara[70]).

3.3.2 Simple Model of Conductivity

The simplest model of conductivity is that in a metal there are certain number, n_0, of electron per unit volume that are free to move under an applied field. These electrons, however, are subject to a damping force because of collisions. Therefore, we can write down the motion equation as:

$$m\frac{d\boldsymbol{v}}{dt} + mg\boldsymbol{v} = e\boldsymbol{\mathcal{E}}(\mathbf{x}, t) \tag{3.3.1}$$

where $g(= 1/\tau)$ is a damping constant that is some sort of average rate of collisions that involve a significant momentum transfer. Collisions occur between electrons, lattice vibrations, lattice imperfections, and impurities. Proper calculation of g involves quantum mechanical considerations. For rapidly oscillating fields, the displacement of electrons is small compared to a wavelength. Hence:

$$m\frac{d\mathbf{v}}{dt} + \frac{m}{\tau}\mathbf{v} = e\boldsymbol{\mathcal{E}_0}e^{-i\omega t} \tag{3.3.2}$$

where $\boldsymbol{\mathcal{E}_0}$ is the electric field at the average position of the electron. The conductivity is given by [123]:

$$\sigma = \frac{n_0 e^2 \tau}{m(1 - i\omega\tau)}, \tag{3.3.3}$$

with

$$\sigma_1 = \frac{n_0 e^2 \tau}{m(1 - \omega^2\tau^2)} \tag{3.3.4}$$

$$\sigma_2 = \frac{n_0 \omega e^2 \tau^2}{m(1 - \omega^2\tau^2)} \tag{3.3.5}$$

The DC conductivity ($\omega \to 0$)is then given by

$$\sigma_0 = \frac{n_0 e^2 \tau}{m}, \tag{3.3.6}$$

For all materials, Hagen and Rubens showed that the conductivity is essentially constant up to near IR frequencies ($\lambda < 2.5 \times 10^{-3} cm$) and the conductivity is essentially real. For IR and optical frequencies, however, the conductivity is complex and depends on frequency [123].

Insofar as it is possible to describe the perfect conductivity of a superconductor by postulating that a certain density (n_s) of its electrons act as if there were no scattering term (

by letting their τ go to infinity), Ohm's law is replaced by an accelerative supercurrent. That is, we have $d\boldsymbol{v}_s/dt = e\boldsymbol{\mathcal{E}}/m$, so that the total supercurrent $\boldsymbol{J}_s$ is governed by [23]

$$d\boldsymbol{J}_s/dt = (n_s e^2/m)\boldsymbol{\mathcal{E}} \tag{3.3.7}$$

3.3.3 Consequences of Symmetry

we conclude with some comments on the implications of crystal symmetry on $\sigma_{\alpha\beta}$ independent of any approximation to it. However, the presence of symmetry axes enables us to reduce the number of components. Let the symmetry axis be the x-axis, $\boldsymbol{x}$ is taken to be a two-or fourfold rotation axis or screw axis, as in Fig.(3.10), and $\boldsymbol{\mathcal{E}}$ is taken parallel to $\boldsymbol{y}$ Fig.(3.10(a)). Now if we reverse the field this reverses J_x. Rotation about $\boldsymbol{x}$ through(π) is equivalent to this reversal Fig.(3.10(b)) but this rotation leaves the physical situation completely unchanged, so that J_x is *not* reversed. Hence, $J_x = 0$ and this is true for a symmetry axis of any kind, implying

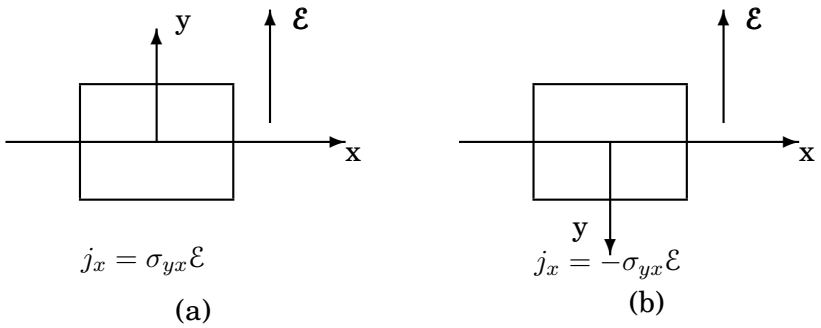

Figure 3.10: Illustrating effect of twofold rotation axis as screw axis,with electric field normal to axis, on components of electrical conductivity tensor. In (b) specimen is rotated about x-axis through π.

$$\sigma_{xy} = \sigma_{yx} = \sigma_{xz} = \sigma_{zx} = 0 \tag{3.3.8}$$

where $\boldsymbol{x}$ is a symmetry axis. Let $\boldsymbol{x}$ be a fourfold rotation axis or screw axis, as in Fig.(3.11) in which $\boldsymbol{x}$ is taken perpendicular to the paper, represent identical physical situations and

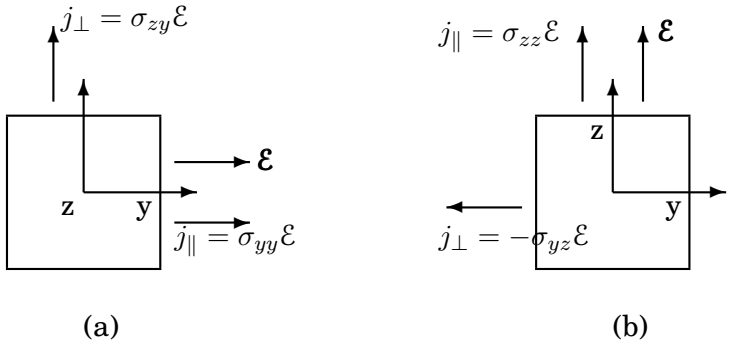

Figure 3.11: Illustrating effect of fourfold rotation axis or screw axis,with electric field normal to axis, on components of electrical conductivity tensor. In (b), field $\boldsymbol{\mathcal{E}}$, normal to x - direction, is rotated through $\pi/2$ relative to (a).

neither $J_\perp$ nor $J_\parallel$ changes (except in direction) as $\boldsymbol{\mathcal{E}}$, perpendicular to $\boldsymbol{x}$, is rotated through

$(\pi/2)$. It follows that $J_\perp = 0$ and

$$\sigma_{zy} = \sigma_{yz} = 0, \sigma_{yy} = \sigma_{zz}. \tag{3.3.9}$$

If $\boldsymbol{x}$ is a fourfold rotation axis or screw axis, so that there are only two independent components of the conductivity tensor [67].

3.3.4 Electrical Conductivity of the Normal State

An electronic property much studied experimentally is the complex frequencydependent conductivity $\sigma(\omega)$. As is well known the Landau Fermi liquid theory (LFLT) predicts that the real part of the conductivity, $\sigma_1(\omega)(= \sigma_R)$, follows the Drude law, which yields that for high (infrared) frequencies, $\sigma_{Drude}(\omega) \propto \omega^{-2}$. The Drude law is obeyed for ordinary metals, both the non superconductors (e.g., noble metals) as well as conventional superconductors (e.g., Al, Hg) above the critical temperature T_c. We actually only calculate the real part $\sigma_1(\omega)$ of the conductivity which is given by the imaginary part of the current-current correlation function Eq.(2.8.35). For the imaginary part the sum over Matsubara frequencies and the momentum integral converge sufficiently rapidly so that their order can be interchanged. Details of this calculation can be found in Appendix F. The result for $\sigma_1(\omega)$ in this case is sufficiently simple so that the integral involved in calculating the imaginary part $\sigma_2(\omega)$ as Hilbert transform of $\sigma_1(\omega)$ can be performed analytically.

The local electrical conductivity can be calculated by means of the *Kubo* formula, as described in section 2.8.2.

$$\sigma_1(\omega) = -\frac{e^2\, Im\chi(\omega)}{\omega} \tag{3.3.10}$$

where $\chi(\omega) = \chi(i\nu_m \to \omega + i\delta)$ is the complex susceptibility, (see section 2.8.1). It is given by Eq.(2.8.42)

$$\begin{aligned}\chi_{\alpha\beta}(\omega) =& \frac{1}{2\pi i}\int_{-\infty}^{\infty} d\omega_0\, f(\frac{\omega_0}{T})\, Sp \int \frac{d^3p}{(2\pi)^3}\frac{2p_\alpha}{2m}\frac{2p_\beta}{2m} \\ &\times \Big\{G_A(\mathbf{p},\omega_0-\omega)2iIm\, G_R(\mathbf{p},\omega_0) + G_R(\mathbf{p},\omega_0+\omega)2iIm\, G_R(\mathbf{p},\omega_0)\Big\}.\end{aligned} \tag{3.3.11}$$

We do not consider magnetic impurities or external magnetic fields, so that *Green's* functions are diagonal and independent of spin. The sum over spin states designated (Sp) in (3.3.11) thus simply contributes a factor 2. Then

$$\begin{aligned}\chi_{\alpha\beta}(\omega) =& (2/\pi)\int_{-\infty}^{\infty} d\omega_0\, f(\frac{\omega_0}{T}) \int \frac{d^3p}{(2\pi)^3}\frac{p_\alpha p_\beta}{m^2}\Big\{ \\ & G_A(\mathbf{p},\omega_0-\omega)Im\, G_R(\mathbf{p},\omega_0) + G_R(\mathbf{p},\omega_0+\omega)Im\, G_R(\mathbf{p},\omega_0)\Big\} \\ =& (2/\pi)\int_{-\infty}^{\infty} d\omega_0\, f(\frac{\omega_0}{T}) \int \frac{d^3p}{(2\pi)^3}\frac{p_\alpha p_\beta}{m^2} \\ & Im\, G_R(\mathbf{p},\omega_0)\Big\{G_R(\mathbf{p},\omega_0+\omega) + G_A(\mathbf{p},\omega_0-\omega)\Big\}\end{aligned} \tag{3.3.12}$$

From section 2.6.3 on the spectral function and using the Eq.(2.6.25), we have [78]

$$Im\, G_R(p,\omega_0) = -\,(1/2)A(\mathbf{p},\omega_0), and \tag{3.3.13}$$

$$Im\Big[G_R(\mathbf{p},\omega_0+\omega) + G_A(\mathbf{p},\omega_0-\omega)\Big] = -\,(1/2)\Big[A(\mathbf{p},\omega_0+\omega) - A(\mathbf{p},\omega_0-\omega)\Big]. \tag{3.3.14}$$

Where $A(\mathbf{p},\omega_0)$ is the electron spectral function [124], then

$$Im\,\chi_{\alpha\beta}(\omega) = \frac{1}{2\pi}\int_{-\infty}^{\infty} d\omega_0\, f(\omega_0/T)\int \frac{d^3p}{(2\pi)^3}\frac{p_\alpha p_\beta}{m^2}A(p,\omega_0)\Big\{A(p,\omega_0+\omega)-A(p,\omega_0-\omega)\Big\} \quad (3.3.15)$$

For isotropic systems [see Table (1.3)]: All diagonal components of χ are equal while nondiagonal components vanish. In Appendix F we show that for a parabolic band (nearly free electron model) one obtains

$$\begin{aligned}\sigma_1 =& \frac{e^2}{\omega} Im\,\chi_{\alpha\alpha} = (\frac{p_f^3}{3\pi^2})\frac{e^2\tau}{m(1+\omega^2\tau^2)}\\ =& \frac{n_0e^2\tau}{m(1+\omega^2\tau^2)} = \sigma_0\frac{1}{(1+\omega^2\tau^2)}\end{aligned}$$

where m is an (effective) mass, $n_0(=p_f^3/3\pi^2)$ is the density of particles contained in the *Fermi* sphere of radius p_f, and τ is a relaxation time.

Using the Kramer-Krönig relation for conductivity , the imaginary part of conductivity σ_2 is given by

$$\begin{aligned}\sigma_2(\omega) =& -\frac{\mathcal{P}}{\pi}\int_{-\infty}^{\infty}\frac{\sigma_1(\omega)}{(\omega_0-\omega)}d\omega_0\\ =& -\sigma_0\frac{\mathcal{P}}{\pi}\int_{-\infty}^{\infty}\frac{1}{(1+\omega^2\tau^2)}\frac{d\omega_0}{(\omega_0-\omega)}\\ =& -\frac{\sigma_0}{\tau^2}\frac{\mathcal{P}}{\pi}\int_{-\infty}^{\infty}\frac{1}{(\omega^2+\frac{1}{\tau^2})}\frac{d\omega_0}{(\omega_0-\omega)}\end{aligned}$$

Using Hilbert transform

$$\pi^{-1}\mathcal{P}\int_{-\infty}^{\infty} f(x)(x-y)^{-1}\,dx = -\frac{y}{a(y^2+a^2)}, \quad (3.3.16)$$

the imaginary part of conductivity σ_2 will be

$$\sigma_2(\omega) = \frac{\sigma_0}{\tau^2}\frac{\omega}{\frac{1}{\tau}(\omega^2+\frac{1}{\tau^2})}$$

or

$$\sigma_2(\omega) = \frac{\sigma_0\omega\tau}{(1+\omega^2\tau^2)} = \frac{ne^2}{m}\frac{\omega\tau^2}{1+\omega^2\tau^2}$$

As we have seen the real part of electrical conductivity obeys the Drude law in agreement with the Landau Fermi liquid theory(LFLT). In the clean limit $\tau\to\infty$ σ_2 will be $(\frac{1}{\omega}\frac{n_0e^2}{m})$ as discussed previously in sections 2.8.2.1 and 3.3.2.

Chapter 4

Summary of Conclusion

- Using the complete elliptic integral we have got a suitable form for DOS $N(\omega)$ for $E > 0$ and $E < 0$, and also a suitable form for its Hilbert transform $F(\omega)$.

- The Hopping integral B as we have seen affect the behaviour and the position of the DOS, and also affect the behaviour of Fermi surface resulting in what is called hot spots.

- In the presence of impurity, whatever the model of the DOS, we get a virtual or resonance states, just the value of U that control the presence and the position of that generated states.

- The model of DOS affect very much the behaviour (we mean the shape) of the DOS Hilbert transform $F(\omega)$.

- We have seen also the importance of the dispersion relation $\varepsilon(\mathbf{k})$, and also the importance of the presence of the next-nearest hoping integral B.

- Theoretically, if we controlled the parameters $\varepsilon(\mathbf{k})$ and U, we can get (construct) a superconductor with the features that we need.

- Hot spots together with pseudogap are the key to solve the mystery of superconductivity in HTSCs.

- Holes (hole-pairing) play the major role in superconductivity.

- Because of hot spots and its lower effective mass [than that of electrons], hole pairs are the accepted [for us at least] regime responsible for superconductivity. Sure we are not talking about zero electron pairs, we do mean the superconductor materials look like the semiconductors, the deference between them is that in case of semiconductors we talk about electrons and holes, in superconductors case we instead talk about electron pairs and hole pairs.

- D-wave in general is the favor pairing symmetry of the order parameter, for electron-, hole-doped cuprates, except in the case of overdoped electron regime.

- We have got an expression for generalized susceptibility (in turn electrical conductivity)

agrees with what we can call Durst and Lee approach. And then have calculated the electrical conductivity for isotropic systems, we have found that its behaviour obeys Drude law in accordance with the prediction of Fermi Landau liquid theory.

Appendix A

Schrödinger, Heisenberg, and Interaction Pictures

In the Schrödinger picture of quantum mechanics, the time evolution of the dynamical system is described solely by the wave functions, and the dynamical operators (c'_λs or ψ's) are time-independent. The situation is quite the opposite in the Heisenberg picture. There, the time dependence is within the operators, and the state vectors are time-independent [125].

A.1 Schrödinger Picture

The state vector satisfies the Schrödinger equation

$$i\frac{\partial \Psi^S(t)}{\partial t} = H\Psi^S(t) \tag{A.1.1}$$

This has the formal solution (if H does not depend explicitly on the time)

$$\Psi^S(t) = e^{-iHt}\Psi^S(0) \tag{A.1.2}$$

A.2 Heisenberg Picture

We define the state vector to agree with the Schrödinger state vector at $t = 0$:

$$\Psi^H = e^{-iHt}\Psi^S(0) \tag{A.2.1}$$

The operators change with time, in such away that the matrix element of an operator between two states in the Heisenberg picture is the same as the matrix element of the corresponding operator between the corresponding two states in the Schrödinger picture[81]:

$$< \Psi_a^S(t)|\mathcal{O}_S|\Psi_b^S(t) > =< \Psi_a^H|\mathcal{O}_H(t)|\Psi_b^H > \tag{A.2.2}$$

Using (A.1.2), we have

$$< \Psi_a^S(0)|e^{iHt}\mathcal{O}_S e^{-iHt}|\Psi_b^S(0) > =< \Psi_a^H|\mathcal{O}_H(t)|\Psi_b^H >,$$

so that

$$\mathcal{O}_H(t) = e^{iHt}\mathcal{O}_S e^{-iHt} \tag{A.2.3}$$

or simply

$$\mathcal{O}_H(t) = e^{iHt}\mathcal{O}e^{-iHt} \tag{A.2.4}$$

Where e^{-iHt} is a unitary operator and carries out the time evolution from $t = 0$ to t. Eq.(A.2.4) represents the Heisenberg picture of operators.
Taking the time derivative of Eq.(A.2.4)

$$\begin{aligned} i\frac{\partial \mathcal{O}}{\partial t} &= i\Big[iHe^{iHt}\mathcal{O}e^{-iHt} + e^{iHt}\mathcal{O}(-iH)e^{-iHt}\Big] \\ &= [\mathcal{O}(t), H] \end{aligned} \tag{A.2.5}$$

Eq.A.2.5 is the Heisenberg equation of motion for operators[72].
For systems where H does not depend explicitly on time $H^S = H^H$,i.e., the Hamiltonian is a constant of the motion. H may still be expressed with either Schrödinger or Heisenberg operators, and although the total Hamiltonian is the same in the two pictures, various parts of it may be quite different in the two pictures[81].

A.2.1 Heisenberg Picture in Fock Space:

As in Eq.(A.2.5) the equation of motion for c_λ's reads[72; 126]

$$\begin{aligned} i\frac{\partial c_\lambda(t)}{\partial t} &= [c_\lambda, H] \\ &= [c_\lambda, \sum_{\lambda'} \varepsilon_{\lambda'}\, c^\dagger_{\lambda'} c_{\lambda'}] \\ &= \varepsilon_\lambda c_\lambda \\ \Rightarrow c_\lambda(t) &= c_\lambda(0)e^{-i\varepsilon_\lambda t} \end{aligned} \tag{A.2.6}$$

A.2.2 Field operators in terms of Heisenberg picture and grand canonical Hamiltonian in real- and imaginary-time:

In real time:

$$\psi(\mathbf{r}, t) = e^{ikt}\psi(\mathbf{r})e^{-ikt}, \quad and \tag{A.2.7}$$

$$\psi^\dagger(\mathbf{r}, t) = [\psi(\mathbf{r}, t)]^\dagger \tag{A.2.8}$$

In imaginary time [127]:

$$\psi(\mathbf{r}, \tau) = e^{k\tau}\psi(\mathbf{r})e^{-k\tau}, \quad and \tag{A.2.9}$$

$$\psi^\dagger(\mathbf{r}, \tau) = e^{k\tau}\psi(\mathbf{r})e^{-k\tau} \neq [\psi(\mathbf{r}, \tau)]^\dagger \tag{A.2.10}$$

A.3 Interaction Representation for Operators

This representation is useful when the *Hamiltonian* is of the form

$$H(t) = H_0 + H'(t) \tag{2.8.1}$$

H_0 is considered soluble and time-independent and the perturbation part $H'(t)$ depends explicitly on time . Then the time development operator is no longer given by e^{-iHt}. When $H'(t)$ can be considered as a small perturbation it is useful to transform into the so-called interaction picture according to

$$A_I(\boldsymbol{r}', t) = e^{iH_0 t} A(\boldsymbol{r}', t) e^{-iH_0 t} \tag{A.3.1}$$

A.4 The Equation of Motion for $\rho(t)$

We start with the *Schrödinger* equation

$$i|\dot{\psi}> = H|\psi> \qquad (|\dot{\psi}>= \frac{\partial}{\partial t}|\psi>)$$

so that

$$-i < \dot{\psi}| =< \psi|H$$

The density operator is defined as

$$\rho = \sum_n P_n |\psi_n >< \psi_n|$$

The time derivative of (ρ) is

$$\begin{aligned}
i\frac{\partial \rho}{\partial t} &= i\frac{\partial}{\partial t}\{\sum_n P_n\{|\psi_n >< \psi_n|\}\\
i\frac{\partial \rho}{\partial t} &= \sum_n P_n\{-|\psi_n > (-i) < \dot{\psi}_n| + (i)|\dot{\psi}_n >< \psi_n|\}\\
&= \sum_n P_n\{-|\psi_n >< \psi_n|H + H|\psi_n >< \psi_n|\}\\
&= \sum_n P_n\{H|\psi_n >< \psi_n| - |\psi_n >< \psi_n|H\}\\
&= \sum_n \{HP_n|\psi_n >< \psi_n| - P_n\psi_n >< \psi_n|H\}\\
&= [H\rho - \rho H]\\
&= [H, \rho]
\end{aligned}$$

Or

$$i\frac{\partial \rho}{\partial t} = [H, \rho]$$

Appendix B

Elliptic Integrals

An elliptic integral is an integral involving a rational function which contains square roots of cubic or quartic polynomials. Generally, the elliptic integrals CANNOT be expressed in terms of elementary functions[128]. We are interested in elliptic integrals of the first kind.

B.1 Elliptic Integral of the First Kind

Let the elliptic modulus k satisfy $0 < k^2 < 1$, and the Jacobi amplitude be given by $\phi = \text{am}\, u$. The incomplete elliptic integral of the first kind, see Fig.(B.1), is then defined

$$F(\phi, k) = \int_0^{\phi} \frac{d\theta}{\sqrt{(1 - k^2 \sin^2 \theta)}}. \tag{B.1.1}$$

The elliptic integral of the first kind is implemented in Mathematica as EllipticF[ϕ, m] (note the use of the parameter $m = k^2$ instead of the modulus k).
Letting

$$t \equiv \sin\theta \tag{B.1.2}$$

$$dt = \cos\theta d\theta \tag{B.1.3}$$

$$= \sqrt{1 - t^2} d\theta, \tag{B.1.4}$$

Then ((B.1.1)) can be written as

$$F(\phi, k) = \int_0^{\sin\phi} \frac{1}{\sqrt{1 - k^2 t^2}} \frac{dt}{\sqrt{1 - t^2}} \tag{B.1.5}$$

$$= \int_0^{\sin\phi} \frac{dt}{\sqrt{(1 - k^2 t^2)(1 - t^2)}}. \tag{B.1.6}$$

Letting

$$v \equiv \tan\theta \tag{B.1.7}$$

$$dv = \sec^2\theta d\theta = (1 + v^2) d\theta, \tag{B.1.8}$$

then the integral can also be written as

$$F(\phi, k) = \int_0^{\tan\phi} \frac{dv}{\sqrt{(1 + v^2)(1 + k'^2 v^2)}}, \tag{B.1.9}$$

where $k^{'2} = 1 - k^2$ is the complementary elliptic modulus[129]. The inverse function of F(ϕ,k) is given by the Jacobi amplitude

$$F^{-1}(u,k) = \phi = am(u,k). \tag{B.1.10}$$

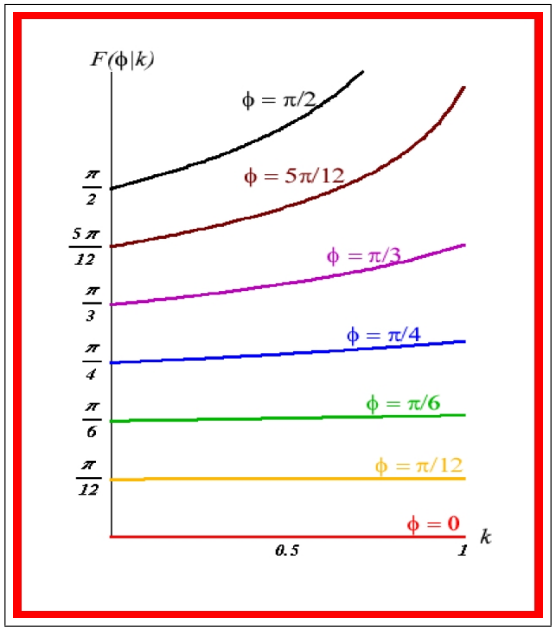

Figure B.1: Elliptic Integral of the First Kind, taken from website[128]

B.2 Complete Elliptic Integrals

For the amplitude $\phi = \pi/2$, the elliptic integrals are said to be complete[128], Fig.(B.2).

$$K(k) = F(\frac{\pi}{2}, k) = \int_0^{\pi/2} \frac{d\theta}{(\sqrt{(1 - k^2 \sin^2\theta)})} = \int_0^1 \frac{(dt)}{(\sqrt{((1-k^2t^2)(1-t^2))})}. \tag{B.2.1}$$

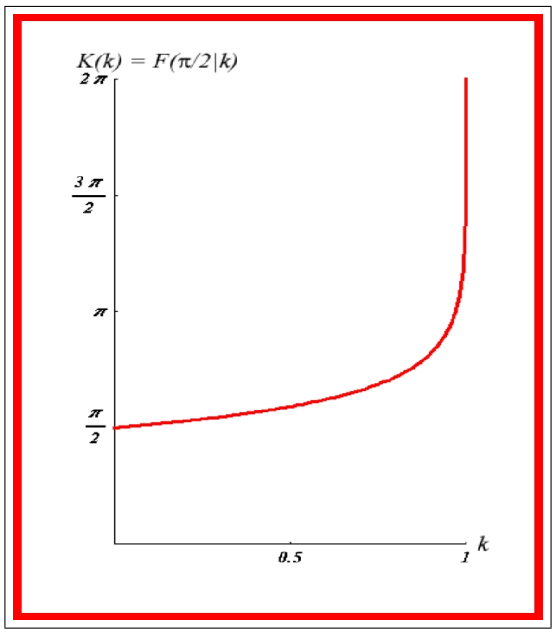

Figure B.2: Complete Elliptic Integrals of the first kind, taken from website[128]

Appendix C

The Calculation of the Density of States and Its Hilbert Transform

The density of states $N(\omega)$ is obtained from the imaginary part of the one-particle Green's function $G^0(\mathbf{k},\omega)$, and the function $F(\omega)$ is its real part $ReG^0(\mathbf{k},\omega)$

$$\begin{aligned}\int \frac{d^2k}{(2\pi)^2} G^0(k) =& \mathcal{P}\int \frac{d^2k}{(2\pi)^2}\frac{1}{\omega-\varepsilon(k)} - i\pi\int \frac{d^2k}{(2\pi)^2}\delta(\omega-\varepsilon(k)) \\ =& F(\omega) - i\,\pi\, N(\omega)\end{aligned}$$

Density of states:

the 1st step is to convert all quantities into dimensionless units. This corresponds to the following change in notation:

$$k_x a, k_y a \to k_x, k_y,$$

$$\varepsilon_k/2t, \mu/2t, \omega/2t, ... \to \varepsilon_k(k_x,k_y), \mu, \omega, ...$$

Next, we define the functions

$$N(\omega) = \frac{1}{(2\pi)^2}\int_{-\pi}^{\pi} dk_x \int_{-\pi}^{\pi} dk_y \delta(\omega-\varepsilon(k)) \tag{C.0.1}$$

$$\varepsilon(k) = -(\cos k_x + \cos k_y) + 2B(\cos k_x \cos k_y) - \mu$$

and then

$$\omega - \varepsilon(k) = \omega + [\cos k_x + \cos k_y - 2B\cos k_x \cos k_y + \mu]$$

or

$$\omega - \varepsilon(k) = E + \cos k_x + \cos k_y - 2B\cos k_x \cos k_y \tag{C.0.2}$$

(C.0.3)

where $E = \omega + \mu$.
Substituting Eq.(C.0.2) into Eq.(C.0.1), we get

$$\begin{aligned} N(\omega) =& \frac{1}{4\pi^2} \int_{-\pi}^{\pi} dk_x \int_{-\pi}^{\pi} dk_y \delta(E + (\cos k_x + \cos k_y - 2B \cos k_x \cos k_y)) \\ =& \frac{1}{2\pi^2} \int_{0}^{\pi} dk_x \int_{0}^{\pi} dk_y \delta(E + (\cos k_x + \cos k_y - 2B \cos k_x \cos k_y)) \end{aligned}$$

note that the DOS integral is symmetric under the interchanges $k_x \to -k_x, k_y \to k_y$, hence its domain of integration can be reduced from $[-\pi, \pi] \times [-\pi, \pi] \to [0, \pi] \times [0, \pi]$. Subsquently, we can do the change of variables $u = \cos k_x,\ v = \cos k_y$ and obtain

$$\begin{aligned} N(\omega) =& \frac{1}{2\pi^2} \int_{-1}^{1} d\,u \int_{-1}^{1} d\,v\, \delta(E + u + v - 2Buv) \\ & \times \frac{1}{\sqrt{1-u^2}\sqrt{1-v^2}} \end{aligned}$$

where $-2 + 2B \leq E \leq 2 + 2B$.
Performing the v integration first, we find that

$$\begin{aligned} N(\omega) =& \frac{1}{2\pi^2} \int_{L}^{U} du \frac{1}{\sqrt{1-u^2}\sqrt{(1-2Bu)^2 - (E+u)^2}} \\ =& \frac{1}{2\pi^2} \int_{L}^{U} d\,u \frac{1}{\sqrt{(1-u)(1+u)(\frac{1+E}{1-2B} + u)(\frac{1-E}{1+2B} + -u)(1-4B^2)}} \\ =& \frac{1}{2\pi^2\sqrt{1-4B^2}} \int_{L}^{U} d\,u \frac{1}{\sqrt{(u-1)(u-\frac{1-E}{1+2B})(u-[-1])(u-[-\frac{1+E}{1-2B}])}} \end{aligned} \tag{C.0.4}$$

Putting $\alpha_1 = 1$, $\alpha_2 = \frac{1-E}{1+2B}$, $\alpha_3 = -1$, and $\alpha_4 = -\frac{1+E}{1-2B}$ the inegration then has the form

$$N(\omega) = \frac{1}{2\pi^2} \frac{1}{\sqrt{1-4B^2}} \int_{L}^{U} d\,u \frac{1}{\sqrt{(u-\alpha_1)(u-\alpha_2)(u-\alpha_3)(u-\alpha_4)}}$$

The integral lower(L) and upper(U) limits: the limits of integration correspond to the two inner roots of the polynomial under the square root in Eq.((C.0.4)) i.e., $E + u = v - 2Buv$, these limits are different for different conditions for E and B.

$$-1 \leq v = \frac{E+u}{1-2Bu} \leq 1$$

For $2B < 1$:
$1 - 2Bu > 1$ for all $u \Rightarrow$

$$-(1-2Bu) \leq E + u \leq 1 - 2Bu$$

or

$$-(1-2Bu) - E \leq u \leq 1 - 2Bu - u$$

at the same time $-1 \leq u \leq 1$
For the case $E > 0$:
the lower limit is

$$Max\{-1 + 2Bu - E, -1\} = -1$$

i.e., $L = -1 = \alpha_3$, and
the upper limit is

$$u = 1 - 2Bu - E$$

$$\Rightarrow\ u = \frac{1-E}{1+2B}$$

i.e., $U = \frac{1-E}{1+2B} = \alpha_2$
Then the final form of our integral is

$$N(\omega) = \frac{1}{2\pi^2}\frac{1}{\sqrt{1-4B^2}}\int_{\alpha_3}^{\alpha_2} d\,u \frac{1}{\sqrt{(u-\alpha_1)(u-\alpha_2)(u-\alpha_3)(u-\alpha_4)}} \tag{C.0.5}$$

with $\alpha_1 > \alpha_2 > \alpha_3 > \alpha_4$ and $\alpha_2 \geq u \geq \alpha_3$.
The solution of the integration (C.0.5), (see Gröbner-Hofreiter, s.84), is given by

$$N(\omega) = \frac{1}{\pi^2}\frac{1}{\sqrt{1+2BE}}\Big[\frac{1}{\sqrt{(\alpha_1-\alpha_3)(\alpha_2-\alpha_4)}}K\Big(k^2 = \frac{(\alpha_1-\alpha_4)(\alpha_2-\alpha_3)}{(\alpha_1-\alpha_3)(\alpha_2-\alpha_4)}\Big)\Big] \tag{C.0.6}$$

and hence,

$$N(\omega) = \frac{1}{\pi^2}\frac{1}{\sqrt{1+2BE}}K\Big(\frac{1-(\frac{E}{2}-B)^2}{1+2BE}\Big) \tag{C.0.7}$$

For the case $E < 0$:
the upper limit is

$$Min\{1, 1-2Bu-E\} = 1$$

$\Rightarrow u = \frac{1-E}{1+2B}$

so that

$$k^2 = \frac{(\alpha_1-\alpha_2)(\alpha_3-\alpha_4)}{(\alpha_1-\alpha_3)(\alpha_2-\alpha_4)} \tag{C.0.8}$$

$$= \frac{(\frac{E}{2}+B)^2}{(\frac{E}{2}-B)^2-1} \tag{C.0.9}$$

i.e.

$$N(\omega) = \frac{1}{\pi^2}\frac{1}{\sqrt{(\frac{E}{2}-B)^2-1}}K\Big(\frac{(\frac{E}{2}+B)^2}{(\frac{E}{2}-B)^2-1}\Big) \tag{C.0.10}$$

In this case i.e., when the parameter $K^2 > 1$, we must use the relation[130] $Re\{K(k^2)\} = Re\{k^{-1}K(k^{-2})\}$

$$N(\omega) = Sign[E]\frac{1}{\pi^2}\frac{1}{(\frac{E}{2}+B)}K\Big(\frac{(\frac{E}{2}-B)^2-1}{(\frac{E}{2}+B)^2}\Big) \tag{C.0.11}$$

The Function $F(\omega)$

$$\begin{aligned} F(\omega) =& \mathcal{P}\int \frac{dk^2}{(2\pi)^2} \quad \frac{1}{\omega-\epsilon(k)} \\ =& \frac{1}{(2\pi)^2}\mathcal{P}\int_{-\pi}^{\pi} \frac{dk_x dk_y}{\cos k_y + E + [(1-2B)\cos k_y]\cos k_x} \\ =& \frac{1}{(2\pi)^2}\int_{-\pi}^{\pi} dk_y\, \mathcal{P}\int_{-\pi}^{\pi} dk_x \frac{1}{a+b\cos k_x} \\ =& \frac{2}{(2\pi)^2}\int_{-\pi}^{\pi} dk_y\, \mathcal{P}\int_{0}^{\pi} dk_x \frac{1}{a+b\cos k_x} \end{aligned}$$

where, $a = E + \cos k_y, b = (1-2B)\cos k_y$, and ε & E as before.
The method of evaluating this definite integral is based directly on Cauchy's theorem. This integral has the form

$$I = \int_0^{\pi} \frac{d\theta}{a - b\cos\theta}, \quad \text{where } \theta = K_x$$

where a and b are real and $a > b > 0$, see D for the case $b > a$. The integral is an even function of θ, and therefore

$$I = \frac{1}{2}\int_0^{2\pi} \frac{d\theta}{a - b\cos\theta} = \int_0^{2\pi} \frac{e^{i\theta}d\theta}{2ae^{i\theta} - b(e^{2i\theta}+1)}. \tag{C.0.12}$$

Put $e^{i\theta} = z$.
As θ increases from 0 to 2π, z moves round the circle $|z| = 1$. Then

$$I = -\frac{1}{i}\int_c \frac{dz}{bz^2 - 2az + b}, \tag{C.0.13}$$

where the path of integration is around the unit circle. But this is a closed contour and the integral is therefore equal to $2\pi i$ times the sum of the residues at any poles within it. There are two poles, namely, the zeros of the denominator, and their products is 1; write

$$b\alpha = a - \sqrt{(a^2-b^2)}, \quad b/\alpha = a + \sqrt{(a^2-b^2)}, \tag{C.0.14}$$

Then α is within the unit circle and $1/\alpha$ outside, as shown in Fig.(C). Then

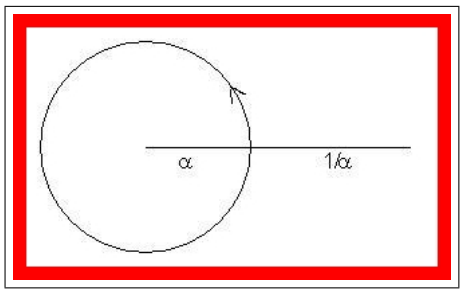

$$I = -\frac{1}{ib}\int_c \frac{dz}{(z-\alpha)(z-1/\alpha)}. \tag{C.0.15}$$

Near α the integrand has the form

$$\frac{1}{\alpha - 1/\alpha}\Big(\frac{1}{z-\alpha} + \text{terms analytic at z}\Big),$$

and the residues is therefore $(\alpha - 1/\alpha)^{-1}$[131]. Hence

$$I = -\frac{2\pi i}{ib(\alpha - 1/\alpha)} = \frac{\pi}{\sqrt{(a^2 - b^2)}}. \tag{C.0.16}$$

i.e.,

$$F(\omega) = \frac{1}{(2\pi)} \int_{-\pi}^{\pi} dk_y \, \frac{1}{\sqrt{(a^2 - b^2)}} \tag{C.0.17}$$

then, $F(\omega)$ is

$$\begin{aligned}
F(\omega) =& \frac{1}{(2\pi)} \int_{-\pi}^{\pi} dk_y \, \frac{1}{\sqrt{[(E + \cos k_x) + (1 - 2B\cos k_y)][(E + \cos k_x) - (1 - 2B\cos k_y)]}} \\
=& \frac{1}{(2\pi)} \int_{-1}^{1} dk_y \, \frac{1}{\sqrt{(1-u^2)([E+u] + [1-2Bu])([E+u] - [1-2Bu])}} \\
=& \frac{1}{(2\pi)} \int_{-1}^{1} dk_y \, \frac{1}{\sqrt{(1-u^2)(E + 1 + (1-2B)u)(E - 1 + (1+2B)u)}} \\
=& \frac{1}{(2\pi)} \int_{-1}^{1} dk_y \, \frac{1}{\sqrt{-(u-1)(u+1)(u + \frac{E+1}{1-2B})(u - \frac{1-E}{1+2B})(1-4B^2)}} \\
=& \frac{1}{(2\pi)} \int_{-1}^{1} dk_y \, \frac{1}{\sqrt{\alpha_0(u-\alpha_1)(u-\alpha_2)(u-\alpha_3)(u-\alpha_4)(1-4B^2)}} \\
=& \frac{1}{(2\pi)} \frac{1}{\sqrt{1-4B^2}} \int_{-1}^{1} dk_y \, \frac{1}{\sqrt{\alpha_0(u-\alpha_1)(u-\alpha_2)(u-\alpha_3)(u-\alpha_4)}}
\end{aligned}$$

with $\alpha_0 < 0$ and $\alpha_1 > \alpha_2 > \alpha_3 > \alpha_4$, see Gröbner and Hofreiter.
The solution for the function $F(\omega)$ has the form

$$F(\omega) = \frac{1}{(\pi)} \frac{1}{\sqrt{1-4B^2}} \frac{2}{\sqrt{(\alpha_1 - \alpha_3)(\alpha_2 - \alpha_4)}} K\Big(\frac{(\alpha_1 - \alpha_2)(\alpha_3 - \alpha_4)}{(\alpha_1 - \alpha_3)(\alpha_2 - \alpha_4)}\Big) \tag{C.0.18}$$

For E we have the next cases, they are:

(1) $E > 2 + 2B$

(2) $-2B < E < 2 + 2B$

(3) $-2 + 2B < E < -2B$

(1) $E > 2 + 2B$:

$\alpha_1 = 1, \alpha_2 = -1,\ \alpha_3 = \frac{1-E}{1+2B},$ and $\alpha_4 = -\frac{E+1}{1-2B}$

$$\begin{aligned}
F(\omega) =& \frac{1}{2} \frac{1}{(\pi)} \frac{1}{\sqrt{(1-4B^2)}} \int_{-1}^{1} du \, \frac{1}{\sqrt{(u-\alpha_1)(u-\alpha_2)(u-\alpha_3)(u-\alpha_4)}} \\
=& \frac{1}{(\pi)} \frac{1}{\sqrt{(1 + 2B - 1 + E)(-1 + 2B + E + 1)}} K\Big(\frac{4(2 + 4BE)}{(E + 2B)(E + 2B)}\Big) \\
=& Sign(E) \frac{1}{(\pi)} \frac{1}{\sqrt{(2B + E)}} K\Big(\frac{4(1 + 2BE)}{(2B + E)}\Big)
\end{aligned}$$

(2) $-2B < E < 2 + 2B$:

$\alpha_1 = 1, \alpha_2 = \frac{1-E}{1+2B},\ \alpha_3 = -1,$ and $\alpha_4 = -\frac{E+1}{1-2B}$

$$F(\omega) = \frac{1}{2}\,\frac{1}{(\pi)}\,\frac{1}{\sqrt{(1-4B^2)}}\,\frac{2}{\sqrt{(1+1)[\frac{1-E}{1+2B}+\frac{1+E}{1-2B}]}}\,K\Big(\frac{1-(\frac{1-E}{1+2B})(-1+\frac{E+1}{1-2B})}{(2\frac{1+1+4BE}{1-4B^2})\cdot 2}\Big)$$

$$F(\omega) = Sign(E)\ \frac{1}{(\pi)}\,\frac{1}{2\sqrt{(2BE+1)}}\,K\Big(\frac{(2B+E)(2B+E)}{4(1+2BE)}\Big)$$

For $E + 2B \geq 0$:

$$F(\omega) = Sign(E)\ \frac{1}{(\pi)}\,\frac{1}{2\sqrt{(2BE+1)}}\,K\Big(\frac{(2B+E)^2}{4(1+2BE)}\Big)$$

(3) $-2 + 2B < E < -2B$:

$\alpha_1 = \frac{1-E}{1+2B}, \alpha_2 = 1,\ \alpha_3 = -\frac{E+1}{1-2B},$ and $\alpha_4 = -1$

$$F(\omega) = \frac{1}{2}\,\frac{1}{(\pi)}\,\frac{1}{2\sqrt{(1-4B^2)}}\,\frac{2}{\sqrt{[\frac{1-E}{1+2B}+\frac{1+E}{1-2B}]\cdot 2}}\,K\Big(\sqrt{\frac{(\frac{1-E}{1+2B}-1)(1-\frac{E+1}{1-2B})}{(\frac{1-E}{1+2B}+\frac{1+E}{1-2B})\cdot 2}}\Big)$$

$$F(\omega) = Sign(E)\ \frac{1}{(\pi)}\,\frac{1}{2\sqrt{(2BE+1)}}\,K\Big(\frac{(-2B-E)^2}{4(1+2BE)}\Big)$$

For $E + 2B \leq 0$:

$$F(\omega) = Sign(E)\ \frac{1}{(\pi)}\,\frac{1}{2\sqrt{(2BE+1)}}\,K\Big(\frac{(-2B-E)^2}{4(1+2BE)}\Big)$$

Note that it is possible to write the function $F(\omega)$, $E < |2 + 2B|$, as

$$F(\omega) = Sign(E)\ \frac{1}{(\pi)}\,\frac{1}{\sqrt{(2BE+1)}}\,K\Big(\frac{(2B+E)^2}{4(1+2BE)}\Big) \tag{C.0.19}$$

$$F(\omega) = \frac{1}{(\pi)}\,\frac{2}{\sqrt{(2B+E)}}\,K\Big(\frac{4(1+2BE)}{(2B+E)^2}\Big) \tag{C.0.20}$$

Appendix D

The Cauchy principle value

The Cauchy principle of an integral may be used to define a less familiar generalized function as follows. First, we define the principle value of the integral of a function, f:

$$P(f) \equiv P\int_{-\infty}^{\infty} f(x)\,dx := \lim_{\epsilon\to 0}\int_{\epsilon<|x|} f(x)\,dx = \lim_{\epsilon\to 0}\Big(\int_{-\infty}^{-\epsilon} f(x)\,dx + \int_{\epsilon}^{\infty} f(x)\,dx\Big). \tag{D.0.1}$$

This defines one possible method for obtaining a number from the integral of a function, f which has a singularity at the origin [132].

D.1 $\mathcal{P}$rinciple value integral

In the previous Appendix we have seen that for $a > b > 0$, the integral I

$$\begin{aligned} I &= \int_0^{\pi} \frac{dk_x}{a + b\cos k_x} \\ &= \frac{2\pi}{\sqrt{a^2 - b^2}} \end{aligned} \tag{D.1.1}$$

Let us now do the $\mathcal{P}$rinciple value integral, to insure that the value of the integral is *zero* for $b^2 > a^2$

$$\mathcal{P} = \lim_{\epsilon\to 0}\Big(\int_0^{x_0-\epsilon} \frac{dk_x}{a + b\cos k_x} + \int_{x_0+\epsilon}^{\pi} \frac{dk_x}{a + b\cos k_x}\Big). \tag{D.1.2}$$

and the solution is [133]

$$\mathcal{P} = \lim_{\epsilon\to 0}(1/\sqrt{b^2-a^2})\Big\{\Big[\ln\frac{b+a\cos(k_x)+\sqrt{b^2-a^2}\sin(k_x)}{a+b\cos(k_x)}\Big]_0^{x_0-\epsilon}$$
$$+\Big[\ln\frac{b+a\cos(k_x)+\sqrt{b^2-a^2}\sin(k_x)}{a+b\cos(k_x)}\Big]_\pi^{x_0+\epsilon}\Big\} \tag{D.1.3}$$
$$= \lim_{\epsilon\to 0}(1/\sqrt{b^2-a^2})\Big\{\ln\Big[\frac{b+a\cos(x_0-\epsilon)+\sqrt{b^2-a^2}\sin(x_0-\epsilon)}{a+b\cos(x_0-\epsilon)}\Big]$$
$$-\ln\Big[\frac{b+a\cos(0)+\sqrt{b^2-a^2}\sin(0)}{a+b\cos(0)}\Big]$$
$$+\ln\Big[\frac{b+a\cos(\pi)+\sqrt{b^2-a^2}\sin(\pi)}{a+b\cos(\pi)}\Big]$$
$$-\ln\Big[\frac{b+a\cos(x_0+\epsilon)+\sqrt{b^2-a^2}\sin(x_0+\epsilon)}{a+b\cos(x_0+\epsilon)}\Big]\Big\} \tag{D.1.4}$$
$$= \lim_{\epsilon\to 0}(1/\sqrt{b^2-a^2})\Big\{\ln\Big[\frac{b+a\cos(x_0-\epsilon)+\sqrt{b^2-a^2}\sin(x_0-\epsilon)}{a+b\cos(x_0-\epsilon)}\Big]$$
$$-\ln\Big[\frac{b+a\cos(x_0+\epsilon)+\sqrt{b^2-a^2}\sin(x_0+\epsilon)}{a+b\cos(x_0+\epsilon)}\Big]\Big\} \tag{D.1.5}$$
$$= \lim_{\epsilon\to 0}(1/\sqrt{b^2-a^2})\Big\{\ln\Big[\frac{b+a\cos(x_0-\epsilon)+\sqrt{b^2-a^2}\sin(x_0-\epsilon)}{a+b\cos(x_0-\epsilon)}$$
$$\times\frac{a+b\cos(x_0+\epsilon)}{b+a\cos(x_0+\epsilon)+\sqrt{b^2-a^2}\sin(x_0+\epsilon)}\Big]\Big\} \tag{D.1.6}$$

$$\cos x_0 = -(a/b),\ \cos^2 x_0 + \sin^2 x_0 = 1 \Rightarrow \sin x_0 = (1/b)\sqrt{b^2-a^2} \tag{D.1.7}$$

$$\begin{aligned}\cos(x_0\mp\epsilon) &= \cos x_0\cos\epsilon \pm \sin x_0\sin\epsilon \\ &= -(a/b)\pm(\epsilon/b)\sqrt{b^2-a^2} \qquad \text{(D.1.8)}\\ a+b\cos(x_0\mp\epsilon) &= a+b[-(a/b)\pm(\epsilon/b)\sqrt{b^2-a^2}] \\ &= \pm\epsilon\sqrt{b^2-a^2} \qquad \text{(D.1.9)}\\ \sin(x_0\mp\epsilon) &= \sin x_0\cos\epsilon \mp \cos x_0\sin\epsilon \\ &= (1/b)\sqrt{b^2-a^2}\pm(a\epsilon/b) \qquad \text{(D.1.10)}\end{aligned}$$

$$\begin{aligned}&b+a\cos(x_0\mp\epsilon)+\sqrt{b^2-a^2}\sin(x_0\mp\epsilon) = \\ &b+b[-(a/b)\pm(\epsilon/b)\sqrt{b^2-a^2}]+\sqrt{b^2-a^2}\big[(1/b)\sqrt{b^2-a^2}\pm(a\epsilon/b)\big] = \\ &b-(a^2/b)\pm(a\epsilon/b)\sqrt{b^2-a^2}+b-(a^2/b)\pm(a\epsilon/b)\sqrt{b^2-a^2} = \\ &(2/b)[(b^2-a^2)\pm(a\epsilon)\sqrt{b^2-a^2}]\end{aligned} \tag{D.1.11}$$

then

$$\begin{aligned}
&\ln\Big[\frac{b+a\cos(x_0-\epsilon)+\sqrt{b^2-a^2}\sin(x_0-\epsilon)}{a+b\cos(x_0-\epsilon)} \\
&\quad\times\frac{a+b\cos(x_0+\epsilon)}{b+a\cos(x_0+\epsilon)+\sqrt{b^2-a^2}\sin(x_0+\epsilon)}\Big] \\
&=\ln\Big[\frac{(2/b)[(b^2-a^2)+a\epsilon\sqrt{b^2-a^2}}{(\epsilon)\sqrt{b^2-a^2}}\times\frac{(\epsilon)\sqrt{b^2-a^2}}{(2/b)[(b^2-a^2)-a\epsilon\sqrt{b^2-a^2}}\Big] \\
&=\ln\Big[\frac{1+\frac{a\epsilon\sqrt{b^2-a^2}}{b^2-a^2}}{1-\frac{a\epsilon\sqrt{b^2-a^2}}{b^2-a^2}}\Big] \\
&=\ln\Big[\frac{1+x}{1-x}\Big]\cong 2x \\
&=\frac{2a\epsilon\sqrt{b^2-a^2}}{b^2-a^2}
\end{aligned} \tag{D.1.12}$$

Then

$$\begin{aligned}
\mathcal{P}&=\lim_{\epsilon\to 0}\frac{1}{\sqrt{b^2-a^2}}\Big\{\frac{2a\epsilon\sqrt{b^2-a^2}}{b^2-a^2}\Big\} \\
&=0
\end{aligned} \tag{D.1.13}$$

Appendix E

Resolvents And Green's Functions

E.1 Basic Definitions

The resolvent of a Hermitean operator (Hamilton operator) is defined as follows

$$\mathcal{G}(z) = (zI - H)^{-1}, \quad z = \omega + i\delta, \quad , \mathcal{G}(z*) = \mathcal{G}(z)^{\dagger}, \tag{E.1.1}$$

where $\mathcal{I}$ is the unity operator. Any representation of such a resolvent is called a Green's functions, e.g., also the following configuration space representation of $\mathcal{G}$,

$$< \mathbf{r}|\mathcal{G}(z)|\mathbf{r}' >= G(\mathbf{r}, \mathbf{r}'; z). \tag{E.1.2}$$

The so-called side-limits of $\mathcal{G}(z)$ are then defined by

$$\lim_{|\delta|\to 0} \mathcal{G}(z) = \begin{cases} \mathcal{G}^{+}(\omega) & ; \ \delta > 0 \\ \mathcal{G}^{-}(\omega) & ; \ \delta < 0 \end{cases} \tag{E.1.3}$$

$$\mathcal{G}^{+}(\omega) = \mathcal{G}^{-}(\omega)^{\dagger} \tag{E.1.4}$$

and therefore lead to the property,

$$Im\mathcal{G}^{+}(\omega) = \frac{1}{2i}(\mathcal{G}^{+}(\omega) - \mathcal{G}^{-}(\omega)), \tag{E.1.5}$$

or,e.g., by making use of the properties of Dirac delta functions,

$$ImTr\mathcal{G}^{\pm}(\omega) = \mp\pi^{-1} \sum_{k} \delta(\omega - \varepsilon_k), \tag{E.1.6}$$

$$n(\omega) = \mp ImTr\mathcal{G}^{\pm}(\omega), \tag{E.1.7}$$

where Tr denotes the trace of an operator and $n(\omega)$ is the density of states (of a Hamiltonian with discrete eigenvalue spectrum, $\{\varepsilon\}$). A Dirac delta function can therefore be simply viewed as the Cauchy part of a first order pole in the resolvent $\mathcal{G}(z)$

E.2 The Dyson Equation

Suppose H is given in termsof an unperturbed Hamiltonian H_0 and a (Hermitean) perturbation V,

$$H = H_0 + V. \tag{E.2.1}$$

The resolvents of H and H_o

$$\mathcal{G}(z) = (zI - H)^{-1}, \quad \mathcal{G}_0(z) = (zI - H_0)^{-1}, \tag{E.2.2}$$

are then coupled in terms of a Dyson equation,

$$\mathcal{G}(z) = \mathcal{G}_0(z) + \mathcal{G}(z)V\mathcal{G}_0(z) = \mathcal{G}_0(z) + \mathcal{G}_0(z)V\mathcal{G}(z) \tag{E.2.3}$$

which in turn can be solved iteratively (Born series),

$$\mathcal{G}(z) = \mathcal{G}_0(z) + \mathcal{G}_0(z)V\mathcal{G}_0(z) + \mathcal{G}_0(z)V\mathcal{G}_0(z)V\mathcal{G}_0(z) + \ldots. \tag{E.2.4}$$

By reformulating (E.2.4) as

$$\mathcal{G}(z) = \mathcal{G}_0(z) + \mathcal{G}_0(z)(V + V\mathcal{G}_0(z)V + \ldots)\mathcal{G}_0(z), \tag{E.2.5}$$

so-called T-operator can be defined,

$$T(z) = V + V\mathcal{G}_0(z)V + V\mathcal{G}_0(z)V\mathcal{G}_0(z)V + \ldots, \tag{E.2.6}$$

such that

$$\mathcal{G}(z) = \mathcal{G}_0(z) + \mathcal{G}_0(z)T(z)\mathcal{G}_0(z). \tag{E.2.7}$$

or, alternatively,

$$T(z) = V + V\mathcal{G}(z)V, \tag{E.2.8}$$

$$T(z) = V + V\mathcal{G}_0(z)T(z) = V + T(z)\mathcal{G}_0(z)V, \tag{E.2.9}$$

$$\mathcal{G}_0(z)T(z) = \mathcal{G}(z)V, \tag{E.2.10}$$

$$T(z)\mathcal{G}_0(z) = V\mathcal{G}(z). \tag{E.2.11}$$

Since V is assumed to be Hermitean, similar to the resolvents, $\mathcal{G}_0(z)$ and $\mathcal{G}(z)$, the T-opertor satisfies the relation,

$$T(z*) = T(z)^\dagger, \tag{E.2.12}$$

and, in particular, for the side-limits the property

$$T^+(\omega)^\dagger = T^-(\omega) \tag{E.2.13}$$

applies.

E.3 Integrated Density of States: the Lloyd Formula

Substituting (E.2.7) into (E.1.7) yields

$$\begin{aligned} n(\omega) &= -\frac{1}{\pi} Im Tr(\mathcal{G}_0^+(\omega) + \mathcal{G}_0^+(\omega)T^+(\omega)\mathcal{G}_0^+(\omega)) \\ &= n_0(\omega) + \delta n(\omega) \end{aligned}$$

where

$$\begin{aligned} n_0() &= -\frac{1}{\pi} ImTr(\mathcal{G}_0^+(\omega), \\ \delta n(\omega) &= -\frac{1}{\pi} ImTr(\mathcal{G}_0^+(\omega) T^+(\omega) \mathcal{G}_0^+(\omega)) \\ &= -\frac{1}{\pi} ImTr\Big(\mathcal{G}_0^+(\omega)^2 T^+(\omega)\Big) \\ &= \frac{1}{\pi} ImTr\Big(d\mathcal{G}_0^+(\omega) d\omega T^+(\omega)\Big) \end{aligned} \tag{E.3.1}$$

and use was made of the following identity

$$\frac{d\mathcal{G}(z)}{dz} = -\mathcal{G}(z)^2 \tag{E.3.2}$$

Based on (E.2.8), (E.2.10) and (E.2.11) one further can derive that

$$\frac{dT(z)}{dz} = V \frac{d\mathcal{G}(z)}{dz} V \tag{E.3.3}$$

$$= -V \mathcal{G}(z)^2 V \tag{E.3.4}$$

$$= -T(z) \mathcal{G}_0(z)^2 T(z) \tag{E.3.5}$$

$$= T(z) \frac{d\mathcal{G}_0(z)}{dz} T(z), \tag{E.3.6}$$

and therefore

$$T(z)^{-1} \frac{dT(z)}{dz} = \frac{d\mathcal{G}_0(z)}{dz} T(z) \tag{E.3.7}$$

which substituted into (E.3.1) yields

$$\delta n(\omega) = \frac{1}{\pi} Im\, Tr\Big(T^+(\omega)^{-1} \frac{dT^+(\omega)}{d\omega}\Big) \tag{E.3.8}$$

$$= \frac{d}{d\omega}\Big(\frac{1}{\pi} Im\, Tr\, ln\, T^+(\omega)\Big) \tag{E.3.9}$$

The integrated DOS,

$$N(\omega) = \int_{-\infty}^{\omega} d\omega' n(\omega'), \tag{E.3.10}$$

can then be directly expressed as

$$N(\omega) = N_0(\omega) + \delta N(\omega), \tag{E.3.11}$$

where

$$N_0(\omega) = \int_{-\infty}^{\omega} d\omega' n_0(\omega'), \tag{E.3.12}$$

and

$$\delta N(\omega) = \frac{1}{\pi} Im\, Tr\, ln T^+(\omega) \tag{E.3.13}$$

or, in terms of (E.2.6) as

$$\delta N(\omega) = -\frac{1}{\pi} Im\, Tr\, ln\Big(I - \mathcal{G}_0^+(\omega) V\Big). \tag{E.3.14}$$

The above expression is usually referred to as the *Lloyd formula*[134].

Appendix F

The Calculation of $Im\chi_{\alpha\beta}(\mathbf{q},\omega)$

The normal state Green's function which includes elastic scattering of quasiparticles is identical with Eq.(2.6.9) except that the infinitesimal imaginary part $i\delta$ is replaced by the finite quantity $i/2\tau$:

$$G_R(\varepsilon_p) = \frac{1}{\omega_0 - \varepsilon_p + i/2\tau} \tag{F.0.1}$$

The spectral function, defined in (2.6.25), is no longer a δ-function:

$$\begin{aligned} A(\mathbf{p},\omega_0) =& -2ImG_R(\varepsilon_p,\omega_0) \\ =& \frac{1/\tau}{(\omega_0-\varepsilon_p)^2 + (1/2\tau)^2} \end{aligned}$$

Because of the isotropy of the system that has been assumed, we only need to consider

$$Im\chi_{\alpha\alpha} = (1/2\pi)\int \frac{d^3p}{(2\pi)^3}\frac{p_\alpha^2}{m^2}\int_{-\infty}^{\infty} d\omega_0\, f(\frac{\omega_0}{T})A(p,\omega_0)\Big[A(p,\omega_0+\omega) - A(p,\omega_0-\omega)\Big]. \tag{F.0.2}$$

Because each ω_0-integral converges fast enough, we can substitute $\omega_0 - \omega$ for ω_0 in the first term

$$\begin{aligned} Im\,\chi_{\alpha\alpha}(\omega) =& (1/2\pi)\Big\{\int \frac{d^3p}{(2\pi)^3}\frac{p_\alpha^2}{m^2}\Big[\int_{-\infty}^{\infty} d\omega_0\, f(\frac{\omega_0-\omega}{T})A(p,\omega_0)A(p,\omega_0-\omega) \\ & - \int_{-\infty}^{\infty} d\omega_0\, f(\frac{\omega_0}{T})A(p,\omega_0)A(p,\omega_0-\omega)\Big]\Big\} \\ =& (1/2\pi)\int_{-\infty}^{\infty}\Big[\int \frac{d^3p}{(2\pi)^3}\frac{p_\alpha^2}{m^2}A(p,\omega_0)A(p,\omega_0-\omega)\big[f(\frac{\omega_0-\omega}{T}) - f(\frac{\omega_0}{T})\big]\Big]d\omega_0 \\ =& \int_{-\infty}^{\infty}\Big[f(\frac{\omega_0-\omega}{T}) - f(\frac{\omega_0}{T})\Big]K\; d\omega_0 \end{aligned}$$

where

$$K(\omega_0,\omega) = (1/2\pi)\int \frac{d^3p}{(2\pi)^3}\frac{p_\alpha^2}{m^2}\big[A(p,\omega_0)A(p,\omega_0-\omega)\big]$$

When the dispersion relation $\varepsilon(\mathbf{p})$ is isotropic, the integral K can be simplified through the conversion to polar coordinates

$$\begin{aligned}\int \frac{d^3p}{(2\pi)^3}p_x^2 &= \int_0^\infty \frac{dp}{(2\pi)^3}p^4 \int_0^\pi d\theta \sin\theta \sin^2\theta \int_0^{2\pi} \cos^2\phi \, d\phi \\ &= \int_0^\infty \frac{dp}{(2\pi)^3}p^4 \cdot (4/3) \cdot \pi\end{aligned}$$

In view of the dependence of the spectral function on momentum we introduce the energy as new integration variable. In the nearly free electron model, this substitution is particularly simple. Because of the particular form of the spectral function, the main contribution to the energy integral is confined to the neighbourhood of the chemical potential. With

$$\varepsilon = \frac{p^2}{2m} - \mu \quad \Rightarrow \quad d\varepsilon = \frac{p}{m}dp,$$

this justifies the following approximations

$$\begin{aligned}K =& (1/2\pi)(1/6\pi^2)\int_0^\infty dp\,(p^4/m^2)\big[A(p,\omega_0)A(\omega_0-\omega)\big] \\ =& s\int_{-\mu}^\infty d\varepsilon\,\big[A(p,\omega_0)A(p,\omega_0-\omega)\big] \\ =& s\int_{-\infty}^\infty d\varepsilon\,\big[A(p,\omega_0)A(p,\omega_0-\omega)\big]\end{aligned}$$

The ε-integral can then be done with the help of the theorem of residues. Then the following simplification is possible

$$\begin{aligned}A(p,\omega_0)A(p,\omega_0-\omega) =& -\big[G_R(\varepsilon,\omega_0)-G_A(\varepsilon,\omega_0)\big] \\ & \times\big[G_R(\varepsilon,\omega_0-\omega)-G_A(\varepsilon,\omega_0-\omega)\big] \\ =& -\big[G_R(\varepsilon,\omega_0)G_R(\varepsilon,\omega_0-\omega)+G_A(\varepsilon,\omega_0)G_A(\varepsilon,\omega_0-\omega) \\ & -G_R(\varepsilon,\omega_0)G_A(\varepsilon,\omega_0-\omega)-G_A(\varepsilon,\omega_0)G_R(\varepsilon,\omega_0-\omega)\big] \\ =& \big[G_R(\varepsilon,\omega_0)G_A(\varepsilon,\omega_0-\omega)+G_A(\varepsilon,\omega_0)G_R(\varepsilon,\omega_0-\omega)\big]\end{aligned}$$

because (G_RG_R), and (G_AG_A) have poles in one half-plane only and hence do not contribute to the integral. Then

$$\begin{aligned}K =& s\int_{-\infty}^\infty d\varepsilon\left\{G_R(\varepsilon,\omega_0)G_A(\varepsilon,\omega_0-\omega)+G_A(\varepsilon,\omega_0)G_R(\varepsilon,\omega_0-\omega)\right\} \\ =& s\int_{-\infty}^\infty d\varepsilon\left\{\frac{1}{\omega_0-\varepsilon-\frac{i}{2\tau}}\times\frac{1}{\omega_0-\omega-\varepsilon+\frac{i}{2\tau}}+\frac{1}{\omega_0-\varepsilon+\frac{i}{2\tau}}\times\frac{1}{\omega_0-\omega-\varepsilon-\frac{i}{2\tau}}\right\} \\ =& s\int_{-\infty}^\infty d\varepsilon\left\{\frac{1}{\varepsilon-(\omega_0-\frac{i}{2\tau})}\times\frac{1}{\varepsilon-(\omega_0-\omega+\frac{i}{2\tau})}+\frac{1}{\varepsilon-(\omega_0+\frac{i}{2\tau})}\times\frac{1}{\varepsilon-(\omega_0-\omega-\frac{i}{2\tau})}\right\} \\ =& \frac{p_f^3}{3\pi^2 m}\cdot\frac{\tau}{1+\omega^2\tau^2}\end{aligned} \tag{F.0.3}$$

Finally $Im\,\chi_{\alpha\alpha}$ becomes

$$\begin{aligned} Im\,\chi_{\alpha\alpha} =& \Big[\frac{p_f^3}{3\pi^2 m}\,\frac{\tau}{1+\omega^2\tau^2}\Big]\Big\{\int_{-\infty}^{\infty} f(\frac{\omega_0-\omega}{T}) - f(\frac{\omega_0}{T})d\omega_0\Big\} \\ =& \Big[\frac{n_0}{m}\frac{\tau}{1+\omega^2\tau^2}\Big]\omega \end{aligned} \tag{F.0.4}$$

since

$$\int_{-\infty}^{\infty} f(\frac{\omega_0-\omega}{T}) - f(\frac{\omega_0}{T})d\omega_0 = \omega$$

The Fermi Function Integral

W e know that Fermi function is

$$f(\frac{\omega_0}{T}) = \frac{1}{[e^{\frac{\omega_0}{T}}+1]} = -\frac{-e^{-\frac{\omega_0}{T}}}{[1+e^{-\frac{\omega_0}{T}}]}$$

Note that apart from a factor T the numerator is the derivative of the denominator with respect to ω_0. We thus write

$$f(\omega_0) = -\,T\frac{d}{d\omega_0}\ln[1+e^{-\frac{\omega_0}{T}}]$$

so that

$$\begin{aligned} \int_{-\infty}^{\infty} f(\frac{\omega_0-\omega}{T}) - f(\frac{\omega_0}{T})d\omega_0 &= -\,T\big[\ln(1+e^{-\frac{\omega_0}{T}}) - \ln(1+e^{-\frac{\omega_0+\omega}{T}})\big]_{-\infty}^{\infty} \\ &= +\,T\lim_{\Omega\to\infty}\big[\ln\big(1+e^{\frac{\Omega}{T}}\big) - \ln\big(1+e^{\frac{\Omega+\omega}{T}}\big)\big] \\ &= +\,T\lim_{\Omega\to\infty}\Big(\frac{\Omega}{T} - \frac{\Omega+\omega}{T}\Big) \\ &= -\,\omega. \end{aligned}$$

So that

$$\sigma_1 = \frac{n_0 e^2\tau}{m(1+\omega^2\tau^2)}$$

List of Acronyms and Symbols

List of Acronyms

Abbreviation	Details
1DEG	1D Electron Gas
AFM	Antiferromagnetic
ARPES	Angle-Resolved PhotoEmission Spectroscopy(Studies)
BCS	Bardeen, Cooper, Schrieffer
BdG	Bogoliubov-deGennes
BSCCO	$Bi_2Sr_2Ca_2Cu_3O_y$
DDW	D-Density-Wave states
DOS	Density Of States
LDOS	Local Density Of States
GF	Green Function
GL	Ginzburg, Landau
HTSC	High Temperature Superconductor
INS	Inelastic Neutron Scattering
LFLT	Landau Fermi Liquid Theory
LSCO	$La_{2-x}Sr_xCuO_4$
MRI	Magnetic Resonance Imaging
NMR	Nuclear Magnetic Resonance
O.D.	Over Doped
PG	Pseudogap
QI	Quantum Interference
RVB	Resonating Valence Bond
SC	Superconductor
SPQI	Spin-Polarized Quasiparticle Injection
SCTMA	Selfconsistant T-Matrix Approximation
SQUIDS	Superconducting Quantum Interference Devices
SSC	Superconducting Super Collider
STM	Scanning Tuneling Microscopy
TISE	Time Independent Schrdinger Equation
U.D.	Under Doped
YBCO	$YBa_2Cu_3O_7$

List of Symbols

Abbreviation	Details
a	Lattice constant
A	Operator
$\mathbf{A}(\mathbf{r},t)$	Electromagnetic vector potential
A(k,ω)	Spectral function
B	Next-neighbor hopping integral in units of t, and Operator
$\mathbf{B}_c$	Critical magnetic field
$\mathbf{c}_{()}$	Annihilation operator
$\mathbf{c}^{\dagger}_{()}$	Creation operator
e	Electron charge
$\boldsymbol{\mathcal{E}}$	Electric field
E	Energy
E_F	Fermi energy
F	Free energy
$\mathbf{F}_n$	Free energy in the normal phase
$F(\omega)(=ReG^0)$	Hilbert transform of $N(\omega)$
G	Green's function; Reciprocal lattice vector
$\mathcal{G}$	Matsubara Green's function
H	Magnetic field
H_0	Unperturbed Hamiltonian
H'	Interaction(perturbed) Hamiltonian
H.c.	Hermite conjugate
$\hbar$	Plank's constant
J	Electric current
j_c	Critical current
k	Wave vector
k	elliptic modulus
K	Grand Hamiltonian $(=H+\mu N)$
K	Kelvin
k_B	Boltzmann constant
k_F	Fermi wavevector
l_e	electron mean free path
m	mass
$M(\omega)$	Memory function
$n_s(r)$	No. of "Superconducting electrons(Cooper Pairs)"
$n_{i\sigma}$	Occupation number of electrons with spin (σ) at site i.
N, n	Number of particles
$\|N>$	Ground state of system
$N(\omega)$, and $N(\varepsilon)$	Density of states
$\mathcal{P}$	Cauchy principle value
$\mathbf{p}_F$	Fermi momentum
$q(=2e)$	Cooper pair charge
R	Optical reflectivity

Abbreviation	Details
t	time, nearest-neighbour hopping integral
t′	time, next-nearest-neighbour hopping integral
T	Temperature, time-ordering parameter
T_c	Transition temperature
T_a	Annealing temperature
T^*	Peusdogap
U	Potential
v	Velocity
$\mathbf{v}_F$	Fermi velocity
V	Potential, Volume
α, β	Phenomenological parameters, Spin
Δ	Gap parameter
Δ_k	Order parameter
λ	Penetration depth
μ	Chemical potential
ξ	Coherence length
σ	Spin, Conductivity
τ	Imaginary time $(= it)$, or Relaxation time
ϕ	Fourier transform of susceptibility
$\varphi(r)$	Spatially varying phase
χ	Susceptibility
ψ	Complex order parameter, Wave function, and Field operator
ψ_0	Equilibrium value of order parameter in absence of an electromagnetic field, Ground state wavefunction
ω	Frequency
ω_p	Plasma frequency
ρ	Electric resistivity
$\rho(\omega)$	Density of states
ρ_i	Residual resistivity
ρ_{ph}	Phonon resistivity
ρ_{ab}	Resistivity in ab-plane
ρ_c	c-axis resistivity
$\kappa(= \lambda/\xi)$	Ginzburg-Landau parameter

Bibliography

[1] *Characteristic Lengths in Superconductors. Website.* http://hyperphysics.phy-astr.gsu.edu/hbase/solids/supcon.html#c1.

[2] R. W. Dull and H. R. Kerchner. A Teacher's Guide to Superconductivity for High School Students, 1994. http://www.ornl.gov/info/reports/m/ornlm3063r1/pt1.html.

[3] Dirk Reimer and Parts by: R. W. Dull. Applications of Superconductors, 1997. http://www.physnet.uni-hamburg.de/home/vms/reimer/htc/pt4.html.

[4] The Discovery of Superconductivity. Website. http://hyperphysics.phy-astr.gsu.edu/Hbase/solids/scdis.html.

[5] Ornl Research Library, 1996. http://www.ornl.gov/info/reports/m/ornlm3063rl/fig2.gif.

[6] History & Applications of Superconductors. Website. http://www.futurescience.com/manual/sc1000.html#B.

[7] Soltan Eid Abdel-Gawad Soltan. Interaction of Superconductivity and Ferromagnetism in YBCO/LCMO Heterostructures . Dissertation, Max-Planck-Institut Fuer Festkoerperforschung, 2005.

[8] High-Temperature Superconductivity. Website. http://www.electro.patent-invent.com/electricity/inventions/high_temperature_superconductivity.html.

[9] High Temperature Superconductor (HTS), 1998. http://bass.gmu.edu/~pceperle/WebProjectsSpr03/Chen-Superconductors/HTS.htm.

[10] High-Temperature Superconductor. Website. http://www.wikinfo.org/index.php/High-temperature_superconductor.

[11] "High-Temperature Superconductors." History of Science and Technology. Website, 2004. http://www.answers.com/topic/high-temperature-superconductors.

[12] Are Superconductors the Future? Website, 1998. http://www.eapen.com/jacob/superconductors/chapter5.html.

[13] R. J. Cava. The Identification of the First 90 K Superconductor, 1993. http://www.garfield.library.upenn.edu/classics1993/A1993KR78900001.pdf.

[14] M. R. Norman, D. Pines, and C. Kallin. The Pseudogap: Friend or Foe of High T_c? Advances in Physics*, 54:715–733, 2005.*

[15] M. V. Sadovskii. Models of the Pseudogap State in High-Temperature Superconductors. ArXiv Condensed Matter e-prints*, August 2004. cond-mat/0408489.*

[16] Superconductors that Work at Room Temperature.
`http://www.eurekalert.org/pub_releases/2001-11/ns-stw112801.php`.

[17] Superconductivity. Website.
`http://en.wikipedia.org/wiki/Superconductivity`.

[18] High Speed Railways. Website.
`http://www.railway-technology.com/projects/shinkansen/shinkansen5.html`.

[19] Applications Of Superconductors.
`http://www.ornl.gov/sci/htsc/documents/superconductivityposter.pdf`.

[20] BCS Theory. Website.
`http://en.wikipedia.org/wiki/BCS_theory`.

[21] BCS Theory of Superconductivity. Website.
`http://hyperphysics.phy-astr.gsu.edu/hbase/solids/bcs.html`.

[22] Ginzburg-Landau Theory. Website.
`http://en.wikipedia.org/wiki/Ginzburg-Landau_theory`.

[23] Michael Tinkham. Introduction to Superconductivity. McGraw-Hill, Inc., New York, 1996.

[24] Takashi Yanagisawa and Hajime Shibata. Optical Properties of Unconventional Superconductors. preprint: cond-mat/0408054 v1 3 Aug 2004.

[25] P. B. Allen. Electron Self-Energy and Generalized Drude Formula for Infrared Conductivity of Metals. preprint: cond-mat/0407777 v1 29 Jul 2004.

[26] J. Orenstein, G. A. Thomas, A. J. Millis, S. L. Cooper, D. H. Rapkine, T. Timusk, L. F. Schneemeyer, and J. V. Waszczak. Frequency- and Temperature-Dependent Conductivity in $YBa_2Cu_3O_{6+x}$ Crystals. Phys. Rev. B*, 42:6342–6362, 1990.*

[27] A. V. Balatsky. Impurities and Conductivity in a d-Wave Superconductor. STI*, 1994.*

[28] A. J. Berlinsky, D. A. Bonn, R. Harris, and C. Kallin. Microwave Conductivity Due to Impurity Scattering in a d-Wave Superconductor. Phys. Rev. B*, 61:9088, 2000.*

[29] A. C. Durst and P. A. Lee. Microwave Conductivity Due to Scattering from Extended Linear Defects in d-Wave Superconductors . Phys. Rev. B*, 65:094501, 2002.*

[30] A. C. Durst and P. A. Lee. Impurity-Induced Quasiparticle Transport and Universal-Limit Wiedemann-Franz Violation in d-Wave Superconductors. Phys. Rev. B*, 62:1270, 2000.*

[31] Y. H. Yang, D. Y. Xing, Y. G. Wang, and M. Liu. Unitary Limit and Quantum Interference Effect in Disordered Two-Dimensional Crystals with Nearly Half-Filled Bands . Phys. Rev. B*, 68:045113, 2003.*

[32] J. M. Byers, M. E. Flatté, and D. J. Scalapino. Influence of Gap Extrema on the Tunneling Conductance Near an Impurity in an Anisotropic Superconductor. Phys. Rev. Lett.*, 71:3363, 1993.*

[33] R. J. Radtke and M. R. Norman. Relation of Extended Van Hove Singularities to High-Temperature Superconductivity within Strong-Coupling Theory. Phys. Rev. B*, 50:9554, 1994.*

[34] Qiang-Hua Wang and Dung-Hai Lee. Quasiparticle Scattering Interference in High-Temperature Superconductors. Phys. Rev. B*, 67:020511, 2003.*

[35] L. Zhu, P. J. Hirschfeld, and D. J. Scalapino. Elastic Forward Scattering in the Cuprate Superconducting State . Phys. Rev. B*, 70:214503, 2004.*

[36] Y. H. Yang, Y. G. Wang, M. Liu, and D. Y. Xing. Quantum Interference Effect on the Density of States in Disordered d-Wave Superconductors. preprint: cond-mat/0211590, 26 Nov 2002.

[37] S. Haas and K. Maki. Quasiparticle Bound States around Impurities in $d_{x^2-y^2}$-Wave

Superconductors. Phys. Rev. Lett.*, 85:2172, 2000.*

[38] Amit Ghosal, Mohit Randeria, and Nandini Trivedi. Spatial Inhomogeneities in Disordered d-Wave Superconductors: Effect on Density of States and Superfluid Stiffness. preprint: cond-mat/0004481 v1 27 Apr 2000.

[39] Jian-Xin Zhu, D. N. Sheng, and C. S. Ting. Quasiparticle Localization in Disordered d-Wave Superconductors . Phys. Rev. Lett.*, 85:4944, 2000.*

[40] W. A. Atkinson, P. J. Hirschfeld, A. H. MacDonald, and K. Ziegler. Details of Disorder Matter in 2D d-Wave Superconductors. Phys. Rev. Lett.*, 85:3926, 2000.*

[41] U. Michelucci, F. Venturini, and A. P. Kampf. Quantum Interference Phenomena between Impurity States in d-Wave Superconductors. Journal of Physics and Chemistry of Solids*, 68:2283, 2002.*

[42] C. Adagideli, D. E. Sheehy, and P. M. Goldbart. Density of States in d-Wave Superconductors Disordered by Extended Impurities. Phys. Rev. B*, 66:140512, 2002.*

[43] W. A. Atkinson, P. J. Hirschfeld, and L. Zhu. Quantum Interference in Nested d-Wave Superconductors: a Real-Space Perspective . Phys. Rev. B*, 68:054501, 2003.*

[44] Jian-Xin Zhu, T. K. Lee, C. S. Ting, and Chia-Ren Hu. Quasiparticle Resonant States Induced by a Unitary Impurity in a d-Wave Superconductor. Phys. Rev. B*, 61:8667, 2000.*

[45] L. Zhu, W.A. Atkinson, and P. J. Hirschfeld. Two Impurities in a d-Wave Superconductor: Local Density of States. Phys. Rev. B*, 67:094508, 2003.*

[46] G. G. N. Angilella, F. E. Leys, N. H. March, and R. Pucci. Linear Response Function around a Localized Impurity in a Superconductor . Journal of Physics and Chemistry of Solids*, 64:413, 2003.*

[47] E. Z. Kuchinskii and M. V. Sadovskii. Normal Impurities in Superconductors with an "Odd" Pairing. JETP Letters*, 57:515, 1993.*

[48] T. V. Ramakrishnan. Magnetic Field Induced id_{xy} Order in a $d_{x^2-y^2}$ Superconductor. preprint: cond-mat/9803069 v1 6 Mar 1998.

[49] H. Ghosh. Higher Anisotropic d-Wave Symmetry in Cuprate Superconductors. Journal of Physics: Condensed Matter*, 11:L371, 1999.*

[50] H. V. Kruis, I. Martin, and A. V. Balatsky. Impurity-Induced Resonant State in a Pseudogap State of a High-T_c superconductor. Phys. Rev. B*, 64:054501, 2001.*

[51] S. Haas and K. Maki. Temperature Dependence of Impurity Bound States in $d_{x^2-y^2}$-Wave Superconductors. preprint: cond-mat/0011004 v1 1 Nov 2000.

[52] Jian-Xin Zhu, W. Kim, C. S. Ting, and J. P. Carbotte. Quasiparticle States around a Nonmagnetic Impurity in a d-Density-Wave State of High-T_c Cuprates . Phys. Rev. Lett.*, 87:197001, 2001.*

[53] D. K. Morr. Resonant Impurity States in the d-Density-Wave Phase. Phys. Rev. Lett.*, 89:106401, 2002.*

[54] C. Pépin and P. A. Lee. Nonmagnetic Impurities in the Spin-gap Phase of the Cuprates. Physica B: Physics of Condensed Matter*, 259:443, 1999.*

[55] M. Kugler, Ø. Fischer, Ch. Renner, S. Ono, and Yoichi Ando. Scanning Tunneling Spectroscopy of $Bi_2Sr_2CuO_{6+\delta}$: New Evidence for the Common Origin of the Pseudogap and Superconductivity. Phys. Rev. Lett.*, 86:4911–4914, 2001.*

[56] David Se´ne´chal and A.-M. S. Tremblay. Hot Spots and Pseudogaps for Hole- and Electron-Doped High-Temperature Superconductors. Phys. Rev. Lett.*, 92:126401, 2004.*

[57] Je Huan Koo and Guangsup Cho. The Spin-gap in High T_c Superconductivity. J. Phys.: Condens. Matter*, 15:L729–L733, 2003.*

[58] E. Z. Kuchinskii, N. A. Kuleeva, and M. V. Sadovskii. Superconductivity in the "Hot

Spots" Model of the Pseudogap State, 2004.

[59] Fourier Series.
`http://mathworld.wolfram.com/FourierSeries.html`.

[60] Fourier Transform.
`http://mathworld.wolfram.com/FourierTransform.html`.

[61] Hamish D. Meikle. The Fourier Transform and the Helix, 2004.
`http://media.wiley.com/product_data/excerpt/14/35274044/3527404414.pdf`.

[62] Fourier Transform. Website.
`http://www.cs.bgu.ac.il/~dip033/ClassNotes/ImageTransformation2.pdf`.

[63] G. Arfken. Mathematical Methods for Physicists. Academic Press, Inc, New York, 1966,1968.

[64] Convolution Theorem.
`http://mathworld.wolfram.com/Convolution.html`.

[65] F. W. Byron and R. W. Fuller. Mathematics of Classical and Quantum Physics. Addison-Wesley Publishing Company, Inc., 1970.

[66] J. Shumway. Hilbert Transforms and Kramers-KrÖnig Relations, Nov 2001.
`phyastweb.la.asu.edu/phy501-shumway/2001/notes/lec36.pdf`.

[67] W. Jones and N. H. March. Theoretical Solid State Physics. John Wiley & Sons Ltd., London, 1973.

[68] F. J. Murray. Applied Mathematics. Plenum Press, New York, 1978.

[69] G. Arfken. Mathematical Methods for Physicists. Academic Press, Inc, Orlando, Florida, 1985.

[70] A. Isihara. Statistical Physics. Academic Press, New York, 1971.

[71] S. Weβel. Solid State Theory.
`http://www.theo3.physik.uni-stuttgart.de/lehre/ss05/sst/script4.2.pdf`.

[72] R. H. Landau. Quantum Mechanics II. John Wiley & Sons, Inc., New York, 1990.

[73] K. Ingersent. Second Quantization: Creation and Annihilation Operators, Nov 2003.
`www.phys.ufl.edu/~kevin/teaching/6646/03spring/2nd-quant.pdf`.

[74] B. J. Powell. On the Interplay of Superconductivity and Magnetism. *Dissertation, University of Bristol, 2002.*

[75] K. D. Cole. What is Green's Function, 2004.
`http://www.engr.unl.edu/~glibrary/home/whatisG/whatisG.html`.

[76] Richard D. Mattuck. A Guide to Fynman Diagrams in the Many-Body Problem. *McGraw-Hill Puplishing Company Limited, London, 1967.*

[77] J. C. Inkson. Many-Body Theory of Solids. Plenum Press, New York, 1984.

[78] G. D. Mahan. Many Particle Physics. Plenum Press, New York, 1990.

[79] E. N. Economou. Green's Functions in Quantum Physics. Springer -Verlag, Berlin, Heidelberg, 1979.

[80] Imaginary Time.
`http://en.wikipedia.org/wiki/Imaginary_time`.

[81] T. D. Schultz. Quantum Field Theory and the Many-Body Problem. Gordon And Breach, Science Publishers, New York, 1964.

[82] R. L. Liboff. KINETIC THEORY Classical, Quantum, and Relativistic Descriptions. Prentice-Hall International, Inc., New Jersey, 1990.

[83] K. Scharnberg. Priv. Communications.

[84] S. Doniach and E. H. Sondheimer. Green's Functions for Solid State Physicists. Imperial College Press, London, 1998.

[85] P. M. Chaikin and T. C. Lubensky. Principles of Condensed Matter Physics. Cambridge,

University press, 1995.

[86] S. Lundqvist. Many Body Theory. In F. Bassani, G. Caglioti, and J. Ziman, editors, Theory of Condensed Matter*, page 73. IAEA, Vienna, Austria, 1968.*

[87] J. M. Ziman. Elements of Advanced Quantum Theory. Cambridge University Press, London, 1969.

[88] M. Plischke and B. Bergersen. Equilibrium Statistical Physics. Prentice-Hall, Inc, New Jersey, 1989.

[89] W. A. Harrison. Solid State Theory. McGraw-Hill Book Company, New York, 1970.

[90] M. S. Dressellhaus. Solid State Physics. 2001.

[91] J. E. Hirsch. Two-Dimensional Hubbard Model: Numerical Simulation Study. Phys. Rev. B*, 31:4403, 1984.*

[92] Mona Berciu and Sajeev John. Microscopic Model for d-Wave Charge-Carrier Pairing and Non-Fermi-liquid Behavior in a Purely Repulsive Two-Dimensional Electron System. Phys. Rev. B*, 61:16454–16469, 2000.*

[93] N. Bulut. $D_{x^2-y^2}$-Wave Superconductivity and the Hubbard Model. Advances in Physics*, 51(6), 2002.*

[94] D. Manske. Phonons, Electronic Correlations, and Self-Energy Effects in High-T_c Superconductors*. Dissertation, Universität Hamburg, 1997.*

[95] P. Arberg and J. P. Carbotte. Effect of the Impurity Scattering on the Zero-Temperature Penetration Depth in $d_{x^2-y^2}$ Symmetry. Phys. Rev. B*, 50:3250–3255, 1994.*

[96] P. Monthoux and D. Pines. $YBa_2Cu_3O_7$: a Nearly Antiferromagnetic Fermi Liquid. Phys. Rev. B*, 47, 1993.*

[97] A. Damascelli, Z. Hussain, and Zhi-Xun Shen. Angle-Resolved Photoemission Studies of the Cuprate Superconductors. Rev. Mod. Phys.*, 75:473, 2003.*

[98] A. Perali, C. Grimaldi, and L.Pietronero. Nonadiabatic Pairing Effects for Tight-Binding Electrons Interacting with Phonons. Phys.Rev. B*, 58:5736, 1998.*

[99] M. H. Sharifzadeh Amin and P. C. E. Stamp. Vertex Corrections in Antiferromagnetic Spin Fluctuation Theories. Phys. Rev. Lett.*, 77:3017, 1996.*

[100] V. A. Khodel, Victor M. Yakovenko, M. V. Zverev, and Haeyong Kang. Hot Spots and Transition from d-Wave to Another Pairing Symmetry in the Electron-Doped Cuprate Superconductors. Phys. Rev. B*, 69:144501, 2004.*

[101] Arkady V. Krasheninnikov. Lecture7. Tight-Binding in Periodic Solids. Website. `http://beam.acclab.helsinki.fi/~akrashen/escalc/lect07.ps`.

[102] A. Georges, G. Kotliar, W. Krauth, and M. J. Rozenberg. Dynamical Mean-Field Theory of Strongly Correlated Fermion Systems and the Limit of Infinite Dimensions. Rev. Mod. Phys.*, 68:13–125, 1996.*

[103] K. Haule. Diagrammatic Theory of Strongly Correlated Electron Systems. Website, 11-07-2002.
`http://morje.ijs.si/~haule/thesis/html/index.html`.

[104] Maciej Mas-acuteka. Antiferromagnetism and Pairing in Strongly Correlated Systems . Phys. Rev. B*, 55:3943–3953, 1997.*

[105] S. G. Sharapov and J. P. Carbotte. Effects of Energy Dependence in the Quasiparticle Density of States on Far-Infrared Absorption in the Pseudogap State . Phys. Rev. B*, 72:134506, 2005.*

[106] M. Abramowitz and I. Stegun. Handbook of Mathematical Functions, Elliptic Integrals. National Bureau of Standards, 1964.

[107] A. V. Balatsky, M. I. Salkola, and A. Rosengren. Impurity-Induced Virtual Bound States in d-Wave Superconductors. Phys. Rev. B*, 51:15547–15551, 1995.*

[108] H. V. Kruis, I. Martin, and A. V. Balatsky. Impurity-Induced Resonant State in a Pseudogap State of a High-T_c Superconductor. Phys. Rev. B*, 64:054501, 2001.*

[109] Jurij S*makov, Ivar Martin, and Alexander V. Balatsky. Theory of Scanning Tunneling Microscopy Measurement of Single Spin Decoherence in a Superconductor.* Phys. Rev. Lett.*, 88:037003, 2002.*

[110] A. V. Balatsky, I. Vekhter, and Jian X. Zhu. Impurity-Induced States in Conventional and Unconventional Superconductors. Rev. Mod. Phys.*, 78, 2006.*

[111] A. M. Clogston. Impurity States in Metals. Phys. Rev.*, 125:439–443, 1962.*

[112] Victor I. Fistul. Impurities in Semiconductors: Solubility, Migration, and Interactions. CRC Press LLC, Florida, 2004.

[113] Daniela Lindner. Electron Doped Cuprates, 2006. `http://guava.physics.uiuc.edu/~nigel/courses/569/Essays_Spring2006/files/Lindner.pdf`.

[114] D. Manske, I. Eremin, and K. H. Bennemann. Theory for Electron- and Hole-Doped Cuprate Superconductors: d-Wave Symmery Order Parameter. Europhys. Lett.*, 53(3):371, 2001.*

[115] N. A. Kuleeva, E. Z. Kuchinskii, and M. V. Sadovskii. Superconductivity in the"Hot Spots" Model of the Pseudogap State: Impurity Scattering and Phase Diagram. preprint: cond-mat/0406156 v1 7 Jun 2004.

[116] Charge Stripes in High-Temperature Superconductors. Website. `http://www-als.lbl.gov/als/science/sci_archive/stripes.html`.

[117] J. Fink, S. Borisenko, A. Kordyuk, A. Koitzsch, J. Geck, V. Zabolotny, M. Knupfer, B. Büchner, and H. Berger. Dressing of the Charge Carriers in High-T_c Superconductors. Lect. Notes Phys.*, 715:295, 2007.*

[118] T. Eckl, D. J. Scalapino, E. Arrigoni, and W. Hanke. Pair Phase Fluctuations and the Pseudogap. Phys.Rev.B*, 66:140510(R), 2002.*

[119] Paul E. Lammert and Daniel S. Rokhsar. How Much Phase Coherence Does a Pseudogap Need? preprint: cond-mat/0108146 v1 8 Aug 2001.

[120] Hole Superconductivity. Website. `http://physics.ucsd.edu/~jorge/hole.html`.

[121] J. E. Hirsch. Superconductors as Giant Atoms Predicted by the Theory of Hole Superconductivity. Physics Letters A*, 309:457, 2003.*

[122] X. J. Zhou, P. Bogdanov, S. A. Kellar, T. Noda, H. Eisaki, S. Uchida, Z. Hussain, and Z.-X. Shen. One-Dimensional Electronic Structure and Suppression of d-Wave Node State in ($La_{1.28}Nd_{0.6}Sr_{0.12}$)$CuO_4$. Science*, 286:268, 1999.*

[123] Giri Iyengar. Simple Model of Conductivity, 1996. `http://privatewww.essex.ac.uk/~mpthak/A%20tour%20through%20the%20interaction%20between%20humans%20and%20electromagneti/node6.html`.

[124] Feng Yuan and Shiping Feng. Normal-State Pseudogap and Electron Flat Dispersion in Copper Oxide Materials. Physics Letters A*, 271:429–434, 2000.*

[125] Y. S. Kim and M. E. Noz. Phase Space Picture of Quantum Mechanics. World Scientific Publishing Co. Pte. Ltd., New Jersey, 1991.

[126] Sang Pyo Kim. Invariant Operators and Heisenberg Operators for Time-Dependent Generalized Oscillators. Journal of the Korean Physical Society*, 43:11–16, 2003.*

[127] Green's Function. `http://en.wikipedia.org/wiki/Green's_function_(many-body_theory)`.

[128] Efunda Engineering Fundamentals. Elliptic Integrals. Website. `http://www.efunda.com/math/elliptic/elliptic.cfm`.

[129] Wolfram MathWorld. Website.
`http://mathworld.wolfram.com/EllipticIntegraloftheFirstKind.html`.

[130] Igor Khavkine. Mean-Field Analysis of Nematic Order in a Strongly Correlated System, 2003.
`http://www.physics.utoronto.ca/~igor/msc-report.pdf`.

[131] Harold Jeffreys and Bertha S. Jeffreys. Methods of Mathematical Physics. Cambridge, At The University Press, London, 1950.

[132] Chris Foster. Ramblings on Generalised Functions. Website.
`http://www.physics.uq.edu.au/people/foster/gen_fxns.pdf`.

[133] Wolfgang Gröbner and Nikolaus Hofreiter. Integraltafel, Unbestimmte Integrale. Springer-Verlag, Vienna, 1957.

[134] J. Zabloudil, R. Hammerling, L. Szunyough, and P. Weinberger. Electron Scattering in Solid Matter. Springer-Verlag, Berlin Heidelberg, 2005.